Properties of Molecules in Tunnel Junctions

Irene Yeriskin

NATIONAL UNIVERSITY OF IRELAND, CORK

(UNIVERSITY COLLEGE CORK)

College of Science, Engineering and Food Science

Department of Chemistry

Thesis submitted for the degree of Doctor of Philosophy

April 2013

Supervisor:	Prof. Jim Greer
Head of Department:	Prof. Michael Morris

CONTENTS

I, Irene Yeriskin, certify that this thesis is my own work and I have not obtained a degree in this university or elsewhere on the basis of the work submitted in this thesis.

Irene Yeriskin

ABSTRACT

Molecular tunnel junctions involve studying the behaviour of a single molecule sandwiched between metal leads. When a molecule makes contact with electrodes, it becomes open to the environment which can heavily influence its properties, such as electronegativity and electron transport. While the most common computational approaches remain to be single particle approximations, in this thesis it is shown that a more explicit treatment of electron interactions can be required. By studying an open atomic chain junction, it is found that including electron correlations corrects the strong lead-molecule interaction seen by the ΔSCF approximation, and has an impact on junction $I-V$ properties. The need for an accurate description of electronegativity is highlighted by studying a correlated model of hexatriene-di-thiol with a systematically varied correlation parameter and comparing the results to various electronic structure treatments. The results indicating an overestimation of the band gap and underestimation of charge transfer in the Hartree-Fock regime is equivalent to not treating electron-electron correlations. While in the opposite limit, over-compensating for electron-electron interaction leads to underestimated band gap and too high an electron current as seen in DFT/LDA treatment. It is emphasised in this thesis that cor-

recting electronegativity is equivalent to maximising the overlap of the approximate density matrix to the exact reduced density matrix found at the exact many-body solution. In this work, the complex absorbing potential (CAP) formalism which allows for the inclusion metal electrodes into explicit wavefunction many-body formalisms is further developed. The CAP methodology is applied to study the electron state lifetimes and shifts as the junction is made open.

ACKNOWLEDGEMENTS

I would firstly like to acknowledge the guidance and support given by my supervisor Prof. Jim Greer throughout this work. His patience and contagious enthusiasm have been invaluable.

A special thanks to Mark Szepieniec for interesting ideas and discussions during our collaborations. I must thank my co-workers and collaborators Shane McDermott, Dr. Giorgos Fagas and Prof. Rod Bartlett, their input was very valuable to me. I want to thank my thesis review committee Prof. Martyn Pemble and Dr. Shane O'Brien for useful suggestions during our regular meetings.

I must thank my examiners Prof. Martin Paterson and Prof. Justin Holmes for making time to read this thesis and attend my *viva*.

A thanks to Thomas Kelly for his help with MCCI and comments on my work. I also want to thank Dr. Giorgos Fagas, Marios Iakovidis and Dr. Lida Ansari for their help with TiMeS program. Thanks to Alin M. Elena for his help with programming and eternal patience with my questions. I want to thank all members of ETG and especially Dr Simon Elliott for making my stay in the group an educational and pleasant experience. A thanks to Mary O'Regan for helping with all the admin paperwork during my stay at Tyndall.

A special mention to Siobhan O'Halloran, Anna Hauber, Sarah Jones, Thomas Kelly, Mark Szepieniec, Marios Iakovidis and Thomas Sadler who did not just provide support during my research but also became my friends. A thanks to everyone in the post grad room, despite being one of the quietest environments I have worked in, I know people cared. A thank you to all of the Block A lunch group, those who are still around and have long graduated, for making lunch breaks friendly and filled with cake. I have met many talented people during the course of my PhD here and while there is not enough room to name them all, I hope to stay in touch with every single one. I want to mention my fellow graduate phorummers, whose postcards from all over the world made my desk a bright cheerful place to work at.

I want to thank my friends and my family and especially Patrick Tuite for reading and correcting several versions of this thesis. Finally, I want to thank my grandfather for teaching me the value of hard work and patience, it is to him I dedicate this thesis.

I would also like to acknowledge the support of Irish Research Council for Science and Engineering for the funding which covered this project.

LIST OF PUBLICATIONS

AND CONFERENCES ATTENDED

Publications

1. Szepieniec, M.; **Yeriskin, I.**; Greer, J.C.,
   "Quasiparticle energies and lifetimes in a metallic chain model of a tunnel junction", *Journal of Chemical Physics*, **138**, 144105, 2013.

2. **Yeriskin, I.**; McDermott, S.; Bartlett, R.J.; Fagas, G.; Greer, J.C.,
   "Electronegativity and electron currents in molecular tunnel junctions", *Journal of Physical Chemistry C*, **144**, 48, 20564-20568, 2010.

3. **Yeriskin, I.**; Szepieniec, M.; Greer, J.C.
   "Effect of electrodes on junction electronegativity", Paper in progress.

Conferences

1. **Yeriskin, I.**; McDermott, S.; Bartlett, R.J.; Fagas, G.; Greer, J.C.,
   "Electronegativity and electron currents in molecular tunnel junctions", Poster presentation at *Trends in Nanotechnology*, Madrid, Spain, September 2012

2. **Yeriskin, I.**; Greer, J.C.,

   "Complex absorbing potentials from electron self-energies", Oral presentation at *Irish Nanoscale Simulators Meeting*, Dublin, Ireland, May 2012

3. **Yeriskin, I.**; McDermott, S.; Bartlett, R.J.; Fagas, G.; Greer, J.C.,

   "Electronegativity and electron currents in molecular tunnel junctions", Poster presentation at *NanoGiga Challenges 2011*, Moscow, Russia, September 2011, "Outstanding Poster" award received.

OVERVIEW

Microchip components are undergoing constant scaling down to nanometre dimensions in accordance with Moore's law [1]. The molecular and electron transport properties of circuit components change, as quantum mechanical effects play an important role. A way of investigating such properties is by considering single molecule junctions.

In such junctions, a molecule of interest is sandwiched between two metal clusters which are comparable to interconnects in conventional systems. The metal-molecule interface is formed and molecular behaviour changes [2, 3]. It is desirable to understand this interface chemistry, which influences band alignment and charge transfer.

In this thesis, the properties of molecules in tunnel junctions are studied by considering electronegativity, electron state lifetimes and transport. The electron lifetimes arise from the molecule interacting with electrodes. This interface can be described exactly using electrode self-energies, or approximated with a complex absorbing potential (CAP). The CAPs method [4] is further developed to describe the coupling of the device region to the environment by incorporating the potential into Monte-Carlo configuration interaction (MCCI) formalism. Electronegativity of different junctions at several levels of electronic structure treatment is also discussed.

Thesis Structure

Chapter 1

An overview of the current progress in the field of molecular electronics is given. Several experimental and computational techniques are introduced.

Chapter 2

This chapter outlines the foundations of the computational methods employed throughout the thesis and serves as a quick reference for the reader.

Chapter 3

An introduction to open systems and quantum electron transport based on non-equilibrium Green's function (NEGF) is given. The CAPs method as applied within this thesis is discussed.

Chapter 4

Quasiparticle energies and lifetimes are calculated for a gold chain model and benzene-di-amine (BDA) containing junctions. The CAP method within Monte-Carlo configuration interaction (MCCI) formalism is used to investigate the effect of opening the system and electron correlations on quasiparticle peak broadening and electronegativity.

Chapter 5

In this chapter, the effect of accurate description of electronegativity and its influence on electron transport is discussed using a correlated model and electronic structure treatments.

1. INTRODUCTION

In 1974 Aviram and Ratner suggested the use of single molecules as components in future electronics [5], stimulating a large body of experimental and theoretical research and the field of molecular electronics itself. The field of molecular electronics comprises fundamental issues concerning the electronic response of molecules as parts of a mesoscopic structure and a technology-facing area of science [6]. The core idea is to form a molecular junction to replace common transistor components. That is, to design the junction conceptually and experimentally in such a way that it can act as a logic or memory device that can be incorporated into the network of a chip. This idea presents a number of challenges conceptually, experimentally and theoretically [3, 6–12]. Conceptually, one needs to design the architecture of a logic or memory device where a single molecule can provide an interconnect, a switch, a transistor or a more complex function. Experimentally, a challenge is to build a single molecule junction that is stable and can be reproduced a number of times to form a self-assembled array of such junctions. Theoretical challenges are around an accurate description of the molecular region while including large metallic electrodes that form interconnects to an active device.

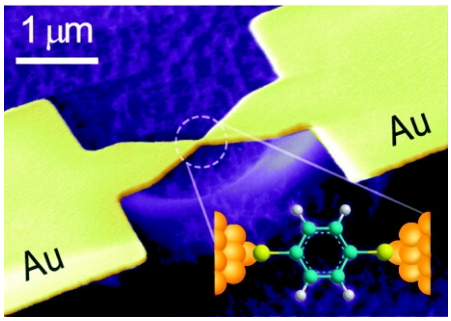

Fig. 1.1: A scanning electron microscopy image of a mechanically controllable break junction; the inset shows a computational model for the junction. Figure from [17].

A molecular junction comprises metal electrodes and a molecule as shown in Figure 1.1. The electrodes are usually either metallic, commonly gold, or a surface and a tip of a scanning tunnelling microscope (STM). The molecule can be a saturated carbon chain (alkane), a conjugated chain (alkene), a single aromatic, or a network of such molecules. A linker (anchor) molecule is a specially designed molecule that allows the species of interest to bond to both metal electrodes. For gold contacts, common linkers are thiol or amine based as they show strong binding energies [13–21], while Au-C linkers have also been explored [22]. Typically thiols and carbon linkers bind covalently to the gold atoms [20, 21], while amines form a donor-acceptor type bonds to under-coordinated gold [13, 14].

Current work in molecular electronics is largely devoted towards studying the conductance of a junction. After a junction is formed, a voltage (V) is applied and current (I) measurements are taken, and the differen-

tial conductance g is determined as

$$g(V) = \delta I(V)/\delta(V). \tag{1.1}$$

For a simple junction where a device region is formed by a chain of atoms such as depicted in Figure 1.2, quantised conductance is observed [23]; that is conductance exhibits steps near 3, 2, 1 or 0 quantum units. The quantum unit of conductance is defined by

$$g_0 = 2e^2/h = (12.9k\Omega)^{-1} \tag{1.2}$$

where e is electron charge and h is Planck's constant and indicates a single conducting state with unity transmission. This quantised conductance was predicted by Landauer [24] and his approach to electron transport forms the basis of the modern transport theories. Quantised conduction occurs when the contact size becomes comparable to the one electron Fermi wavelength [25]. The wavelength for electrons in gold is only a few Ångström, hence the appearance of quantised steps signals the formation of an atomic scale contact between a STM tip and surface.

On the fundamental level, molecular junctions present an opportunity to study the dynamics of a complex system and aid future transistor design when quantum mechanics is required. The computational modelling process, much like experiment, focuses on the accurate measurement of conductance. The first principles or *ab-initio* methods are usually based on Density Functional Theory (DFT) in combination with

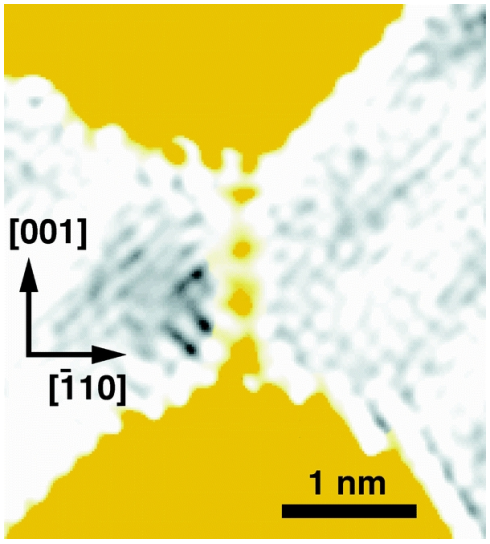

Fig. 1.2: Electron microscope image of a linear chain of four gold atoms (yellow coloured dots) forming a bridge between two gold films. Figure from [26].

non-equilibrium Green's function (NEGF) [8] and will be described in Chapter 2. An advantage of modelling over experiment is that the junction geometry can be relaxed within commonly used formalisms to give an idea of the bonding mechanisms and orbitals involved in the molecule-metal interface, though the junctions are often idealised compared to what is currently possible with laboratory based methods [6, 27].

In what follows, fabrication of molecular junctions is discussed, focusing on the two most common methods at the present time. Once built, the junctions need to be analysed and this is usually carried out with inelastic electron tunnelling spectroscopy (IETS) and recently tip-enhanced Raman spectroscopy (TERS), both methods are discussed with examples specifically relevant to theoretical modelling. One of the most

interesting aspects of molecular electronics is functionalising the molecular region to change its conductance, again this is done experimentally with theoretical evidence to explain the results. Lastly, an overview of theoretical modelling and its application to the field is presented.

1.1 Fabrication of Molecular Junctions

A molecular junction can be built using several techniques [20, 28, 29]. Electron current across a single molecule was first measured within mechanically controllable break junctions (MCBJ) using benzene-di-thiol (BDT) [20]. This method remains in common use, see refs. [10, 17, 30] and references therein. With recent developments in electron microscopy, STM based methods to form a junction have become increasingly popular following the first demonstration of the method by Xu *et al* [28]. Electromigration is another recent method based on a principle similar to MCBJ, however the mechanical force used to rupture the substrate is replaced with electron wind forces [29, 31]. Once a junction is formed, conductance is measured. There may be a range of molecular conformations in the gap between two electrodes and hence bonding patterns can differ, so the electronic response represents the average behaviour over an ensemble of individual molecules. The conductance measurements are generally taken thousands of times with active junctions to provide a reliable statistical result.

1.1.1 Mechanically Controllable Break Junctions

Mechanically controllable break junctions (MCBJs) provide an accurate way of forming a nano-scale band gap to facilitate the measurement of conductance [20, 32, 33]. In a typical set-up, as in Figure 1.3 (left panel), a metal wire is attached to a substrate which rests atop a metal rod. The piezo-driven rod motion displaces the position of the wire on the substrate. This technique gives great control over the size of the gap that is being formed as the wire breaks and allows for multiple contact formations and deformations. The resulting contacts are atomically sharp [32]. To measure the conductance of a particular molecule, the contacts are broken in the presence of the solution containing the adsorbing species. As a result, the atomic contacts are coated with a self-assembled monolayer of the molecule of choice as shown in Figure 1.3 (right panel).

1.1.2 Scanning Tunnelling Microscopy Junctions

A more common way of producing single molecule junctions is to use a substrate and STM tip [13, 20, 28]. The individual molecular junctions are formed by repeatedly moving the STM tip in and out of contact with a gold substrate in a solution of molecules of interest. During the initial stage when the tip is pushed down and then pulled up, the conductance decreases in a step like fashion at integer multiples of the conductance quantum (as is the case for MCBJ), as illustrated in Figure 1.4a. At a certain point when the tip is pulled further away from the substrate, the atomic chain formed between the tip and the substrate breaks. This

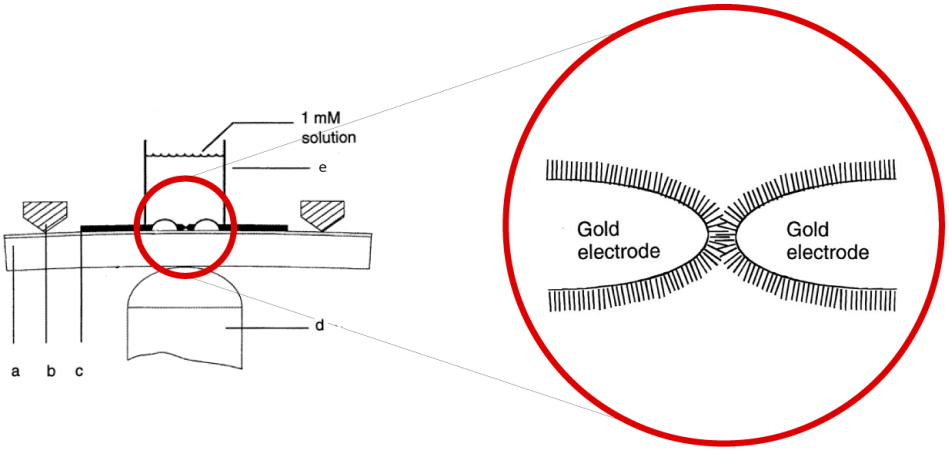

Fig. 1.3: A schematic diagram of a typical MCBJ process on the left: (a) the bending beam; (b) the counter supports; (c) the gold wire used to form contacts; (d) the piezo element (metallic rod) that will fracture the wire; (e) vessel containing solution of molecules. In the right panel, two tips of a molecular wire coated with a self-assembled mono-layer of BDT are brought together until the onset of conductance. Figure from ref. [20].

leads to a new set of peaks but of a different scale, as shown in Figure 1.4b. In the absence of molecules conductance below g_0 is featureless and smooth, as can be seen in Figure 1.4c.

The STM based techniques facilitate the study of the conductance of molecules [16, 34, 35] as a function of their geometry [36, 37] and substituents [38].

1.2 Characterisation Of Molecular Tunnel Junctions

Characterisation of molecular junctions is still in its early stages of development, but the inelastic electron tunnelling spectroscopy (IETS) technique has been used by some groups to yield interesting results,

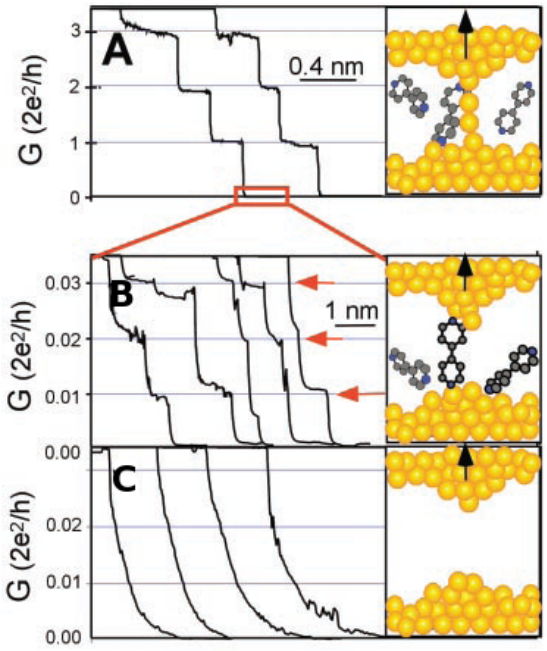

Fig. 1.4: A molecular junction formed by the STM tip method: (a) Step-like conductance observed as gold atomic chains are formed by pulling the STM tip further away from the surface, the steps correspond to multiples of g_0 (conductance quantum); (b) As the atomic chain is pulled apart to the breaking point, bipyridine fills in the gap leading to step-like conductance again but on a smaller scale; (c) A control experiment where the atomic chain is broken in the absence of molecules that can bind to both the surface and the tip, results in smooth conductance with no steps observed. Figure from ref. [28].

as discussed in what follows. Recent progress in tip-enhanced Raman spectroscopy (TERS) had led to the technique being applied to single molecule junctions with a view of providing accurate information on junction geometry.

1.2.1 Inelastic Electron Tunnelling Spectroscopy

IETS is a tool for studying adsorbates on metal surfaces by yielding an accurate vibrational spectra. One of the first applications of IETS was in metal-insulator-metal junctions [39]. In molecular electronics, IETS is commonly used to identify the molecular species in the nanogap between two metal contacts [10, 16, 17, 30, 31, 40, 41]. The device region can be thought of as a barrier through which the electrons tunnel from the left electrode to the right, depending on the chemical potentials of the metals. A bias voltage is applied which initiates electron tunnelling. Elastic tunnelling occurs when the electron has the same initial energy upon entering the barrier as upon emerging from it. Inelastic tunnelling occurs when the electron is scattered or interacts with the vibronic states of the device, this reduces its energy when it reaches the second metal electrode. In Figure 1.5, the moving electronic charge interacts with the molecular dipoles (electronic or vibronic) within the device region to induce excitation of the insulator molecule. This results in the loss of energy of the electron. Since the interaction of the electron with the molecular dipoles of the device region has both long and short range effects, selection rules are relaxed [42]. The applied voltage can be tailored to probe a particular state. For molecular electronics this is usually done to probe the highest occupied molecular orbital (HOMO) and lowest unoccupied molecular orbital (LUMO) levels that are investigated.

While in this thesis the vibrational properties of molecules are not studied, the results obtained from IETS indicate a strong coupling of

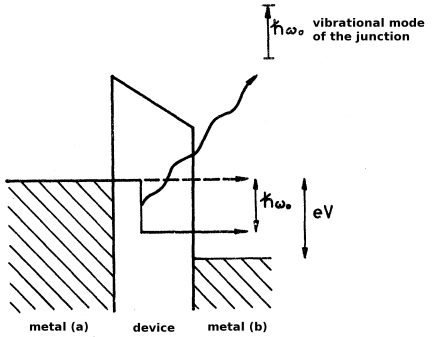

Fig. 1.5: A schematic representation of IETS mechanism, where the hatched regions represent the occupied states in metals (a) and (b). The dashed arrow represents an elastic tunnelling regime, that is, electron does not interact with the device. If the electron does interact with the vibronic or electronic modes of the device region, it loses the energy corresponding to those levels as $\hbar\omega_0$, and results in inelastic tunnelling shown as a solid arrow. This can be achieved by applying a voltage $V_0 = \hbar\omega_0/e$ across the junction. Figure ref. [39].

molecular and metallic states. The IETS method is one of the clearest methods to date that provides information that single molecules are being measured in molecular tunnel junction.

The most recent application of IETS came from Song *et al* where conducting states of BDT were probed to demonstrate gating behaviour of orbitals [40]. A gating voltage V was applied and the peaks of the IET spectrum (Figure 1.6) were assigned using the previous measurements obtained from Raman and infra-red (IR) spectroscopy as well as DFT calculations.

The HOMO of BDT is close in energy to the metal Fermi level E_F and is strongly coupled to the external vibrations resulting in a resonantly enhanced IET spectra [41]. Also, strong coupling has been observed

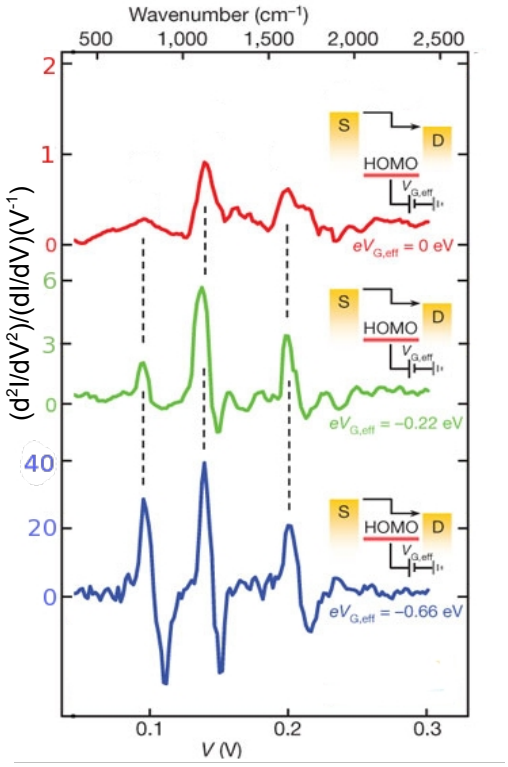

Fig. 1.6: The IET spectra for BDT junction with applied voltage V on the horizontal axis. The colour coded spectra correspond to the insets of the junctions where the molecular HOMO can be seen to move closer to the metal Fermi level as more negative voltages are applied. The dashed vertical lines guide the eye to the peaks as they change with applied voltage, which correspond to different vibrational modes of benzene. The value of $eV_{g,eff}$ corresponds to an effective molecular orbital gating voltage, the details of which are outlined in ref. [40] from where the figure is taken.

when the molecular orbitals are distributed around the bond directly related to the vibrational modes. In the case of BDT this holds for $\pi - \pi$ orbitals. The result of gating by changing V, as shown in Figure 1.6, is that the benzene IET spectra is modified. As the applied gating voltage becomes more negative and brings the HOMO closer to E_F, the

normalised amplitude $(d^2I/dV^2)/(dI/dV)$ for some features increases by more than a factor of 30 and peak shapes change. From this experimental work, further evidence for the need to accurately predict the molecule-metal interface is given.

1.2.2 Tip-Enhanced Raman Spectroscopy

Recent progress in TERS has led to the technique being applied to single molecule junctions with a view of providing accurate information on junction structure [43]. TERS builds on the same principle as surface-enhanced Raman spectroscopy, but a single metal nanoparticle is used to give an even greater electromagnetic field enhancement [44]. Due to the small size of the probe, lateral resolution is improved down to 10 nm. The technique is used in conjunction with STM, where Raman and conductance readings are taken as the junctions form between the surface and STM tip. In Figure 1.7, the red contour illustrates the electromagnetic field distribution, it can be seen that the molecule within the junction experiences the strongest electromagnetic effect. This is a great advantage of TERS compared to other techniques as molecular resolution is obtained.

In the recent experiment of 4,4-bipyridine on a gold (111) surface [43], Raman spectra were obtained by the means of "fishing-mode" where the STM tip is brought close enough to the surface coated with molecules to form a junction, then the current is measured as the "on" state. The tip is then withdrawn until the junction is broken and the current in the "off" state is obtained. The STM feedback loop is formed and brings

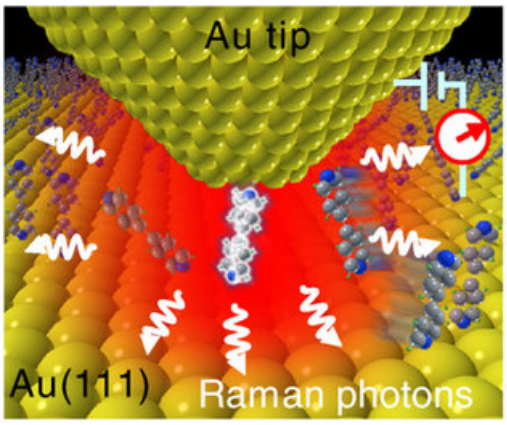

Fig. 1.7: Diagram of the TERS set up illustrating the extent of electromagnetic field (red) as it is felt by the molecule in vicinity of the tip. It is clear that the molecule bonded to the tip experiences the biggest effect. Figure from ref. [43].

the tip back within the junction-forming distance to "fish" for another molecule. The geometry characteristics are then obtained by considering the Raman spectrum, Figure 1.8a, where peak splitting in the "on" state is seen.

At low voltage, the two pyridine rings interact with the two electrodes in a similar way. Increasing the voltage, the bonding on the drain side will also increase, shown in Figure 1.8b, decreasing the Au-N bond from 2.35 Å to 2.15 Å [43]. The C-N bonds become weaker and the parallel C-C bonds become stronger, hence the ring becomes deformed. The drain ring results in a modified stretch frequency of 1631 cm^{-1} while the ring bonded to the source remains at 1609 cm^{-1}.

This work by Liu *et al* shows for the first time how voltage effects the geometry of the junction while being able to assign the changes to specific bonds. Shortly after, computational results by Mirjani *et al* [45]

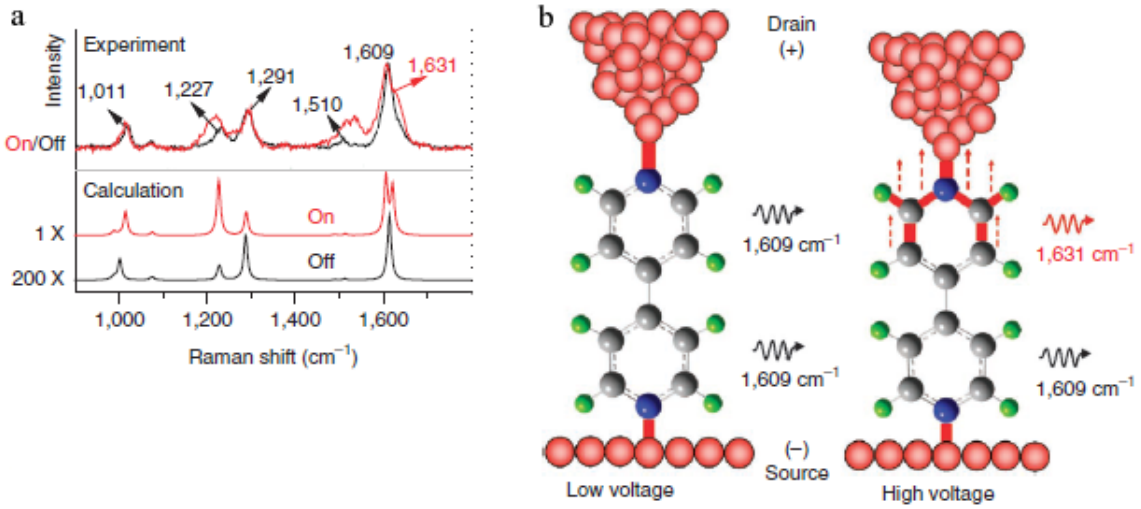

Fig. 1.8: Fishing-mode TERS spectra in (a) for 4,4-bipyridine junction and its computational model representation in (b). The red curve in panel (a) represents the average of all "on" states, while the "black" curve corresponds to the "off" states. The top panel of (a) illustrates the experimental results, and the bottom panel DFT results with B3LYP exchange correlation functional. A clear peak splitting from 1609 cm^{-1} in the "off" state to 1609 cm^{-1} and 1631 cm^{-1} in the "on" state is seen. Panel (b) illustrates the computational model used to explain the origin of peak splitting. At high voltages, the drain bonded benzene ring is seen to distort and result in a modified frequency of 1631 cm^{-1}, while the source bonded benzene remains at 1609 cm^{-1}. The figure is taken from ref. [43].

followed where DFT was used to predict Raman spectra of a collection of charged and neutral molecules with different anchor groups.

1.3 Designing Single Molecule Junctions

Molecular junctions provide a unique opportunity to tailor the band gap of the device region by means of shifting the positions of HOMO and

LUMO levels with respect to the metal Fermi level using various anchor molecules, chemical substituents and different molecular conformations. The relative position of molecular energy levels to metal energy levels is called band alignment and is seen to be the key quantity in molecular electronics which can control electron transport of the junction [2, 46–49]. In this section, the recent experimental and theoretical research that has been successfull in altering conductance is presented.

1.3.1 Linker Groups

Perhaps the most important component of the molecular junction, bar the molecule itself, is the linker (anchor) group. The linker molecule determines the bonding, and in turn the conductance properties of the device. The most common linker molecules for gold electrodes are amine or thiol based. The bonding motifs of linker groups with the metallic surface differ for thiols and amines. For example, thiol linkers conductance can be sensitive to conformation by orders of magnitude [50]. Whereas amines form a weaker but more selective bond [13]. The amine bond hypothesis [13] is that the strongly basic amine group donates its lone pair of electrons to an uncoordinated gold atom to form a Au-N bond. While a thiol has been seen to bind covalently in a variety of ways, for example top and three-fold hollow sites yielding a difference in conductance by up to factors of two to ten [51]. The selective amine bonding results in clearer conductance steps compared to thiols. More electronegative anchor groups have also been used, such as cyano [45], and were seen to significantly modify the position of the HOMO level.

1.3.2 Molecular Substituents

In chemical terms, substituents can be divided into two main types: electron donating groups (EDGs) and electron withdrawing groups (EWGs). Both groups can operate in two main ways by either resonance or induction, the former effect being stronger. It was found that EDGs and EWGs influence the position of the molecular HOMO and LUMO levels and their alignment with the metal E_F leading to the change in observed conduction [38, 52].

In the study by Venkataraman *et al* [38], the gold-BDA-gold (benzene-di-amine) junction used was substituted with a variety of substituents from electron donating methyl and methoxy groups to the most electron withdrawing fluorine and cyano groups. The substituents were added by replacing hydrogen atoms on the benzene ring. EDGs are found to increase conductance as they increase the energy of the HOMO (decreasing ionisation potential (IP)). This is because EDGs have lone electron pairs on them, for *e.g.* in methoxy, oxygen has a lone pair, that delocalises into the π space of benzene, thereby raising the HOMO energy closer to the metal work function. On the other hand, a very electronegative halogen group removes electron density from the σ space of the benzene and lowers the energy of the HOMO.

The experimental findings from ref. [38] have been confirmed by computational modelling within the DFT formalism for both BDA [38] and BDT [52] junctions. Despite different bonding geometries of BDA and BDT, the conceptual findings of substituents effects are equally valid.

1.3.3 Molecular Conformation

The conductance of molecular junctions can also be modified by changing the conformation of the molecule [15, 16, 36, 46]. However, in experimental studies when a junction is formed it consists of several molecular conformations, so only the average conductance can be measured. Bonding to the metal can occur at several sites, each site contributing a different conductance value. Theoretically, it is easier to form an idealised molecular junction of a certain starting geometry and then to allow the geometry to relax. Much like with the molecular substituents, conformation first affects the position of the HOMO and LUMO levels which in turn modify conductance [46].

1.4 Computational Modelling

Computational modelling of single molecule junctions entails dealing with open systems. Opening of a system is achieved by imposing boundary conditions. The most common way of opening a junctions is to use a Green's function self-energy to describe the leads within a single-particle formalism [3, 8]. When a molecule couples to a metal contact, several processes occur [2, 3]: metal and molecular states interact (hybridisation of molecular orbitals occurs), charge transfer from metal states to molecular states takes place and the electronic structure of the molecule may be changed. The convention is to consider the entire system as three sub-systems: left lead, extended molecule (EM) or device and right lead as illustrated in Figure 1.9

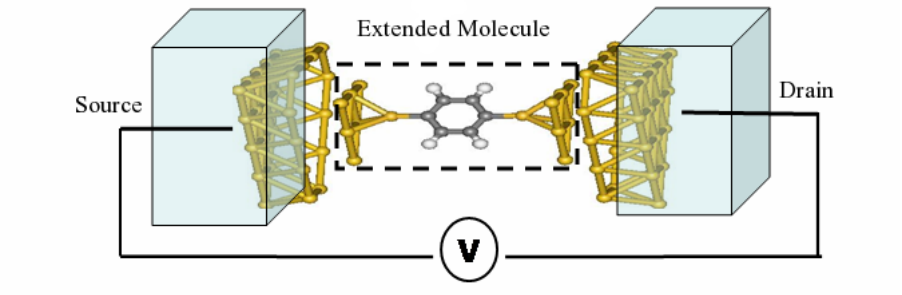

Fig. 1.9: A schematic representation of a typical computational model of a molecular tunnel junction. The source and drain are represented by two large leads, the extended molecule (EM) can be seen to contains parts of the lead called contacts as well as the molecule itself. Figure from ref. [53].

Commonly, a single particle approximation, such as the Kohn-Sham (KS) orbitals within DFT formalism (discussed in Chapter 2), is used to treat the junction's electronic structure. It is well known that there are inherent errors using DFT orbital energies to model the energy gap and alignment to the Fermi level due to self-interaction of electrons [48, 54–58]. For example, DFT calculations place the HOMO level too close to the metal Fermi energy in the case of amine linked junctions [15]. This results in conductance being about seven times larger than experiment [14, 59]. Similary, it has been shown that DFT overestimated electron current for BDT by up to a factor of 10^3 [34, 60]. Therefore, electron-electron interactions need to be included beyond the use of KS orbitals at least into the treatment of the extended molecule, while leaving the leads described by single particle formalisms. Improvements upon the standard DFT approach are achieved by including electron self-interaction by using NEGF [2], however, as the use of KS orbitals

remains a single-particle approach the errors are not completely eliminated [55]. The critical point within this theory is the correct selection of the self-energy approximation which would in turn lead to reliable quasiparticle energies. Further improvement can only be achieved by using many-body theories which account for electron interactions explicitly. Recent calculations based on many-body perturbation theory within the GW approach have been demonstrated to correct level alignment errors associated with KS-DFT and conventional NEGF-DFT approximations [61–63], however, discrepancies with experimental conductance still exist. The GW framework of DFT [64, 65] uses a Green's function G approximation to self-energy which contains a large part of exchange energies and some electron correlation. The dynamically screened Coulomb interaction is W. However, one significant drawback of the GW approximation is the failure to describe the multi-determinant behaviour. The configuration interaction (CI) framework (discussed in Chapter 2) can provide an accurate multi-reference treatment of electronic structure, conductance from which has shown excellent experimental agreement [66–68]. Hence, the need for a multi-determinant description [69] of tunnel junctions to achieve accurate predictions for band alignment and electron transport will be highlighted.

2. COMPUTATIONAL METHODS

The aim of electronic structure calculations is to solve the Schrödinger equation to obtain the electronic ground and excited states energies and wavefunctions. From the wavefunction all properties can be derived, such as dipole moments, polarisability, *etc.* There are several approaches to solving the Schrödinger equation. In this chapter, a brief conceptual summary of the most common electronic structure techniques as they are used in this thesis is given. Single determinant models are introduced first: Hartree-Fock (HF) [70] and the Kohn-Sham form of Density Functional Theory (DFT) [71]; followed by the many-body formalism of configuration interaction (CI) and more specifically the Monte-Carlo configuration interaction (MCCI) method [72–74]. We also discuss the Møller-Plesset (MP) approximation as it is commonly used in quantum chemical calculations and will be referred to in Chapter 5. A brief introduction to the density matrix and Green's function self-energy is also given.

2.1 The Molecular Hamiltonian

Usually, electronic structure calculations begin with a time-independent Schrödinger equation

$$\hat{H}_{tot}\Psi(\mathbf{r},\mathbf{R}) = E\Psi(\mathbf{r},\mathbf{R}) \tag{2.1}$$

where $\mathbf{r}$ are the electronic coordinates and $\mathbf{R}$ are the collective nuclear positions. The molecular Hamiltonian $\hat{H}_{tot}$ consists of nuclear and electronic terms and interaction term coupling the electronic and nuclear degrees of freedom

$$\hat{H}_{tot} = \hat{T}_n + \hat{T}_e + \hat{V}_{ne} + \hat{V}_{ee} + \hat{V}_{nn}. \tag{2.2}$$

The $\hat{T}_n$ and $\hat{V}_{nn}$ are nuclear kinetic and potential energies respectively, dependent only on the nuclear coordinates $\mathbf{R}$

$$\hat{T}_n + \hat{V}_{nn} = -\sum_{A=1}^{M} \frac{\hbar^2}{2M_A} \bigtriangledown_A^2 + \sum_{A=1}^{M}\sum_{B>A}^{M} \frac{Z_A Z_B}{\mid \mathbf{R}_A - \mathbf{R}_B \mid}, \tag{2.3}$$

$\hat{T}_e$ and $\hat{V}_{ee}$ only depend on the electron positions,

$$\hat{T}_e + \hat{V}_{ee} = -\sum_{i=1}^{N} \frac{\hbar^2}{2m_e} \bigtriangledown_i^2 + \sum_{i=1}^{N}\sum_{j>i}^{N} \frac{e^2}{4\pi\epsilon_0} \frac{1}{\mid \mathbf{r}_i - \mathbf{r}_j \mid} \tag{2.4}$$

The $\hat{V}_{ne}$ term depends on both the position of nuclei and electrons,

$$\hat{V}_{ne} = \sum_{A=1}^{M}\sum_{i=1}^{N} \frac{Z_A e^2}{4\pi\epsilon_0 \mid \mathbf{R}_A - \mathbf{r}_i \mid}. \tag{2.5}$$

where i, j in the above are the electron coordinate indices and A, B are nuclear coordinate indices, $Z_{A,B}$ are nuclear charges, m_e is the mass of an electron and M_A is a nuclear mass, $\bigtriangledown_i^2$ and $\bigtriangledown_A^2$ are Laplacian operators which involve differentiation with respect to the coordinates of the i'th electron and A'th nucleus, respectively. There are several assumptions used when constructing this Hamiltonian: gravity, nuclear forces and non-electromagnetic forces are all ignored as they are weak compared to the electromagnetic force. In the Born-Oppenheimer approximation, it is assumed that the nuclei are stationary and the electrons move in the mean field of the nuclei. That is, the motion of the nuclei and electrons is decoupled. This type of Hamiltonian is used throughout this thesis.

The operators may be grouped based on the number of electron indices:

$$\hat{h}_i = -\frac{\hbar^2}{2m_e} \bigtriangledown_i^2 - \sum_A^M \frac{Z_A}{\mid \mathbf{R}_A - \mathbf{r}_i \mid}, \tag{2.6}$$

$$\hat{g}_{ij} = \frac{1}{\mid \mathbf{r}_i - \mathbf{r}_j \mid}. \tag{2.7}$$

The one-electron operator $\hat{h}_i$ describes the motion of electron i in the field of all the nuclei, and $\hat{g}_{ij}$ is a two-electron operator giving the electron-electron repulsion. So, an electronic Hamiltonian can be written compactly as

$$\hat{H} = \sum_i^N \hat{h}(i) + \sum_i^N \sum_{j>i}^N \hat{g}(i,j). \tag{2.8}$$

The Schrödinger equation cannot be solved exactly for any Coulomb

system that contains more than one electron. This is because the electron-electron repulsion term is not separable; this term couples the electrons together which repel each other while being attracted to the nucleus. Hence, the motion of all the electrons are correlated. The correlation energy and its calculation are discussed in more detail in Section 2.4. In the work that follows atomic units (a.u.) ($\hbar = m_e = e = 1$) are used, unless otherwise specified.

2.2 Slater Determinants

An atomic orbital (AO) is defined as the wavefunction for a single electron in an atom. Molecular orbitals (MOs) are often expanded as a linear combination of AOs. Since electrons have spin, they are defined within coordinate space (spatial orbitals) or coordinate and spin space (spin orbitals). A spin orbital, $\chi(\mathbf{x})$ consists of the two orthonormal functions α (spin up) and β (spin down) as a wavefunction describes both the spatial distribution and spin of an electron. Hence, for every spatial orbital ψ, there are two spin orbitals

$$\chi(\mathbf{x}) = \begin{cases} \psi(\mathbf{r})\alpha(\varphi) \\ \text{or} \\ \psi(\mathbf{r})\beta(\varphi) \end{cases}, \tag{2.9}$$

where $\mathbf{r}$ is the position vector of a single electron in space, φ is the coordinate in spin space, and $\mathbf{x}$ is a spin and space coordinate.

Electrons obey the Pauli Exclusion principle which states that two

fermions can not be simultaneously in the same quantum state. Hence, an antisymmetric wavefunction for two electrons is written as

$$\chi(\mathbf{x_1}, \mathbf{x_2}) = -\chi(\mathbf{x_2}, \mathbf{x_1}), \tag{2.10}$$

with the antisymmetry enforcing the Pauli exclusion principle.

The antisymmetric wavefunction for an N electron system can be written as a determinant:

$$\chi(\mathbf{x_1}, \mathbf{x_2} \ldots \mathbf{x_N}) = (N!)^{-1/2} \begin{vmatrix} \chi_i(\mathbf{x_1}) & \chi_j(\mathbf{x_1}) & \ldots & \chi_k(\mathbf{x_1}) \\ \chi_i(\mathbf{x_2}) & \chi_j(\mathbf{x_2}) & \ldots & \chi_k(\mathbf{x_2}) \\ \vdots & \vdots & & \vdots \\ \chi_i(\mathbf{x_N}) & \chi_j(\mathbf{x_N}) & \ldots & \chi_k(\mathbf{x_N}) \end{vmatrix} \tag{2.11}$$

where $(N!)^{-1/2}$ is the normalisation factor when using orthonormal spin orbitals. This is the so-called Slater determinant [75, 76]. Interchanging the coordinates of two electrons is the same as interchanging two rows of the determinant, and changes the sign of the determinant enforcing the anti-symmetry requirement. The Slater determinant incorporates exchange correlation, that is the motion of electrons with parallel spins is correlated, in that non-classical effects beyond electrostatics are introduced. However, the electrons of opposite spins remain uncorrelated.

Slater determinants can also be used to express excited state wavefunctions. Let us consider the Schrödinger equation

$$H\Psi_0 = E\Psi_0, \tag{2.12}$$

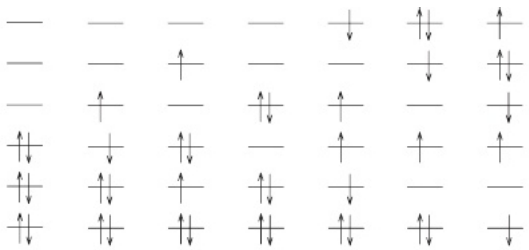

Fig. 2.1: Excited Slater determinants, from l-r: ground state, S-type, S-type, D-type, D-type, T-type, Q-type, denoting singles, doubles, tripes, quadruples, respective. Figure from ref. [77].

let Ψ_0 be N-electron determinant approximation to the ground state wavefunction. The excited Slater determinants are defined as Ψ_S (Single), which is a new Slater determinant different from Ψ_0 in one spin orbital, Ψ_D (Double) if two spin orbitals differ, and so on. In Figure 2.1 a collection of such determinants is illustrated.

The total number of excited determinants that can be generated depends on the size of the basis set, the larger the basis, the larger the number of virtual orbitals, and the greater the number of the Slater determinants. The number of N-electron Slater determinants increases combinatorially as the number of molecular orbitals (MOs) describing excitations is increased.

2.3 Single Determinant Models

A Slater determinant can represent a set of non-interacting electrons that serve as a first approximation to a set of interacting electrons. In the following section, Hartree-Fock (HF) theory and the Kohn-Sham ap-

proach to DFT will be introduced to understand how spin orbitals may be employed and to understand their use as a single determinant approximation to the N-electron wavefunction and charge density, respectively. The use of orbitals in KS-DFT is a theoretical device to describe the electron density. However, as will be discussed, the use of KS eigenvalues to describe electronic spectra equates to their use in a single particle theory, or single determinant approximation.

2.3.1 Hartree-Fock Theory

The HF method seeks to approximately solve the Schrödinger equation by assuming that the wavefunction can be approximated by a single Slater determinant. The energy in a single normalised Slater determinant is,

$$E = \langle \Psi | \hat{H}_e | \Psi \rangle \tag{2.13}$$

Having selected a trial wavefunction, $|\Psi\rangle = |\chi_1 \chi_2 \dots \chi_a \chi_b \dots \chi_N\rangle$, the HF equations can be derived using the variational principle. An equation (2.1) for the electronic Hamiltonian is considered first,

$$\hat{H}_e = \sum_{i}^{N} \hat{h}(i) + \sum_{i}^{N} \sum_{j,j \neq i}^{N} \hat{g}(i,j).$$

The two-electron term gives rise to two contributions: a Coulomb interaction term and an exchange term. In an exact theory, the Coulomb term is represented by the two-electron operator r_{ij}^{-1} felt by electron 1 and associated with the instantaneous position of electron 2, however in

the HF approximation it is an average term. A Coulomb operator is defined as

$$\hat{J}_b(1) = \int d\mathbf{x}_2 \mid \chi_b(2) \mid^2 r_{12}^{-1} \tag{2.14}$$

as an average local potential at point $\mathbf{x}_1$ due to an electron in χ_b. The exchange integral has no classical analogue and can be thought of as the energy associated with exchanging two electrons of the same spin,

$$\hat{K}_b(1)\chi_a(1) = \left[\int d\mathbf{x}_2 \, \chi_b^*(2) r_{12}^{-1} \chi_a(2)\right] \chi_b(1). \tag{2.15}$$

The HF method is a constrained minimisation method, meaning the total energy is minimised under the constraint that the MOs remain orthogonal and normalised. The constraint condition is handled by Lagrange multipliers leading to an eigenvalue equation with the Fock operator as

$$\hat{f}(1) = \hat{h}(1) + \sum_b \left[\hat{J}_b(1) - \hat{K}_b(1)\right]. \tag{2.16}$$

The Fock operator contains the one-electron energy operator describing the kinetic energy of electrons and their attraction to the nuclei, while the two-electron operator describes the repulsion of an electron in the mean field of all other electrons. The energy operator is non-separable in electron coordinates due to the Coulomb operator, and hence the solution to the HF differential equation cannot be a single (separable) Slater determinant. Because the energy is described as an average repulsion between an electron and all the other electrons distributed in orbitals, the total energy cannot be exact.

The variational principle states that the best wavefunction of this functional form is the one which gives the lowest possible energy. The expectation value for energy can be written as,

$$E = \langle \Psi | \hat{H}_e | \Psi \rangle,$$

the energy, E is minimised with respect to the choice of the spin orbitals χ; this leads to the HF equation which determines the optimal spin orbitals. Because the HF Hamiltonian operator is hermitian ($H^\dagger = H$), the orbitals can be chosen to be orthonormal[1].

This leads to a HF equation $\hat{F}\,\chi_{HF} = \epsilon\,\chi_{HF}$ that is solved iteratively, *i.e.* the results must eventually become self-consistent. The orbitals χ_{HF} obtained in this way lead to the HF approximation to the ground state wavefunction Ψ.

Introducing a basis set transforms the HF equations into the Roothaan equations and leads to the wavefunction becoming a linear combination of atomic orbitals (LCAO). For the work that follows in this thesis, it is useful to express the Roothaan equations in matrix form [70]. Two matrices are defined: an overlap matrix **S** and the Fock matrix **F**. The overlap matrix has elements

$$S_{\mu\nu} = \int d\mathbf{r}_1\, \phi^*_\mu(1)\phi_\nu(1), \tag{2.17}$$

and is a Hermitian matrix. The finite set of K atomic basis functions

[1] $\langle \chi_i | \chi_j \rangle = \delta_{i,j}$, $\delta_{i,j}$ = Krönicker-delta function

$\{\phi_\nu\}$ is assumed to be normalised, although not orthogonal to each other, hence the magnitude of the diagonal elements is $0 \leq | \ S \ | \leq 1$. Their sign depends on the relative orientation and separation of the two basis functions. The Fock matrix, $\mathbf{F}$ has elements

$$F_{\mu\nu} = \int d\mathbf{r}_1 \, \phi^*_\mu(1) f(1) \phi_\nu(1), \tag{2.18}$$

and is also a Hermitian matrix representation of the Fock operator. The integrated Hartree-Fock equations can be written as [70],

$$\sum_\nu F_{\mu\nu} C_{\nu i} = \epsilon_i \sum_\nu S_{\mu\nu} C_{\nu i} \qquad i = 1, 2, \ldots, K, \tag{2.19}$$

these are the Roothan equations, which are written as a matrix equation,

$$\mathbf{FC} = \mathbf{SC}\boldsymbol{\epsilon}, \tag{2.20}$$

where $\mathbf{C}$ is a square matrix of the expansion coefficients C_{μ_i} of χ, and $\boldsymbol{\epsilon}$ is a diagonal matrix of the orbital energies ϵ_i. The matrix representation of the HF equations is the form that will be used in this thesis. The computational cost of the HF method increases as N^3 (where N is the number of AOs) due to the need to solve a matrix eigenvalue problem, hence making it as time-consuming a calculation as KS-DFT (discussed next), but less computationally heavy than MP2 and configuration interaction (CI) which will be discussed in what follows.

2.3.2 Kohn-Sham Density Functional Theory

Thomas-Fermi theory

Density Functional Theory (DFT) is based on Thomas-Fermi theory [78, 79], dating back to 1927. The original theory proposes to use the kinetic, exchange and correlation energies for a homogeneous gas to construct similar expressions for an inhomogeneous gas. This is an early outline of the Local Density Approach (LDA) but unlike in modern DFT-LDA, Thomas-Fermi LDA is applied also to the kinetic energy. It is assumed that when the energy density is calculated locally in the inhomogeneous system it will exhibit approximately the homogeneous gas behaviour. In the 1930's, the theory was extended by Dirac who formulated the local approximation for exchange, leading to the energy functional[2] in an external potential V_{ext}, [79]:

$$\begin{aligned} E_{TF}[\rho] &= C_1 \int d^3r\, \rho(\mathbf{r})^{5/3} + \int d^3r\, V_{ext}(\mathbf{r})\rho(\mathbf{r}) \\ &+ C_2 \int d^3r\, \rho(\mathbf{r})^{4/3} + \frac{1}{2}\int d^3r d^3r'\, \frac{\rho(\mathbf{r})\rho(\mathbf{r}')}{\mid \mathbf{r}-\mathbf{r}' \mid} \end{aligned} \qquad (2.21)$$

where the first term is the local approximation to the kinetic energy with $C_1 = \frac{3}{10}(3\pi^2)^{2/3} = 2.871$ a.u., the third term is the local exchange with $C_2 = -\frac{3}{4}(\frac{3}{\pi})^{1/3}$ and the last term is the classical electrostatic (Hartree) energy. Minimising this energy functional for all possible $\rho(\mathbf{r})$, subject to the constraint on the total number of electrons to be equal to the total

[2] A functional is a prescription for producing a number from a function which in turn depends on a set of variables. A function is a prescription which produces a number from a set of variables.

charge, leads to an approximation for the ground state energy.

The advantage of density based methods is that they are, in principle, computationally less demanding compared to a wavefunction method such as HF as discussed previously, and they explicitly include electron correlations. This is because the electron density can be expressed as

$$\rho = \sum_{i=1}^{N} \mid \chi_i \mid^2, \tag{2.22}$$

with an increased number of electrons, the charge density matrix has the same number of variables. However in practice, there is no method yet to solve for the density without the re-introduction of MOs.

In 1964, a proof by Hohenberg and Kohn [80] that the ground state electronic energy is determined entirely by the electron density ρ gave mathematical grounds to the ideas behind Thomas-Fermi theory. The proof of the theorems is widely available in literature [79] and shall be omitted in this thesis, suffice it to say that the theorems relate a functional of the charge density to the ground state electronic energy.

A drawback to DFT is that the functional connecting the electron density and ground state energy is not explicitly known. Much of the work done in the DFT field is directed toward designing and improving such approximate functionals.

The Kohn-Sham Approximation to Density Functional Theory

The DFT formulation implemented in modern quantum chemistry packages is the theory formulated in Kohn-Sham (KS) orbitals [71] [3]. This leads to the computational effort being more demanding due to the re-introduction of the orbitals.

The KS Ansatz can be used to show that the ground state density of the original interacting system is equal to that of some chosen non-interacting system that can be considered exactly soluble with all the difficult many-body terms incorporated into an exchange-correlation functional of the density. The accuracy of the ground state energy and density is determined by the approximation used to describe the exchange-correlation functional. The solution for the KS ground state is the minimisation with respect to either the density $\rho(\mathbf{r}, \varphi)$ or the effective potential, V_{eff}. The KS variational equation can be written as,

$$\begin{aligned} \frac{\delta E_{KS}}{\delta \chi_i^*(\mathbf{x})} &= \frac{\delta T_S}{\delta \chi^* *_i (\mathbf{x})} \\ &+ \left[\frac{\delta E_{ext}}{\delta \rho(\mathbf{x})} + \frac{\delta E_{Hartree}}{\delta \rho(\mathbf{x})} + \frac{\delta E_{xc}}{\delta \rho(\mathbf{x})}\right] \frac{\delta \rho(\mathbf{x})}{\delta \chi_i^*(\mathbf{x})} \\ &= 0, \end{aligned} \tag{2.23}$$

where T_S, the independent-particle kinetic energy, is explicitly expressed as a functional of the orbitals but all the other terms are considered as functionals of density. Hence the minimisation is with respect to the KS

[3] In this thesis, when a reference to DFT, it is specifically to KS-DFT

orbitals. The KS Schrödinger-like equation is

$$(H_{KS} - \epsilon_i)\chi_i(\mathbf{x}) = 0, \tag{2.24}$$

where H_{KS} is the KS Hamiltonian with eigenvalues ϵ_i and $\mathbf{x}$ are a combined spin and space coordinate as before. The Hamiltonian consists of two parts

$$\begin{aligned} H_{KS}(\mathbf{x}) &= -\frac{1}{2}\bigtriangledown^2 + V_{KS}(\mathbf{x}), & (2.25)\\ V_{KS}(\mathbf{x}) &= V_{ext}(\mathbf{x}) + \frac{\delta E_{Hartree}}{\delta n(\mathbf{x})} + \frac{\delta E_{xc}}{\delta n(\mathbf{x})} \\ &= V_{ext}(\mathbf{x}) + V_{Hartree}(\mathbf{r}) + V_{xc}(\mathbf{x}), & (2.26) \end{aligned}$$

where attempting to describe the exchange-correlation functional $V_{xc}(\mathbf{r})$ is the subject of much work in the DFT field. The Kohn-Sham orbitals are not strictly quasiparticles, but their energy eigenvalues are often used to approximate properties of a system in a single particle picture. This section is referred to when describing junctions in the DFT treatment and implementing various exchange-correlation functionals in this work.

2.4 Configuration Interaction

For many chemical reactions and in the case of molecular junctions, a more accurate determination of the energy or a multi-reference wavefunction is required. This is generally obtained by using many-electron formalisms which treat correlation energy explicitly. While being computationally demanding, the results contain significant information on

the energy and the character of the many-electron wavefunction of the system. Configuration interaction (CI) is one example of a many-electron formalism and is the one used in this thesis.

The HF method generates solutions to the Schrödinger equation where the electron-electron interaction is replaced by an average interaction. In a sufficiently large basis set for atoms and molecules, HF can account for 99% of the exact energy. However in chemical reactions that require an accurate description of the excited state or transition complexes, the neglected 1% plays an important role. The correlation energy can be defined as the difference between the HF energy and the exact energy:

$$E_{corr} = E_{total} - E_{HF}. \tag{2.27}$$

The first linear variational principle for many-body wavefunctions was written by MacDonald in 1933 and became known as the superposition of configurations or configuration interaction [81]

$$\Psi = \sum_i c_i \Psi_i, \tag{2.28}$$

where Ψ is the many-electron wavefunction. The N-electron basis Ψ_i are Slater determinants, which are often called "spin-orbital configurations", or sums of Slater determinants which are known as configuration state functions (CSFs) and have the same symmetry properties as Ψ.

As the HF energy follows from a variational principle it is an upper bound to the exact energy, hence the correlation energy is negative. Con-

figuration interaction is a means to obtain the correlation energy. The method consists of diagonalising an N-electron Hamiltonian in an N-electron basis. Since the HF method determines the energetically "best" one-determinant trial wavefunction, it is often used as a starting point for CI. To improve on a single determinant HF wavefunction, the trial wavefunction is written in a multi-determinant form. Because the starting wavefunction is expanded to include more determinants, it is more correct to think of the electron distribution not as orbitals but as an electron density obtained from a many-electron wavefunction,

$$\Psi = c_0\Psi_{HF} + \sum_{i=1} c_i\Psi_i. \tag{2.29}$$

In general, c_0 is close to one for a molecular problem, unless the system is multi-reference, that is several states are nearly degenerate and can mix strongly in the overall wavefunction. The CI method calculates the remaining coefficients c_i. The starting point contains N electrons and K basis functions with $N/2$ occupied spatial molecular orbitals for a closed shell state and $K-N/2$ unoccupied (virtual) orbitals. There are typically more virtual orbitals than occupied orbitals. The total CI wavefunction is made up of excited Slater determinants. Subscripts indicate the excitations Single (S), Double (D), triple (T), *etc.* as described in Section 2.2,

$$\Psi_{CI} = c_0\Psi_{HF} + \sum_S c_S\Psi_S + \sum_D c_D\Psi_D + \sum_T c_T\Psi_T + \ldots = \sum_{i=0} c_i\Psi_i. \tag{2.30}$$

A restriction is placed on the summation indices to ensure that a given excitation is counted only once. CI is a variational technique, the energy should be minimised under the constraint that the total CI wavefunction is normalised. The expectation value of the many-body Hamiltonian operator using the wavefunction Ansatz equation (2.30) is the CI energy,

$$E = \frac{\langle \Psi_{CI}|H|\Psi_{CI}\rangle}{\langle \Psi_{CI}|\Psi_{CI}\rangle}. \tag{2.31}$$

The energy is minimised with respect to the coefficients c_i, leading to a matrix eigenvalue equation,

$$\mathbf{Hc} = \mathbf{ScE}, \tag{2.32}$$

where the matrix elements of the many-electron Hamiltonian are $\langle \Psi_i|H|\Psi_j\rangle$. The overlap matrix, $\mathbf{S}_{ij} = \langle \Psi_i|\Psi_j\rangle$ for orthonormal Slater determinants will be unity. In general, one deals with non-orthogonal CSFs and the overlap matrix elements are $\langle \Psi_i|\Psi_j\rangle$.

Since this is a many-particle method, as can be anticipated it is computationally more demanding than single particle theories. The size of the full CI space can be calculated using Weyl's dimensional formula as the number of CSFs,

$$M = \frac{2S+1}{K+1}\binom{K+1}{N/2-S}\binom{K+1}{N/2+S+1}, \tag{2.33}$$

where N is the number of electrons, K is the number of orbitals, and S is the total spin. It becomes clear that even with the reduction of CI space

due to spin constraints, the increase in the size of the wavefunction length with an increasing number of electrons is dramatic. A full configuration interaction (FCI) will give the exact energy within a given basis set, however it is only feasible for few small systems, due to the size of the resulting CI matrix.

The size of the CI calculation and the accuracy of the energy obtained can be controlled by the size of an active space and by freezing occupied orbitals. The active space can be defined as all the CSFs that are available for the calculation, both occupied and virtual. The more virtual states that are available, the more accurate the calculation will be. Some occupied orbitals which are low in energy that will not be easily excited can be frozen, limiting the CSFs just to the higher lying occupied orbitals which will readily participate in the excitations into the virtual orbitals. This is known as the "frozen core approximation" and can significantly aid in limiting the size of the CI matrix. The correlation of the core electrons contributes to the total energy as well, however it can be essentially considered as a constant factor [74].

The implementation of CI used in this work is Monte-Carlo configuration interaction (MCCI) [72–74, 82]. The MCCI formalism has several advantages over direct CI and its applicability to the ground state energy [72, 73, 83], electronic spectra and excited states in atoms and molecules [82, 84–87] and for calculations of dissociation energies [88] as well as large systems [89] has been demonstrated.

The main advantage of MCCI is how it selects the CSFs. Starting from a set of CSFs (which initially may be a single CSF), then addi-

tional CSFs are randomly generated relative to that trial vector with no restriction on the interacting configuration subspace. The CI matrix diagonalisation problem is solved on the subspace defined by the resulting expanded vector. This vector is then "pruned" by removing the CSFs whose associated coefficient in the CI eigenvector has a magnitude lower than a given coefficient threshold (c_{min}). This "pruned" vector now serves as a trial vector for the generation of new random CSFs, and this sequence is repeated until convergence in the energy and CI vector length is reached. The selection criteria can be lowered to include more and more CSFs, approaching the exact energy and wavefunction. A reference space consists of a set of strongly interacting CSFs, which are usually quickly found. Each of these CSFs can then interact with a set of single, double, and higher order excitations which may be selected later in the process. The parameters that control the calculation are involved in regulating the convergence behaviour of energy and the CI vector. The convergence of MCCI relates to how many steps are necessary until the wavefunction and energy satisfy given thresholds, illustrated in Figure 2.2. This primarily depends on how good the initial vector was. In the branching step the new configurations are generated. If only a small amount of new configurations is generated, then the previous step CI vector will be a good approximation to the current vector. However, if a large number of new configurations is obtained, the the convergence is slower. A small change in the magnitude of the coefficients speeds up the convergence process.

In this thesis, a complex MCCI program is used which is the standard

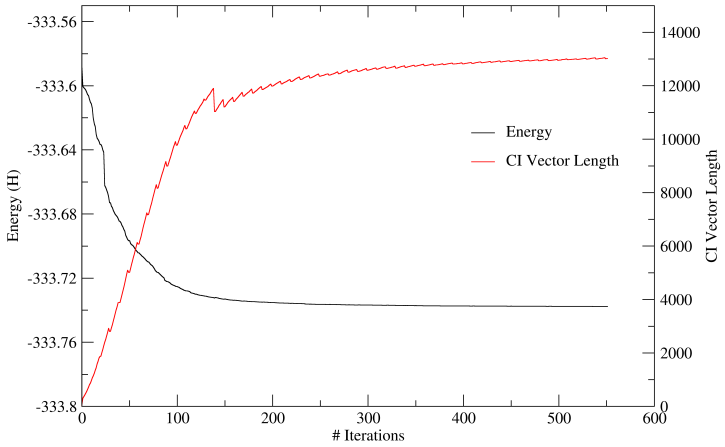

Fig. 2.2: Convergence behaviour of MCCI for the chain-BDA-chain junction studied in Chapter 4 for a fixed value of c_{min} of 8×10^{-4}. The total energy is seen to rapidly decrease (shown in black) as the number of CSFs increases (shown in red). The small jumps seen in the CI vector length curve correspond to the full pruning steps.

MCCI modified to treat the complex symmetric generalised eigenvalue problem that arises when adding the complex absorbing potential (CAP) (which is discussed in more detail in Chapter 3) as a one-body operator to the many-electron Coulomb Hamiltonian [90][4]. MCCI uses a Lanczos method for matrix diagonalisation. The projection method outlined in ref. [91] is introduced to solve the complex symmetric generalised eigenvalue problem.

Further details on development of MCCI can be found in ref. [72–74, 82, 85, 90, 92].

[4] Algorithm modifications have been carried out by Mark Szepieniec.

2.5 Density Matrix

We have mentioned that wavefunctions for molecules become more and more complex as system sizes become larger and computational facilities improve. The information on the single electron distribution is contained within an electron density and spin density. In this section, the density matrix is discussed, which is later referred to in Chapter 5.

The probability of finding an electron in volume element $d\mathbf{r}$ and with spin between s and $s + \mathrm{d}s$ (where $\mathrm{d}s$ is a spin element) is determined by the density function [93],

$$\rho(\mathbf{x}) = \sum_{i}^{n_{occ}} \mid \chi_i(\mathbf{x}) \mid^2, \tag{2.34}$$

where as before χ_i is a spin orbital and $\mathbf{x}$ stands for space and spin coordinates collectively, and n_{occ} is the total number of occupied orbitals. For a many electron system with a wavefunction $\Psi(\mathbf{x}_1, \mathbf{x}_2, \ldots, \mathbf{x}_N)$, then the probability of electron 1 being in space volume $d\mathbf{x}_1$ and other electrons anywhere is,

$$\rho(\mathbf{x}_1) = \int \Psi(\mathbf{x}_1, \mathbf{x}_2, \ldots, \mathbf{x}_N)\Psi^*(\mathbf{x}_1, \mathbf{x}_2, \ldots, \mathbf{x}_N)d\mathbf{x}_2 \ldots d\mathbf{x}_N, \tag{2.35}$$

and the probability of finding any of the N electrons in $d\mathbf{x}_1$ is N times the above equation, so the corresponding density function $\rho_1(\mathbf{x}_1)$ defined

as [93],

$$\rho_1(\mathbf{x}_1) = N \int \Psi(\mathbf{x}_1, \mathbf{x}_2, \ldots \mathbf{x}_{N-1}, \mathbf{x}_N)\Psi^*(\mathbf{x}_1, \mathbf{x}_2, \ldots \mathbf{x}_{N-1}, \mathbf{x}_N) d\mathbf{x}_2 \ldots d\mathbf{x}_N, \tag{2.36}$$

where $\mathbf{x}_1$ is a point at which the density is being evaluated as opposed to an electron coordinate. As an example particularly illustrative to electronic structure calculations, an energy operator that contains the one-electron terms is considered

$$\hat{h}(i) = -\frac{1}{2} \bigtriangledown^2 (i) + V(i), \tag{2.37}$$

for each electron i and the two-electron term for electron repulsion

$$\hat{g}(i,j) = 1/r_{ij}, \tag{2.38}$$

for a pair of electrons i, j. Due to the symmetry of $\Psi^*\Psi$, each term of the expectation value will contribute equally, so one can write N times the result for the first electron to obtain the density function $\rho(\mathbf{x}_1; \mathbf{x}'_1)$. The expectation value of the one-electron operator $\langle \sum_i \hat{h}(i) \rangle$ is

$$N \int\limits_{\mathbf{x}'_1 = \mathbf{x}_1} \hat{h}(1)\Psi(\mathbf{x}_1, \mathbf{x}_2, \ldots, \mathbf{x}_N)\Psi^*(\mathbf{x}'_1, \mathbf{x}_2, \ldots \mathbf{x}_{N-1}, \mathbf{x}_N) d\mathbf{x}_1 d\mathbf{x}_2 \ldots d\mathbf{x}_N \Big|_{\mathbf{x}'_1 = \mathbf{x}'_1}, \tag{2.39}$$

where $\mathbf{x}'_1 = \mathbf{x}_1$ is true after $\hat{h}(i)$ operates on functions of $\mathbf{x_1}$ only, but before completing the integration, in this way the variables that are primed are immune to the action of the operator. The right-hand side

contains the density function $\rho(\mathbf{x}_1;\mathbf{x}'_1)$ also known as reduced density matrix (RDM) as only the $\mathbf{x}_1$ coordinate is used,

$$\langle \sum_i \hat{h}(i) \rangle = \int\limits_{\mathbf{x}'=\mathbf{x}} \hat{h}(1)\rho(\mathbf{x}_1;\mathbf{x}'_1)\, d\mathbf{x}_1. \tag{2.40}$$

The expectation value of the two-electron operator can be expressed as a pair function π, [93],

$$\langle \sum_{i,j} \hat{g}(i,j) \rangle = \int\limits_{\substack{\mathbf{x}'_1=\mathbf{x}_1 \\ \mathbf{x}'_2=\mathbf{x}_2}} \hat{g}(1,2)\pi(\mathbf{x}_1,\mathbf{x}_2;\mathbf{x}'_1,\mathbf{x}'_2)\, d\mathbf{x}_1\ d\mathbf{x}_2. \tag{2.41}$$

Summing the expectation values for the operators $\hat{h}(i)$ and $\hat{g}(i)$ gives an expression for the energy of the many-electron system as a collection of terms with a classical interpretation for the distribution function of electrons or pairs of electrons aside from the quantum mechanical expectation value of kinetic energy.

$$\begin{aligned} E &= -\frac{1}{2} \int\limits_{\mathbf{x}'_1=\mathbf{x}_1} \bigtriangledown^2 \rho(\mathbf{x}_1;\mathbf{x}'_1)\, d\mathbf{x}_1 + \int\limits_{\mathbf{x}'_1=\mathbf{x}_1} \hat{V}\rho(\mathbf{x}_1;\mathbf{x}'_1)\, d\mathbf{x}_1 \\ &+ \frac{1}{2} \int\limits_{\substack{\mathbf{x}'_1=\mathbf{x}_1 \\ \mathbf{x}'_2=\mathbf{x}_2}} \hat{g}(1,2)\pi(\mathbf{x}_1,\mathbf{x}_2;\mathbf{x}'_1,\mathbf{x}'_2)\, d\mathbf{x}_1 d\mathbf{x}_2, \end{aligned} \tag{2.42}$$

because the energy involves only the one and two electron distributions directly, it is in principle possible to obtain useful molecular properties for any state of any system without detailed reference to the wavefunction.

2.6 Møller-Plesset Perturbation Theory

Up to now methods based on the variational principle have been discussed. In this section, a perturbation technique common to quantum chemistry calculations is discussed. The Møller-Plesset (MP) perturbation theory is a method of adding correlation energy to the Hartree-Fock equations by means of the Rayleigh-Schrödinger perturbation theory, usually calculated to second-order. A zeroth-order Hamiltonian is considered first,

$$\hat{H}_0|\Psi_i^{(0)}\rangle = E_i^{(0)}|\Psi_i^{(0)}\rangle, \tag{2.43}$$

where the superscript (0) indicates zeroth-order to the i'th state (subscript). The perturbation $\hat{V}$ is added giving a new perturbed Hamiltonian,

$$\hat{H} = \hat{H}_0 + \lambda\hat{V}, \tag{2.44}$$

where at $\lambda = 0$ the zeroth-order energy is obtained.

The exact eigenvectors, and eigenvalues of $\hat{H}$ are expanded in a Taylor series in λ,

$$\mathcal{E} = E_i^{(0)} + \lambda E_i^{(1)} + \lambda^2 E_i^{(2)} + \ldots \tag{2.45}$$

$$|\Psi_i\rangle = |\Psi_i^{(0)}\rangle + \lambda|\Psi_i^{(1)}\rangle + \lambda^2|\Psi_i^{(2)}\rangle + \ldots, \tag{2.46}$$

the $E_i^{(n)}$ is the n'th order energy to the i'th state. The energies are expressed in terms of the zeroth-order wavefunction $|\Psi_i^{(0)}\rangle$ to obtain the first (MP1) and second (MP2) order energy corrections. Solving order

by order in the expansion, [70], one obtains,

$$E_i^{(0)} = \langle \Psi_i^{(0)} | \hat{H}_0 | \Psi_i^{(0)} \rangle, \tag{2.47}$$

$$E_i^{(1)} = \langle \Psi_i^{(0)} | \hat{V} | \Psi_i^{(0)} \rangle, \tag{2.48}$$

$$E_i^{(2)} = \langle \Psi_i^{(0)} | \hat{V} | \Psi_i^{(1)} \rangle, \tag{2.49}$$

the zeroth-order energy is just the Hartree-Fock total energy if $|\Psi_i^{(0)}\rangle$ is expressed in HF orbitals and the first-order correction can be shown to be zero by Brillouin's theorem. Hence, the lowest contribution to the correlation energy is in the second-order MP correction (MP2).

The unperturbed Hamiltonian can be written as a sum of one-particle Hamiltonians

$$\hat{H}_0 = \sum_i \hat{h}_0(i) \tag{2.50}$$

and similarly, the perturbation as the difference between $\hat{H}_0$ and the exact Hamiltonian $\hat{H}$ is written as

$$\hat{V} = \hat{H} - \hat{H}_0. \tag{2.51}$$

Then the zeroth-order wavefunction is the HF wavefunction and zeroth-order energy is the sum of the HF spin orbital energies of occupied orbitals $\{\epsilon_i\}$. The convention used within this thesis is that i and j label occupied orbitals, a and b are virtual orbitals and p, q are general HF orbitals. Then, the second-order correction to ground state energy can

be written as

$$E_i^{(2)} = \frac{1}{4}\sum_{ijab}\frac{|\ \langle ij\ ||\ ab\rangle\ |^2}{\epsilon_i+\epsilon_j-\epsilon_a-\epsilon_b}, \tag{2.52}$$

and the second-order correlation energy correction to the HF energy is,

$$\begin{aligned} E_i &= E_i^{(0)} + E_i^{(2)} \\ &= \sum_i \epsilon_i + \frac{1}{4}\sum_{ijab}\frac{|\ \langle ij\ ||\ ab\rangle\ |^2}{\epsilon_i+\epsilon_j-\epsilon_a-\epsilon_b}, \end{aligned} \tag{2.53}$$

which typically contains 80-90% of the correlation energy [77]. The expressions for higher order energies may be derived, however they do not contribute significantly more to the correlation energy of many molecular systems and are computationally intensive to calculate. The MP2 method is one of the most commonly used post Hartree-Fock methods in quantum chemistry.

2.7 Electron-Electron Self-Energy and Green's Function

The Green's function is one of the most powerful and useful techniques in many-body theory. In Chapter 5, the Green's function calculated ionisation potential (IP) and electron affinity (EA) are used and compared to those obtained from an analytical model and electronic structure computational packages. The application of Green's function methods is a very wide field, the discussion in this thesis is limited only to the many-electron Green's function of the Hartree-Fock (HF) theory and the resulting self-energy.

It is known that the Hartree-Fock Green's function, $\mathbf{G}_0(E)$, has poles

at the eigenvalues of the Hamiltonian that approximate the energy differences between the N and $(N \pm 1)$-particle systems, *i.e.* at the orbital energies ϵ [70],

$$\mathbf{G}_0(E) = (E\mathbf{I} - \boldsymbol{\epsilon})^{-1}. \tag{2.54}$$

where $\boldsymbol{\epsilon}$ is a diagonal matrix of the HF orbital energies and $\mathbf{G}_0(E)$ has poles at values of E for which the inverse $(E\mathbf{I} - \boldsymbol{\epsilon})^{-1}$ does not exist.

If $|\Psi_0^N\rangle$ is the HF wavefunction for the N-particle system, $|\Psi_i^{N-1}\rangle$ is an approximate wave function for the $(N-1)$-electron system obtained by removing an electron from a filled level i, $|\Psi_a^{N+1}\rangle$ is an approximate $(N+1)$-particle wave function formed from adding an electron to a virtual state a, then the IP and EA are

$$-IP = \epsilon_i = \langle\Psi_0^N|H|\Psi_0^N\rangle - \langle\Psi_i^{N-1}|H|\Psi_i^{N-1}\rangle \tag{2.55}$$

$$-EA = \epsilon_a = \langle\Psi_a^{N+1}|H|\Psi_a^{N+1}\rangle - \langle\Psi_0^N|H|\Psi_0^N\rangle. \tag{2.56}$$

The above IPs and EAs do not allow for orbital relaxation because $|\Psi_a^{N+1}\rangle$ and $|\Psi_i^{N-1}\rangle$ are not the HF wave functions of the $(N+1)$ and $(N-1)$ particle systems respectively as they contain the spin orbitals of the N-particle system. The exact IP or EA can be obtained by including the relaxation energy of the $(N-1)$ system ($(N+1)$ for EA) and the difference in correlation energies between the N and $(N-1)$ (or $(N+1)$) systems [70].

The many-body Green's function, $\mathbf{G}(E)$ has poles at the exact energy differences between the N and $(N \pm 1)$-particle systems. It is reasonable

to view the Hartree-Fock Green's function as a single determinant approximation to the many-body Green's function. Obtaining approximations for $\mathbf{G}(E)$ beyond $\mathbf{G}_0(E)$ will lead to improvement in Koopmans[5] IPs and EAs while retaining the one-particle treatment associated with HF theory. To improve Koompans' IPs and EAs an effective energy dependent potential is introduced, called the electron-electron self-energy, making the Green's function an integral equation known as the Dyson equation [70]

$$\mathbf{G}(E) = \mathbf{G}_0(E) + \mathbf{G}_0(E)\mathbf{\Sigma}(E)\mathbf{G}(E), \tag{2.57}$$

where $\mathbf{\Sigma}(E)$ is the matrix representation of the exact self-energy in a HF basis. The Green's function can be corrected by expanding equation (2.57) in a perturbation expansion of self-energy

$$\mathbf{\Sigma}(E) = \mathbf{\Sigma}^{(2)}(E) + \mathbf{\Sigma}^{(3)}(E) + \dots. \tag{2.58}$$

In particular, the second-order correction is of interest, so the matrix elements for $\mathbf{\Sigma}^{(2)}(E)$ are [70]

$$\Sigma_{ij}^{(2)}(E) = \frac{1}{2}\sum_{ars}\frac{\langle rs||ia\rangle\langle ja||rs\rangle}{E+\epsilon_a-\epsilon_r-\epsilon_s} + \frac{1}{2}\sum_{abr}\frac{\langle ab||ir\rangle\langle jr||ab\rangle}{E+\epsilon_r-\epsilon_a-\epsilon_b}, \tag{2.59}$$

where $\langle rs||ia\rangle = \langle rs \mid ia\rangle - \langle rs \mid ai\rangle$. So if the exact self-energy is used, then the exact value of the many-body Green's function can be

[5] Koopmans' theorem states that if one considers an N-particle system with an added or subtracted electron, and assumes the MOs are identical for all systems, the the energy difference between the $N+1$ and N states corresponds to IP given by the eigenvalue of the HOMO orbital and that of $N+1$ and N states corresponds to EA given by the eigenvalue of the LUMO orbital.

obtained. However, there are approximations, such that at zero self-energy the many-body Green's function has the value of $\mathbf{G}_0(E)$. As such, the many-body Green's function provides a way to generalise the HF theory while retaining the single-particle picture by introducing an energy-dependent self-energy, and this approach is also at the heart of the *GW* approximation.

The Green's function can also be related to the previously discussed density matrix. It is achieved by integrating over a contour such as Coulson contour which encloses the pole residues giving density matrix elements rs

$$\rho_{rs} = \frac{\hbar}{2\pi i} \oint \mathbf{G}_{rs}(E)\, dE. \tag{2.60}$$

It is important to note that the second-order correction in self-energy is similar to the second-order energy obtained with many-body perturbation theory, equation (2.52) and can also be related to the RDM. This will be used again in Chapter 5 where the calculation of IPs and EAs using the Green's function formalism and electronic structure computational packages is discussed.

2.8 Conclusion

The fundamental concepts employed in electronic structure theory calculations with discussion specifically directed towards molecular tunnel junctions as used in this thesis were outlined. In the chapters that follow, there will be references to these treatments when describing the systems studied.

3. QUANTUM ELECTRON TRANSPORT

The core work of this thesis focuses on properties of open quantum systems, specifically in molecular electronics. This chapter introduces the concept of an open system and the implications of exposing a device to the environment. This is followed by discussing electrode self-energies which are complex entities used to account for semi-infinite leads. A non-equilibrium Green's function (NEGF) based transport method is discussed, particularly with reference to the Transport in mesoscopic systems (TiMeS) program used in this thesis. Finally, a method to account for semi-infinite leads using an *ab-initio* energy-independent complex absorbing potential (CAP) derived from electrode self-energies is described.

3.1 What is an Open System?

The discussion of open systems has been a popular topic in engineering and other disciplines [94]. Their description from *ab-initio* methods is challenging, as will be explained in the following. An open system can be understood as a system that exchanges information with its environment, for example in some chemical reactions, it is found that particles rearrange or destroy themselves and create stable atomic configurations,

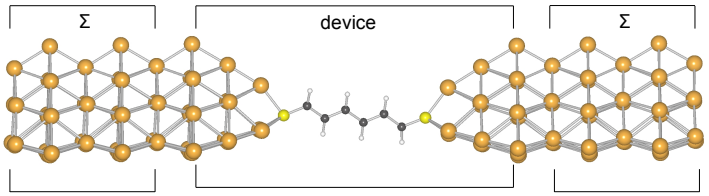

Fig. 3.1: Computational description of a junction: the device region is described by DFT, HF or CI Hamiltonian and the leads are incorporated via self-energies (Σ).

such as when a photon is absorbed, where there is an injection source and an absorbing drain for electrons, or where there is a decay of an excited level. In molecular electronics, an open quantum system is where a closed region is coupled to semi-infinite leads and is driven from equilibrium. To achieve this, a molecule is bonded to at least two reservoirs with which it can exchange electrons so that non-equilibrium states can be created and maintained. In a typical experimental set-up, the junction consists of an organic molecule bonded between two metallic probes. These probes can be a surface and a STM tip or two surfaces, *etc.* In real world applications, this component could be integrated into a circuit in a variety of ways making it a switching or memory device.

A typical molecular junction is illustrated in Figure 3.1. In molecular electronics, the device region is generally described using DFT and NEGF methods, though sophisticated many-body formalisms are more accurate and is the route taken in this work. The metal electrodes are treated within a single particle approximation using complex energy-dependent self-energies $\mathbf{\Sigma}$. The transmission is calculated on a finite device (or

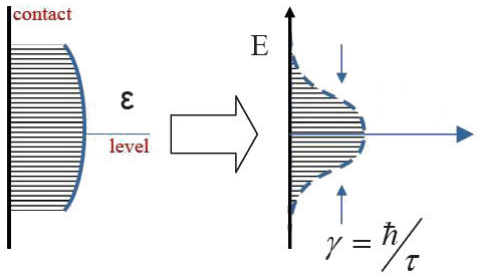

Fig. 3.2: Level broadening of a molecular energy level ϵ when coupling to a metallic contact resulting in a broadened state of width γ which is related to the life-time of the new state τ. Figure from ref. [96]

EM) region which incorporates fractions of both the right and left leads, providing the boundary conditions on the surfaces of the leads. These boundary conditions are found using Green's function methods with self-energies.

An isolated molecule has sharp infinite lifetime energy levels, while the metallic lead is better described by a continuum of states, *i.e.* a density of states. Upon coupling to the continuum, the discrete quantum energy levels broaden with a lifetime τ and shift, as illustrated in Figure 3.2. The open system energy and wavefunction become complex-valued properties on the device region [95]. Such a decaying state is an example of a resonance, *i.e.* a broadened energy level with a finite lifetime,

$$\omega_i = \epsilon - i\gamma/2 \tag{3.1}$$

where ω_i is known as the Siegert energy [97], ϵ is the resonance position and γ the decay associated with the irreversible transition from the discrete state to the continuum. The decay lifetime of the resonance can be

obtained from its line width as

$$\tau = \hbar/\gamma. \tag{3.2}$$

While studying resonances can provide valuable information on the state of the system such as transport properties, decay lifetimes and strength of coupling to electrodes, calculating their properties is not trivial. A decaying wavefunction (Siegert state) is not square-integrable, *i.e.* the wavefunction is non-normalisable, so a Gaussian basis set expansion cannot be used to describe them [98]. That is, with conventional basis-set-dependant methods it is not feasible to describe both bound and continuum states simultaneously because a decaying state diverges at large distances. A complete *ab-initio* description of such systems is, therefore, generally difficult. Partitioning methods which divide the space into closed and open environments are one of ways to overcome the issue and are described in ref. [95]. Another way of achieving this is by using a CAP [99, 100], which is discussed in Section 3.3.

3.2 Electron Transport Through Mesoscopic Systems

A general transport problem comprises of two bulk electrodes and a device as illustrated in Figure 3.1. The two leads are described using two chemical potentials, μ_L for the left (L) lead and μ_R for the right (R) lead which control electron exchange with the device. When there is no applied bias, $\mu_L = \mu_R$, the junction is in thermodynamic equilibrium and there is no current flow.

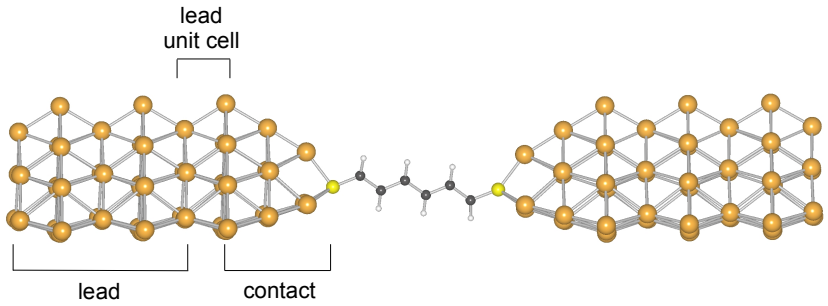

Fig. 3.3: The terminology used when talking about the lead structures.

From an electronic structure viewpoint, the system is seen to have an infinite size Hamiltonian, **H**, which is not easily treated. A solution is to assume that the lead structures are perfectly crystalline and have a regular periodic structure with a unit cell repeating in the direction of transport, allowing them to be readily described using self-energies. The problem is formulated in matrix notation.

3.2.1 Lead-Device Hamiltonian Structure

We begin the discussion of lead and device Hamiltonians by defining the terminology used. A typical junction is shown in Figure 3.3. A lead defines a large semi-infinite structure that is locally in equilibrium, it can be periodic and described using unit cells. A unit cell of a lead is defined as the smallest repeated unit that repeats in the direction of transport. A contact is the part of the lead that is bonded to the linker molecule of the device. A principal layer (PL) is composed of unit cells and chosen such that only the nearest PLs interact, that is, PL 1 and 3 have negligible interaction, *i.e.* all interaction matrix elements between

non-neighbouring PLs are zero or very close to it. For example, consider a tight-binding system of a chain of N atoms in the device region. Then, one atom forms a PL. Similarly, in a system of N atoms with N_i basis functions per atom in each PL, the Hamiltonian matrix representing this PL is of dimension,

$$N = \sum_{i}^{N_{atoms}} N^{i}_{atoms} \times N^{i}_{orbitals}, \tag{3.3}$$

the total number of basis functions per region of interest, the size of the Hamiltonian matrix is $N \times N$. This can be applied to any Hamiltonian to determine its dimension. The entire system is described by the Hamiltonian $\mathbf{H}$ given by,

$$\mathbf{H} = \begin{pmatrix} . & . & . & . & . & . & . & . & . & . & . \\ . & . & 0 & \mathbf{H}_1^{\dagger} & \mathbf{H}_0 & \mathbf{H}_{LD} & 0 & . & . & . & . \\ . & . & . & 0 & \mathbf{H}_{DL} & \mathbf{H}_D & \mathbf{H}_{DR} & 0 & . & . & . \\ . & . & . & . & 0 & \mathbf{H}_{RD} & \mathbf{H}_0 & \mathbf{H}_1 & 0 & . & . \\ . & . & . & . & . & 0 & \mathbf{H}_1^{\dagger} & \mathbf{H}_0 & \mathbf{H}_1 & 0 & . \\ . & . & . & . & . & . & . & . & . & . & . \end{pmatrix}, \tag{3.4}$$

where the matrix $\mathbf{H}_0$ is the Hamiltonian for the unit cells of the left (L) and right (R) leads (which are described here for symmetrical electrodes but a simple generalisation allows them to be different). The interactions between two unit cells is described by a matrix $\mathbf{H}_1$ of the size $N \times N$. The matrices $\mathbf{H}_{DL} = \mathbf{H}_{LD}^{\dagger}$ and $\mathbf{H}_{DR} = \mathbf{H}_{RD}^{\dagger}$ are of the size $N \times M$ and are the interaction matrices between the EM region and the leads. These

can be rectangular matrices, hence the dimension $N \times M$. These matrices are incorporated into the EM matrix and are used for determining the surface Green's function $\mathbf{g}$ and self-energy $\mathbf{\Sigma}$, hence the need to include lead components into the device region description. The surface Green's function contains all the information about the electronic structure of the device-lead interface at equilibrium.

3.2.2 Electrode Self-Energies

In the present context, the self-energies are used to describe the effect of a semi-infinite lead. The elements of the self-energy matrix $\mathbf{\Sigma}$ contain information about the chemical coupling of the individual PL orbitals with the device. It is important that at this point one differentiates between the electron-electron self-energy discussed in Section 2.7 and the lead-device interaction. The electron-electron self-energy can be thought of as a correlation energy correction to a HF operator, whereas presently the discussion is of the treatment of the interaction of an electron with the environment of the leads within a single electron approximation.

The derivation of the Green's function and self-energy is explained in ref. [3]. Here, the results are summarised and their relevance to subsequent work presented in this thesis is highlighted.

Let the device interact with one lead, for simplicity,

$$\begin{bmatrix} \mathbf{H}_D & \mathbf{H}_{DR} \\ \mathbf{H}_{RD}^{\dagger} & \mathbf{H}_R \end{bmatrix}, \tag{3.5}$$

where $\mathbf{H}_R$ is a large matrix compared to $\mathbf{H}_D$ and represents the leads. The overall Green's function can be partitioned to,

$$\begin{bmatrix} \mathbf{G}_D & \mathbf{G}_{DR} \\ \mathbf{G}_{RD} & \mathbf{G}_R \end{bmatrix} = \begin{bmatrix} (E+i0^+)\mathbf{I}-\mathbf{H}_D & -\tau \\ -\tau^\dagger & (E+i0^+)\mathbf{I}-\mathbf{H}_R \end{bmatrix}^{-1}. \quad (3.6)$$

We solve for the device Green's function $\mathbf{G}_D$,

$$\begin{bmatrix} \mathbf{G}_D & \mathbf{G}_{DR} \\ \mathbf{G}_{RD} & \mathbf{G}_R \end{bmatrix} \begin{bmatrix} (E+i0^+)\mathbf{I}-\mathbf{H}_D & -\tau \\ -\tau^\dagger & (E+i0^+)\mathbf{I}-\mathbf{H}_R \end{bmatrix} = \mathbf{I}. \quad (3.7)$$

$\mathbf{G}_D$ is sought as the aim is to include the infinite leads and to describe their effect on the device region while reducing the dimensions of the problem to be solved numerically. Then,

$$[(E+i0^+)\mathbf{I}-\mathbf{H}_D]\mathbf{G}_D - \tau^\dagger \mathbf{G}_{DR} = \mathbf{1} \quad (3.8)$$

$$-\tau \mathbf{G}_D + \mathbf{G}_{DR}[(E+i0^+)\mathbf{I}-\mathbf{H}_R] = 0. \quad (3.9)$$

Re-arranging for $\mathbf{G}_D$,

$$\mathbf{G}_{DR} = \tau \mathbf{G}_D [(E+i0^+)\mathbf{I}-\mathbf{H}_R]^{-1}, \quad (3.10)$$

$$\left[(E+i0^+)\mathbf{I}-\mathbf{H}_D\right]\mathbf{G}_D - \mathbf{1} = \tau^\dagger \mathbf{G}_{DR}, \quad (3.11)$$

$$= \tau^\dagger \tau \mathbf{G}[(E+i0^+)\mathbf{I}-\mathbf{H}_R]^{-1} \quad (3.12)$$

$$\Rightarrow \mathbf{G}_D = [(E+i0^+)\mathbf{I}-\mathbf{H}_D - \tau^\dagger \tau [(E+i0^+)\mathbf{I}-\mathbf{H}_R]^{-1}]. \quad (3.13)$$

Alternatively, one can write,

$$\mathbf{G}_D = [(E + i0^+)\mathbf{I} - \mathbf{H}_D - \mathbf{\Sigma}]^{-1} \equiv [E\mathbf{I} - \mathbf{H}_D - \mathbf{\Sigma}]^{-1}, \tag{3.14}$$

where the self-energy $\mathbf{\Sigma}$ is given by

$$\mathbf{\Sigma} = \tau \mathbf{g}_R \tau^\dagger \quad \mathbf{g}_R = [(E + i0^+)\mathbf{I} - \mathbf{H}_R]^{-1}, \tag{3.15}$$

and $\mathbf{g}_R$ is a surface Green's function. From this, it is noted that self-energy is energy dependent. It accounts for the periodic boundary conditions often used in the construction of the lead regions and for the interaction of the lead with the device region [101].

3.2.3 TiMeS Mesoscopic Electron Transport

TiMeS is a software package used to calculate electron transmission through tunnel junctions by using NEGF and scattering matrix methods [101–103]. The input consists of Hamiltonians expressed in a localised basis resulting in that no specific geometry data is read into the program. The electrodes Hamiltonian as described in Section 3.2.1 is approximated by a continuum of free or quasi-free states incorporated into the calculation *via* the self-energy correction as discussed in Section 3.2.2.

The transmission function can be calculated from the knowledge of the molecular energy levels and the nature and the geometry of the contacts. One can see this by expressing the Green's function matrix of the full problem $\mathbf{G}^{-1} = \mathbf{G}_D^{-1} + \mathbf{\Sigma}_L + \mathbf{\Sigma}_R$, in terms of the bare device Green

function $\mathbf{G}_D$ and the self-energy correction $\mathbf{\Sigma}_{L,R}$ due to the presence of the leads.

The TiMeS approach is based on three steps: incorporating the leads *via* the surface Green's function self-energy, constructing the coupling matrix between the surface of the two leads and the scattering region, $\mathbf{G}_D$, then the scattering matrix is extracted from $\mathbf{G}$ [102].

The potential drop occurs only over the EM region and there is no change to the electronic structure of the lead reservoirs as they are assumed to be in local thermodynamic equilibrium. The leads are not affected by either the voltage drop or coupling to the device due to their large structure and electrostatic screening. Therefore, one only needs to concentrate on the device region and the electrodes are treated by $\mathbf{\Sigma}_L$ and $\mathbf{\Sigma}_R$. We calculate the retarded self-energies, $\mathbf{\Sigma}^r_{L,R}$, from the retarded surface Green's function, $\mathbf{g}^r_{L,R}$, on the PL directly attached to the device and is used in the evaluation of the lead self-energies.

$$\begin{aligned} \mathbf{\Sigma}^r_L(E) &= \left[(E+i0^+)\mathbf{S}_{DL} - \mathbf{H}_{DL}\right] \mathbf{g}^r_L(E) \\ &\times \left[(E+i0^+)\mathbf{S}_{LD} - \mathbf{H}_{LD}\right] \qquad (3.16) \\ \mathbf{\Sigma}^r_R(E) &= \left[(E+i0^+)\mathbf{S}_{DR} - \mathbf{H}_{DR}\right] \mathbf{g}^r_R(E) \\ &\times \left[(E+i0^+)\mathbf{S}_{RD} - \mathbf{H}_{RD}\right]. \qquad (3.17) \end{aligned}$$

Since self-energy is energy dependent, the Green's function is evaluated iteratively. The device retarded Green's function can the be calculated as,

$$\mathbf{g}^r_D = \left[(E+i0^+)\mathbf{S}_D - \mathbf{H}_D - \mathbf{\Sigma}^r_L(E) - \mathbf{\Sigma}^r_R(E)\right]^{-1}. \qquad (3.18)$$

The scattering wavefunction can be obtained by constructing the eigenstates from $\mathbf{g}_D^r$ and a scattering matrix containing transmission coefficients as derived in ref. [102]. TiMeS is used to calculate quasiparticle energies and electron transport in Chapters 4 and 5. A modified version of TiMeS is used to extract self-energies when constructing a CAP introduced in the next section.

3.3 Complex Absorbing Potentials

3.3.1 Introduction

It has been mentioned in this thesis that, the electronic interaction of a molecule making contact with electrodes is determined by the coupling of discrete molecular states to the continuum electrode density of states. This interaction can be described exactly using the energy-dependent self-energy. While widely accepted, this concept is difficult to implement in the correlated many-body framework as there is no immediate corresponding quantities to single-electron self-energies within CI formalisms. That is, relating the electron reservoirs to the device region becomes non-trivial. Essentially, a method is needed to describe electrode-device interaction independently of single particle energies.

If one considers $\mathbf{H}$, the matrix representation of the many-electron Hamiltonian in a CSF basis, $\mathbf{S}$ is the overlap matrix (metric) for the CSF basis, E is the many-electron energy and $\vec{c}$ is the vector of the

expansion coefficients or "CI vector",

$$\mathbf{H}\vec{c} = \mathbf{S}\vec{c}E. \tag{3.19}$$

The matrix elements of **H** and **S** are constructed from one- and two-electron integrals defined in the single particle basis used to construct the CSFs. However, in this treatment of the many-electron problem no reference is made to single particle or quasiparticle energies. Hence the inclusion of continuum states (electrodes) *via* an energy-dependent self-energy is not evident.

There are two ways to transmit the information contained within self-energies which is to use either the formally exact smooth exterior scaling (SES) or an energy-independent CAP. The SES method [104], which despite being exact is cumbersome to implement for our intended use with configuration interaction. The idea of SES is to rotate the wavefunction into the complex plane making it square-integrable. SES involves construction and knowledge of an analytic continuation of the scattering potential, which maybe difficult to obtain or may not exist. The idea of the CAP is to introduce an absorbing boundary condition in the exterior region of the molecular scattering target, *i.e.* outside the device region which absorbs outgoing wavefunctions. It was first introduced by Kosloff and Kosloff [105] in time-dependent wavepacket propagation. Since then, CAPs have been used to include leads into a many-particle formalism using self-energies [4, 90]; and the converse, Driscoll *et al* [106] used CAPs as a more efficient way to derive self-

energies.

The CAP concept is a more suitable solution for use with CI. Just like SES, it makes all wave-functions square-integrable and likewise has been extensively studied [95, 99, 100, 107, 108].

3.3.2 CAP Methodology

A previously published method for an *ab-initio* CAP generation was developed for a tight-binding chain model[1] [4]. The goal of the following section is to generalise this approach and make it more applicable towards realistic systems. While the detail of the CAP construction is outlined in ref. [4], here the essential points are covered and the modifications carried out to apply the method to more general electronic structure treatments are developed. A closed system Hermitian Hamiltonian defined by $\mathbf{H}_D$ and bound states $|\chi_i\rangle$ with sharp energies ϵ_i is considered

$$\mathbf{H}_D \mid \chi_i\rangle = \epsilon_i \mid \chi_i\rangle, \tag{3.20}$$

$$\langle\chi_j \mid \mathbf{H}_D = \epsilon_j\langle\chi_j \mid, \tag{3.21}$$

$$\langle\chi_j \mid \chi_i\rangle = \delta_{ij}. \tag{3.22}$$

Let the two electrodes be described by known left $\mathbf{\Sigma}_L(\omega)$ and right $\mathbf{\Sigma}_R(\omega)$ self-energies for a complex eigenvalue ω. For a tight-binding model these can be evaluated analytically *via* a Green's function approach. To deter-

[1] A tight-binding model can be thought of as electrons being under such a large potential that they spend most of their time bound to ionic cores, *i.e.* the opposite to a free electron model. As a result, interaction of an electron in an atomic orbital within the tight-binding approach is very limited.

mine the self-energies for more realistic systems, a modified version of the TiMeS program [101] is used. These self-energies are evaluated on the lead PL region of the system and are added to to the device Hamiltonian $\mathbf{H}_D$ accordingly to yield the complex eigenvalue problem

$$[\mathbf{H}_D + \lambda\mathbf{\Sigma}_L(\omega_i^\lambda) + \lambda\mathbf{\Sigma}_R(\omega_i^\lambda)]|U_i^\lambda\rangle = \omega_i^\lambda|U_i^\lambda\rangle, \tag{3.23}$$

$$\langle V_i^\lambda|[\mathbf{H}_D + \lambda\mathbf{\Sigma}_L(\omega_i^\lambda) + \lambda\mathbf{\Sigma}_R(\omega_i^\lambda)] = \langle V_i^\lambda|\omega_i^\lambda, \tag{3.24}$$

where the parameter λ is introduced to allow for an adiabatic coupling between the electrode states and the extended device region "molecular states". At $\lambda = 0$, the states on the extended device region are obtained as described by eigenvectors $|\chi_i\rangle$, that may be chosen real, and real eigenvalues ϵ_i. As λ is increased, the device region and the electrode single particle states begin to couple until at $\lambda = 1$ the Siegert resonances ω_i [97], right eigenvectors $|U_i\rangle$, and left eigenvectors $\langle V_i|$ are obtained describing the open system. The introduction of the adiabatic coupling of the self-energies permits to "label" the molecular states and to follow their evolution as the system is opened. This holds if the evolution of the eigenvalues follow a smooth trajectory[2]. This will be discussed in Appendix A, that the adiabatic hypothesis does not always hold. The adiabatic coupling allows the calculation of an *ab-initio* CAP by selecting those eigenvalues that correspond to the uncoupled device region states. At $\lambda = 1$, the real part of ω_i gives the energy of the i'th resonance including the shift from the original eigenvalue with the imaginary part

[2] A trajectory of the real part of the eigenvalue describes the evolution of the real eigenvalue as it shifts when the system is opened with increasing λ.

giving the broadening.

The goal is to build an energy-independent complex potential $\mathbf{W} = \mathbf{W}_L + \mathbf{W}_R$ from the corresponding right and left self-energies, such that the Hamiltonian $\mathbf{H}_D + \mathbf{W}$ has the eigenvalues equivalent to using the explicit self-energies. Such a Hamiltonian is not readily constructed for each ω_i, as a Hamiltonian $\mathbf{H}_D + \mathbf{\Sigma}_L(\omega_i) + \mathbf{\Sigma}_R(\omega_i)$ with its own set of complex eigenvalues is used. The set of non-Hermitian operators that are of interest, do not have biorthogonal vectors obeying the traditional definition of the inner product, equation (3.22), that is $\langle V_i|U_j\rangle \neq \delta_{ij}$. The current and previous version of CAPs construction consider formalisms that yield eigenvalues which approximate ω_i and eigenvectors that approximate $\langle V_i|$ and $|U_i\rangle$ while satisfying biorthogonality. Given such a set of approximate eigenvectors, the CAP is written as

$$\mathbf{W} = \sum_i |U_i'\rangle\omega_i\langle V_i'| - \mathbf{H}_D, \tag{3.25}$$

which for biorthogonal $|U_i'\rangle$ and $\langle V_i'|$ will give by construction an operator $\mathbf{H}_D + \mathbf{W}$ with correct eigenvalues and approximate eigenvectors.

In practice, the problem is formulated in a real basis of the device region, so the CAP is built accordingly by using

$$\mathbf{W} = \mathbf{S}_0\mathbf{X}\boldsymbol{\omega}\mathbf{X}^\dagger - \mathbf{H}_D, \tag{3.26}$$

where $\mathbf{S}_0$ is the overlap for the atomic basis used to describe the system, $\mathbf{X}$ is the matrix of the eigenvectors of the Hamiltonian $\mathbf{H}_D$, and $\boldsymbol{\omega}$ is the

diagonal matrix of the eigenvalues ω_i calculated at $\lambda = 1$. Since the self-energy is a property of the electrode only for properly defined electrodes and device regions, the CAPs are generated on a single PL of the lead, and then transformed to the molecular orbital basis of the device region, which contains a lead PL on either side.

3.4 Conclusion

In this chapter, the concept of open systems and electron transport through them has been introduced. A method to generate a CAP for a tight-binding model has been generalised further to be applied to chain systems described by HF or DFT Hamiltonians, or for systems where the energy level spacing is such that there is no curve crossings, *i.e.* eigenvalue trajectories are smooth, as the system is opened. While previously the self-energy was analytically evaluated, it is now obtained from the electron transport code TiMeS and is evaluated on the lead area only. Inclusion of the overlap matrix enables the use of non-orthogonal orbitals as required for application in quantum chemistry.

This prescription for constructing a CAP is applied to a model system consisting of an extended molecule model using atomic chains for the electrodes and molecular regions as described in Chapter 4 to study the effect of correlations and excitation on energy level alignments. In addition, this new methodology is applied to a BDA junction using two gold chain electrodes to study the effect of opening the system on junction electronegativity while explicitly treating electron correlations. A

proposition to generalise the method further to 3D systems such as metal clusters as electrode models is discussed in Appendix A and several observations are made there.

4. QUASIPARTICLE ENERGIES AND LIFETIMES IN A MOLECULAR TUNNEL JUNCTION

In this chapter, the methods of CAPs and MCCI are applied to study the effect of metal electrodes on electronegativity and quasiparticle spectrum of two molecular junctions [90].

4.1 Introduction

In Chapter 1 the importance of band alignment for accurate predictions of electron transport was highlighted. Now the shift of the molecular HOMO and LUMO levels as electrodes are introduced is discussed. In addition, the junction IP and EA energies and how they change as the system is opened are also studied. The MCCI and CAPs methods are used to obtain quasiparticle excitation spectra of a molecular junction. A quasiparticle can be defined as a "low-energy excitation that acts like weakly interacting electrons" [79], or just as an electron surrounded by its polarisation cloud treated together. Using quasiparticles is a useful way to describe strongly interacting systems in terms of weakly interacting quasiparticles. An accurate quasiparticle spectrum can describe processes such as electron addition and removal, *i.e.* EA and IP energies.

Atomic gold chains as model electrodes for a molecular junction are used. Experimentally, atomic chains can be fabricated by single atom deposition onto a surface [109], using a STM tip [110] or by the MCBJ technique. Atomic nanowires are of fundamental interest as they exhibit known properties, such as quantised conduction. Technologically, they could potentially play the role of interconnects as minimisation to molecular level occurs. One of the first theoretical studies of atomic chains is by Lang [111] where the electrodes were treated as jellium (*i.e.* constant electron density) and were treated within the DFT/LDA formalism.

Since then, improvements in quantum transport calculations have been made through combining DFT with NEGF [2] and recently an increased interest in the *GW* approximation for molecular electronics has been seen. The NEGF/DFT formalism implies single determinant or quasiparticle treatment due to the use of KS orbitals. In *GW* the electron self-energy is approximated using a perturbation expansion with respect to quasiparticle interactions, it is expressed as a product of the single-particle Green's function G and the screened interaction W. Like DFT-NEGF, DFT-*GW* also implies a quasiparticle description. Alternatively to DFT methods, one can use CI and calculate transport through correlated scattering [66].

The impact of lead excitations as they couple to the molecular region is also explicitly considered, as these have been shown to play an important role in electron transport [112]. In the work of Galperin *et al* an interacting two level analytical model was used, where free electron reservoirs were described by the NEGF formalism. The energy transfer

interaction that occurs during excitation/de-excitation of the molecule (device) accompanied by electron-hole pair annihilation/creation in the metal leads. The authors find that such energy transfer can have a significant effect on electron current, hence suggesting that lead excitations play an important role in electron transport and in general cannot be disregarded [112].

A tunnel junction consisting of a gold chain and BDA is also considered in this chapter. The effect of adding metallic character to a molecule is known to modify its electronic structure and result in molecule-metal states hybridisation, which influences band alignment. Recently, BDA in gaseous phase was studied using the *GW* approach and the spectra was compared to experimental results [62, 113]. A significant improvement on DFT results was reported. However, the *GW* approach being a perturbation approach cannot deal with multi-determinant states as has been demonstrated by Pavlyukh and Hübner using a multi-reference ground state of the C_2 molecule [114].

4.2 Method

4.2.1 Model Set-Up

The atomic chain model studied is built from three atomic gold chains with inter-atomic spacing of 0.28 nm based on atomic gold chains on nickel surfaces studied experimentally in ref. [109]. The central device region is formed by 20 atoms with each explicit lead region being symmetric and consisting of 24 atoms. The width of the gap between the

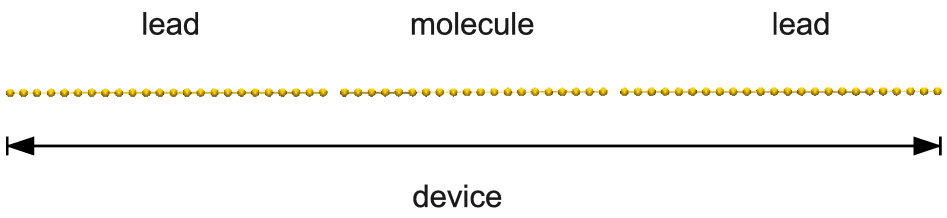

Fig. 4.1: Extended device region studied which incorporates a 12 atom portion of the leads on either side of the 20 atom molecule. The left and right leads are described by a CAP derived from self-energy.

leads and the device controls the strength of the molecule-electrode coupling; varying the spacing allows for different couplings to be studied, Figure 4.1.

The gold atoms are described by a single 6s electron and a 68-electron effective core potential [115] yielding a single half-filled one-dimensional band. The Fock and overlap matrices in the Hartree-Fock (HF) approximation are calculated using the Turbomole [116] programme package. These matrices are used to calculate electron transmission in the absence of electron correlations with the Green's function based approach implemented within TiMeS [101]. The one- and two-electron integrals from the HF calculations are generated using a modified version of Turbomole and then used to construct the Hamiltonian matrix elements used as input for MCCI.

Benzene-di-amine junction model

The three BDA-based systems are described within DFT with the PBE Generalized Gradient Approach (GGA) exchange correlation functional

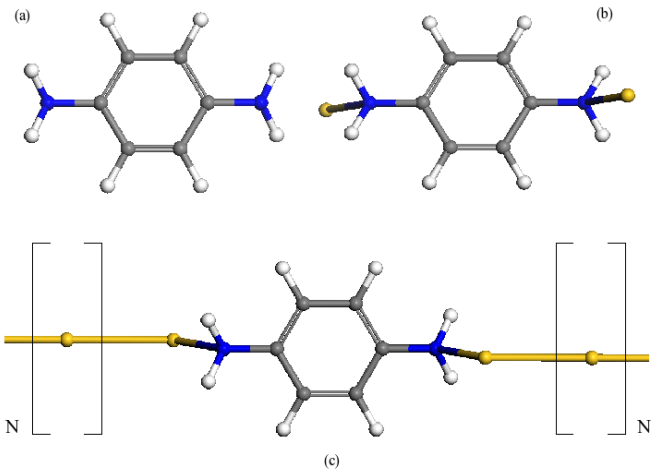

Fig. 4.2: The three systems studied are (a) BDA, (b) Au-BDA-Au and (c) chain-BDA-chain, where $N = 12$ indicates the twelve atom gold chain electrodes. The atom colour scheme is: Au is yellow, Nitrogen is blue, Carbon is grey and Hydrogen is white.

[117]. The nitrogen and carbon atoms are treated with a triple-ζ polarised basis sets, while split-valence basis are used to describe hydrogen atoms. A single BDA molecule is relaxed and forms the building block for the other junctions. Two gold contact atoms described by 8 electrons with a split valence polarised basis and a corresponding 60 electron core potential [116] are bonded to BDA and relaxed, this junction is referred to as Au-BDA-Au. The chain-BDA-chain junction is formed by attaching the 12 atom gold chain electrodes with 0.28 nm inter-atomic spacing to both contact atoms to form right and left electrodes. The three systems are illustrated in Figure 4.2. The many-particle basis for MCCI were prepared using a modified version of Turbomole. For the Au-BDA-Au model, the energy range for the KS orbitals to be included as excitations for the CI calculation was 5.45 eV above HOMO and 4.12

eV for chain-BDA-chain junction, while a larger range of 6.40 eV above the HOMO was used for BDA. The MCCI calculations were carried out with a coefficient threshold (c_{min}) of 8×10^{-4}.

4.2.2 Complex Absorbing Potentials

The CAP is constructed following the method outlined in Chapter 3. The device region is given by an explicit model that includes the molecule as well as a region that defines the bonding of the molecular region to the electrodes, recall, that this is referred to as the extended molecule (EM) or "device". The portion of the electrodes not explicitly included into the EM is then described by single-electron self-energies which are used to construct the energy independent CAP.

The adiabatic hypothesis is followed when building the CAP with bare Hamiltonian eigenvalues ϵ_i at $\lambda = 0$ perturbed towards the complex broadened resonances ω_i at $\lambda = 1$. The real part of ω_i includes the shift from the original position of ϵ_i as illustrated in Figure 4.3a. The imaginary component can be related to the lifetime of the new state, as the system is opened and is shown in Figure 4.3b. It is noted that both the real and imaginary eigenvalue trajectories follow smooth curves. While there are crossing points in the imaginary plane, because the trajectories are smooth, the adiabatic hypothesis holds. The CAP is constructed within the real basis of the extended device region as described in Section 3.3.1.

Two CAPs are constructed: one in real HF basis to be used with the chain model and one in DFT basis to be used with chain-BDA-chain,

thus demonstrating the applicability of the approach within different single particle approximations for molecular tunnel junctions.

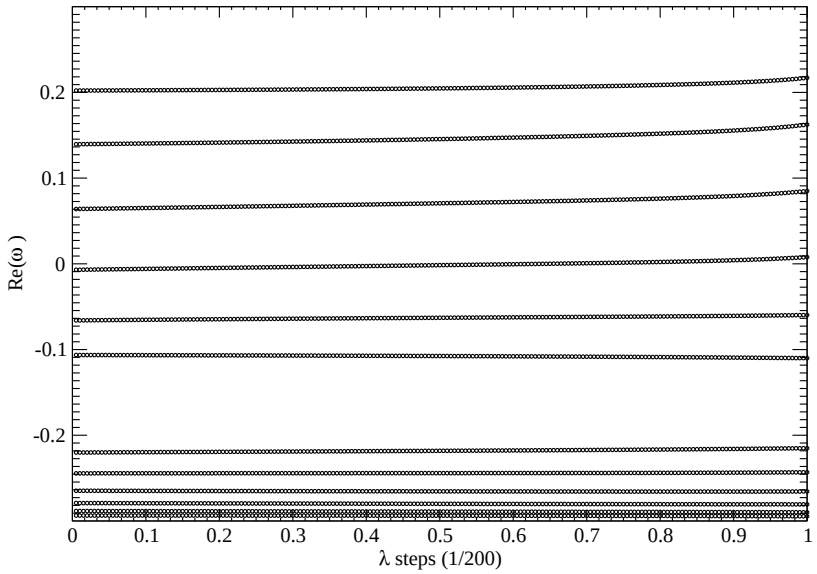

(a) The trajectories of the real component of ω_i depicting the shift in the eigenvalue from it's original state at $\lambda = 0$ towards the broad resonance at $\lambda = 1$

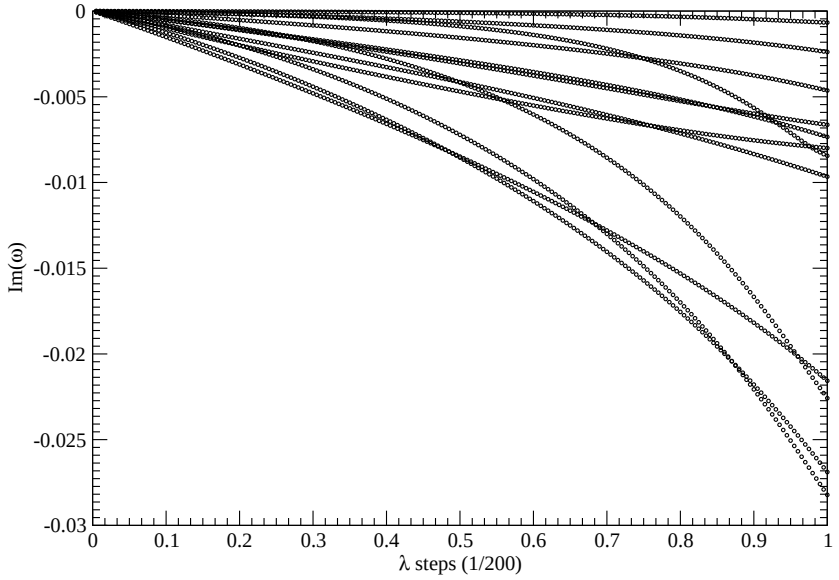

(b) The extent of state broadening as the system is being opened at the final broadened state and life-time achieved at $\lambda = 1$ by following the imaginary component ω_i.

Fig. 4.3: Adiabatic generation of complex resonances for the gold chain model with HF formalism. Note that opening the system in the weak coupling limit does not cause a large shift in the resonance positions, whereas the imaginary part of the eigenvalue introduces broadening. Energies are expressed in Hartrees.

4.2.3 Verification of the CAP

To verify the CAP constructed using the method described in Chapter 3, the energy level shifts and broadening are calculated and compared against those obtained directly using self-energies within the TiMeS program. This is done using the chain model described in the HF basis.

The TiMeS approach uses explicit self-energies to describe the electrodes and calculates the Green's function which is then implemented within the scattering matrix formalism to generate the electron transmission, as was discussed in Section 3.2.3. The resulting HF quasiparticle spectrum gives energy shifts and broadenings which serve as the reference point for the subsequent calculations, both when replacing self-energy using CAPs and when correlations are introduced.

The transport calculation is then repeated but using the CAP in place of self-energy in the definition of the Green's function $\mathbf{G}$ and spectral densities $\mathbf{\Lambda}_{L,R}$ leading to the following:

$$\mathbf{W} = \mathbf{W}_L + \mathbf{W}_R, \tag{4.1}$$

$$\mathbf{G}^{-1} = [E\mathbf{S} - (\mathbf{H}_D + \mathbf{W})], \tag{4.2}$$

$$\mathbf{\Lambda}_{L,R} = i\left(\mathbf{W}_{L,R} - \mathbf{W}_{L,R}^{\dagger}\right). \tag{4.3}$$

The transmission is then calculated as,

$$T = Tr\left[\mathbf{\Lambda}_L \mathbf{G} \mathbf{\Lambda}_R \mathbf{G}^{\dagger}\right], \tag{4.4}$$

where the CAP plays the role of the self-energy for incorporating the

leads. The resulting comparison obtained is shown in Figure 4.4. The good agreement between the CAP and self-energy based transmission is clearly seen especially in the energy gap of interest around the HOMO-LUMO molecular levels.

It is useful to examine if transmission can be approximated as Lorentzian peaks. If so, then the quasiparticle energies that will be calculated as the difference between many-electron energy states at a later stage can be used to generate Lorentzian transmission resonances. This will provide a way to compare the complex quasiparticle states to the Green's function transmissions. To establish whether this comparison can be made, the complex eigenvalues ω_i obtained from the CAP using equations (3.23) and (3.24) with $\lambda = 1$ and with the CAP replacing $\Sigma_L(\omega_i)$ and $\Sigma_R(\omega_i)$ are used,

$$f(\epsilon;\omega_i) = \frac{(\gamma/2)^2}{(\epsilon - Re(\omega_i))^2 + (\gamma/2)^2}, \tag{4.5}$$

where $\gamma = 2Im(\omega_i)$ is the width of the Lorentzian peak and is inversely proportional to the lifetime of the quasiparticle state. In Figure 4.5, the Lorentzian resonances are compared to the ones calculated using explicit self-energies from the Green's function for the chain model with weak molecule-lead coupling of 0.45 nm lead-device separation.

The Green's function resonances (shown in black) derived from a complex-valued HF problem can be thought of as Koopmans' resonances, and will be referred to as such in this chapter. The Lorentzian resonances derived from $\mathbf{H}_D + \mathbf{W}$ (shown in red) display a very good agreement with the Koopmans peaks, both in terms of the resonance peak position and

broadening. The inset of Figure 4.5 illustrates in detail the region around the HF HOMO showing that the resonances from the Green's function transmission and those derived from the CAPs agree to an accuracy that is more than sufficient for the subsequent application in this work.

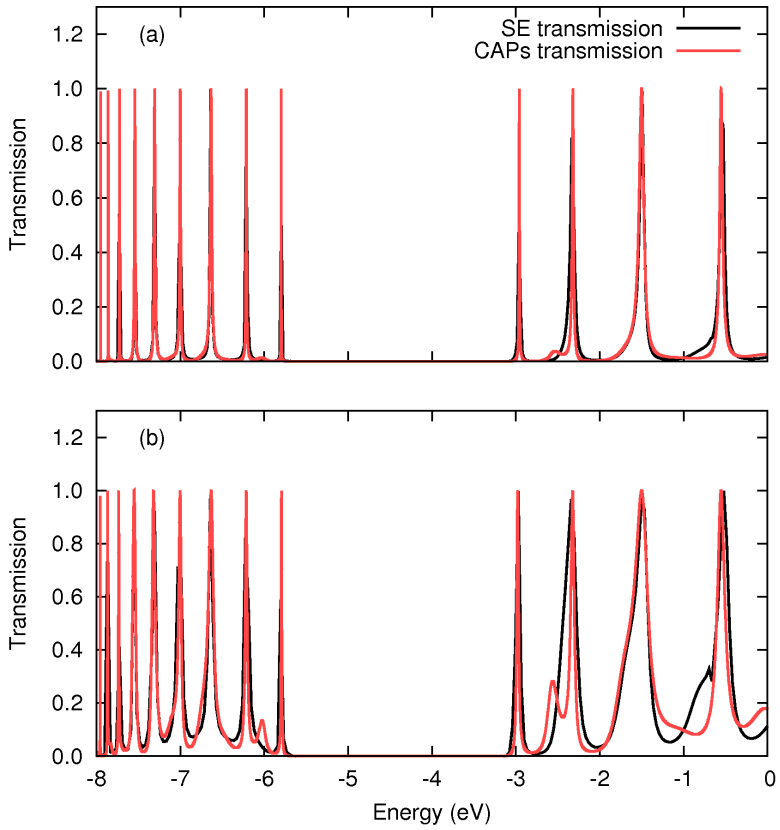

Fig. 4.4: Electron transmission through the chain junction obtained using self-energies and Green's function formalism (black) and transmission using a CAP (red). The lead-molecule separation is 0.45 nm in panel (a) and 0.40 nm in panel (b).

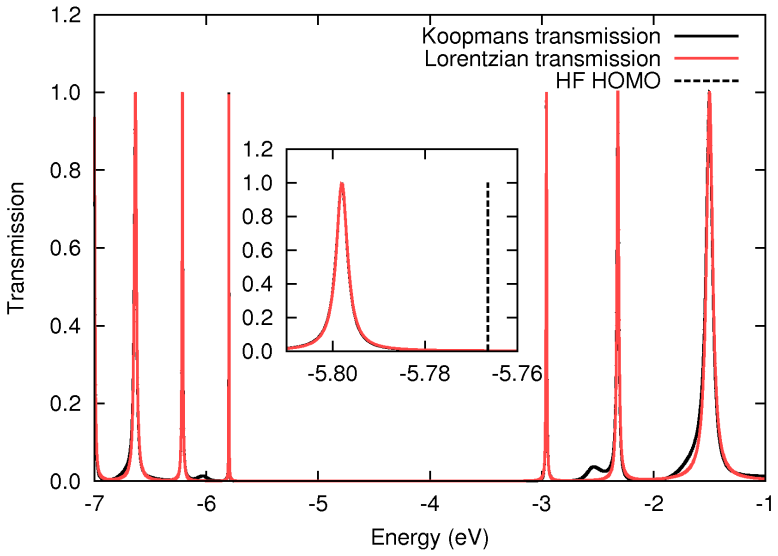

Fig. 4.5: Comparison of Green's function transmission (black) and Lorentzian broadened complex eigenvalues obtained from solving $\mathbf{H}_D + \mathbf{W}$ (red) for the chain junction with 0.45 nm lead-device separation. The shift in the position of the HOMO level relative to the HF value (dashed black line) is illustrated in the inset.

4.2.4 Complex Symmetric CI Approximation

All CI calculations were performed using the complex version of MCCI [90] as described in Section 2.4. The use of MCCI in this work enables the study of the evolution of quasiparticle energies as electron correlations are introduced. This is achieved by starting with a single determinant picture (we will further discuss the use of single determinant approximation and electron correlation in Chapter 5) and then systematically increasing electron correlation, by varying the parameter c_{min} which controls the threshold of included CI expansion coefficient values. At a lower value of c_{min}, more CSFs are included in the calculation leading to improving the description of correlation energy.

In the analysis for the chain model, several approximations for the CI wavefunction expansion are used. The first approximation is the "singles approximation" based on a singles expansions of the CI vector,

$$|\Psi_0\rangle + |\Psi_S\rangle = \left(1 + \sum_{i,a} c_i^a \hat{a}_a^\dagger a_i\right) |\Psi_0\rangle \tag{4.6}$$

with $|\Psi_0\rangle$ as the HF reference state, $|\Psi_S\rangle$ consists of singly excited CSFs. The index i labels occupied orbitals, a labels virtual, c_i^a is the CI coefficient for a singly excited CSF, and $\hat{a}^\dagger$ and $\hat{a}$ are creation and annihilation operators, respectively. This form of the wavefunction allows for the investigation of the effect of optimising the single particle orbitals[1]. To better explain this, one can consider Thouless' theorem [118] which states that any N-particle determinant $|\Psi_A\rangle$ which is not orthogonal to $|\Psi_B\rangle$ can be written in the form

$$|\Psi_A\rangle = \exp\left(\sum_{i,a} c_i^a \hat{a}^\dagger \hat{a}_i\right) |\Psi_B\rangle. \tag{4.7}$$

The exponential operator acts as a rotation to the single particle basis. For appropriately chosen coefficients c_i^a, $|\Psi_A\rangle$ can be written as the single particle determinant which optimises the energy. If the weight of the HF reference state $|\Psi_0\rangle$ is large in the singles wavefunction in equation (4.6), then the expansion coefficients c_i^a will be small. Then equation (4.6) becomes an approximation to the Thouless form equation (4.7), accurate to first order in the c_i^a.

[1] We recall that in the HF formalism the orbitals are optimised by minimising the energy in a Slater determinant approximation to the wavefunction.

The difference between the N and $(N+1)$ many-particle states, and the N and $(N-1)$ states, yields the EA, and IP energies, respectively,

$$\omega_{EA} = \Omega^{N+1} - \Omega^{N}, \tag{4.8}$$

$$\omega_{IP} = \Omega^{N} - \Omega^{N-1}, \tag{4.9}$$

where Ω^N is the N-electron state energy and Ω^{N+1}, Ω^{N-1} are $(N+1)$ and $(N-1)$-electron state energies. These can be thought of as charging the molecule by adding or subtracting electrons from the ground state. In this work, the focus is on the IP and EA of the explicit device region as these can be related to the quality of an electronic structure description of transport [119], which will be shown more explicitly in Chapter 5 where different electronic structure theory formalisms are used to investigate transport properties of a molecular tunnel junction.

The energies obtained from Koopmans' theorem do not account for orbital relaxation: the theorem assumes that the spin orbitals in the $(N \pm 1)$-electron single determinant states are identical with those of the N-electron single determinant state. That is, the relaxation of the spin orbitals in $(N \pm 1)$-electron states is neglected and the spin orbitals of the N-electron single determinant state are not the optimum orbitals for either $(N+1)$- or $(N-1)$-electron states. Hence, sometimes Koopmans approximation is referred to as a "frozen orbitals" approximation. The neglect of orbital relaxation typically results in too positive of an IP and too negative of an EA. Since Koopmans' theorem is a single determinant approach, electron correlations are also neglected.

Another formalism that is often used at the single determinant level is ΔSCF (self-consistent field (SCF)) where the energy difference between separate SCF calculations on the molecule and cation (anion) is taken, hence the name ΔSCF. The ΔSCF method accounts for orbital relaxation, however the total energy tends to be too high as again electron correlations are not included. A proper inclusion of correlation energy would lower the value of the ground state energy more than cation state. Hence, the ΔSCF approximation tends to underestimate the IP. Then, the Koopmans and ΔSCF values generally bracket the true IP and EA energies.

Let us consider the transmission spectra in Figure 4.4, the resonance peaks correspond to N-particle single determinant HF states broadened by opening the system using self-energies. Hence, the HOMO state corresponds to the IP for the extended molecule region, excluding the effects of orbital relaxation of the other single electron states that occurs when an electron is removed. Similarly, the LUMO level corresponds to the EA value on the molecular region, with all the orbitals frozen as an electron is added. So one can think of the HOMO and LUMO levels in Figure 4.4 as Koopmans IP and EA in a single determinant picture. Using a many-electron framework and including all single excitations into the CI wavefunction, means letting all other electrons relax on the EM region, as the charge state is changed by either adding or subtracting electrons. From Thouless' theorem, it can be deduced that the CI singles energies Ω^{N+1} and Ω^{N-1} are approximations to optimised single determinant energies with orbital relaxations included for the device region. Hence

equations (4.8) and (4.9) correspond to ΔSCF EA and IP values.

For chain-BDA-chain model that is studied, the IP and EA values obtained from the MCCI calculations when excitations beyond CI singles are included and compare to DFT/PBE charge states. These peaks are also compared to the equivalent values obtained when the junction is opened by introducing the CAP. Hence, this approach provides a way to study what role electron correlations and environment play on electronegativity.

4.3 Quasiparticle States and Life-times

In these calculations, two types of CI singles approximations are considered. In molecular singles, only one-electron excitations involving orbitals localised on the molecular region are allowed. The molecular orbitals were chosen by comparing the eigenvalues of $\mathbf{H}_D + \mathbf{W}$ to those obtained with the Green's function electron transport method, as Green's function peaks correspond to molecular states. In the second approximation, referred to as extended device excitations, all singles excitations whether arising from the device or leads are allowed. Two c_{min} values used are 0.003 and 0.001 and the calculations are repeated for the molecular excitations, referred to as the CI(0.003)-molecule and CI(0.001)-molecule. For the device approximation only the threshold of 0.003 is used and will be referred to as CI(0.003)-device. It is estimated that with the present CI treatment, over 90% of total correlation energy is obtained for the weakly coupled case of 0.45 nm lead-device separation. This is

calculated using the method outlined in ref. [83].

The electron transmission peaks in Figure 4.5 correspond to resonances associated with the single particle energies. For a valid comparison, the quasiparticle energies ω_i taken as energy differences between many-electron single determinant HF states obtained from solving $\mathbf{H}_D + \mathbf{W}$ are used. Since the molecular Hamiltonian is coupled to the leads *via* the CAP, the many-electron energies are also complex and contain the energy shift and finite lifetime. The resonance lifetime is calculated as $\tau = \hbar/\gamma$ where $\gamma = 2Im(\omega)$. The effect of systematically increasing correlations on these resonant energies is studied next.

4.3.1 Molecular Excitations

In this Section, only excitations from the MOs localised on the molecular region are considered. The weaker coupling case is defined to be the 0.45 nm separation between the electrodes and molecular region. As can be seen in Figure 4.5 opening the system by introducing the leads *via* CAPs shifts the HOMO level by 32 meV from the HF HOMO level and introduces state broadening with a lifetime of approximately 223 fs. Including molecular singles, allows for orbital relaxation in the charged states and attempt to correct for the over-estimation of the band gap that is typical of HF.

The result of the ΔSCF calculations is illustrated in Figures 4.6a for the HOMO and 4.6b for the LUMO, where the energy shifts and broadenings are seen. The HOMO peak shifts upward in energy by 288 meV and the LUMO peak shifts downward in energy by 260 meV from

the Koopmans positions. This is accompanied by a significant decrease in the electron lifetimes relative to Koopmans values with the HOMO lifetime reducing to 59 fs and LUMO to 17 fs. The shorter lifetimes reflect increased coupling between molecular and lead states.

The CI calculations are first carried out at the threshold of 0.003, resulting in a shift of the HOMO peak downward and the LUMO peak upward, increasing the band gap relative to the ΔSCF calculation, as shown in Figures 4.6a and 4.6b. The c_{min} coefficient is lowered to 0.001 increasing the correlations, which narrows the band gap by slightly shifting both levels back in the opposite direction.

These findings are consistent with the literature: Koopmans EA and IP are underestimated [70] and ΔSCF overestimates the band gap [120]. The introduction of correlations energies serves to renormalise the band gap with the HOMO and LUMO states being bracketed by the Koopmans and ΔSCF values. The added correlations do not seem to affect the resonant broadening to a great extent beyond that seen in the ΔSCF approximation. It can be concluded, that in the weakly coupled case the molecular region behaves similar to an isolated molecule with additional features of small energy state shifts and lifetime broadening due to the inclusion of the electrodes.

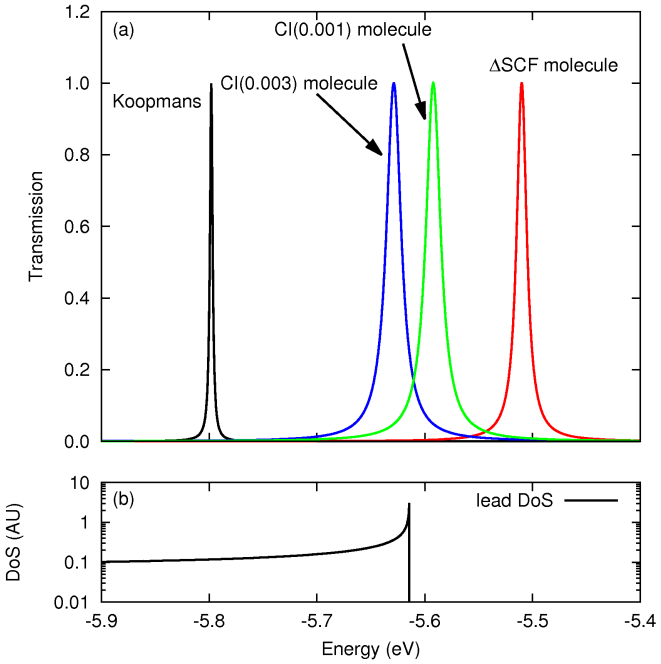

(a) HOMO quasiparticle peaks.

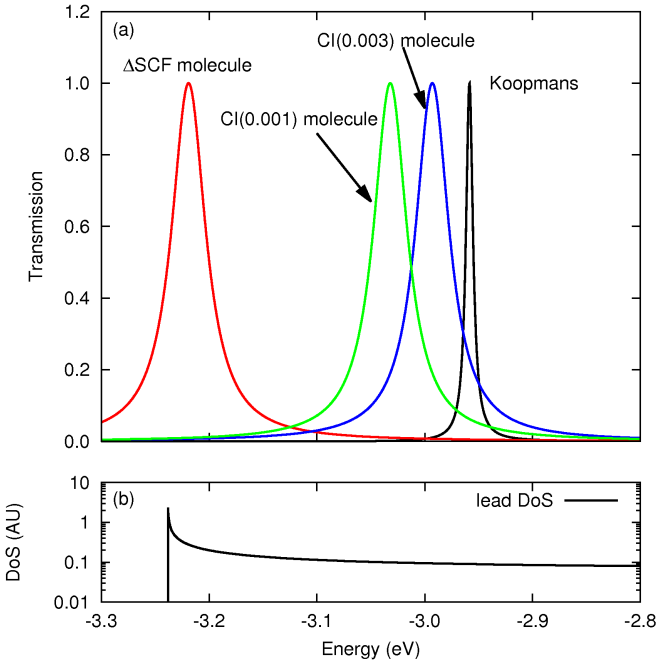

(b) LUMO quasiparticle peaks.

Fig. 4.6: HOMO and LUMO energy states for the weakly coupled system (0.45 nm lead-device separation). The excitations are restricted to the orbitals localised on the molecular region. The approximations used are: Koopmans (black), ΔSCF (red) and the MCCI results with c_{min} of 0.003 (blue) and 0.001 (green). Density of states of the lead is shown in panel (b) for both figures.

In the stronger coupling case the molecule-lead separation is reduced to 0.40 nm. The same calculations as above were repeated with the results summarised in Figures 4.7a and 4.7b. As before, the ΔSCF approximation narrows the band gap and the level broadening is significantly greater compared to the Koopmans band gap. The HOMO state lifetime decreases to 17 fs in ΔSCF from 71 fs in Koopmans approximation, while the LUMO decreases to 7 fs from 26 fs. Similarly as for the weak coupling regime, the resonance lifetimes are not significantly changed when electron correlations are introduced, but the peak positions do shift. As a result, the band gap is also renormalised with increased correlations and the correlated resonances are bracketed by the Koopmans and ΔSCF values, as was the case for a weakly coupled system.

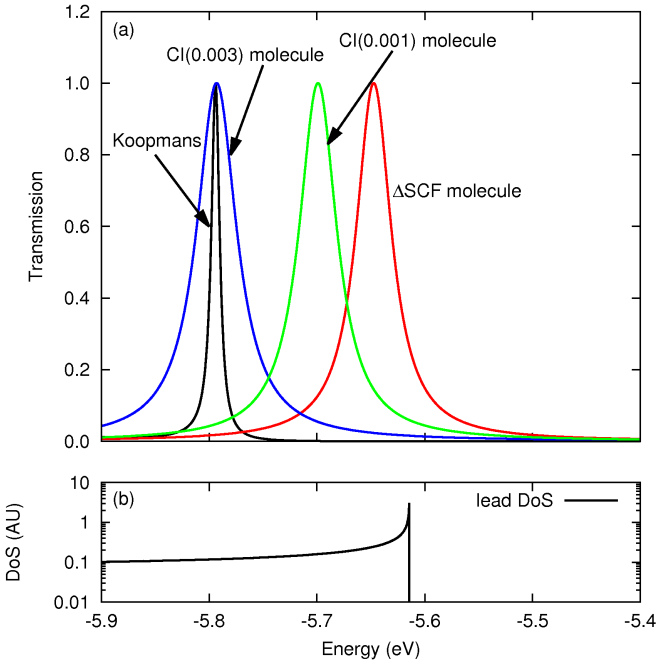

(a) HOMO quasiparticle peaks.

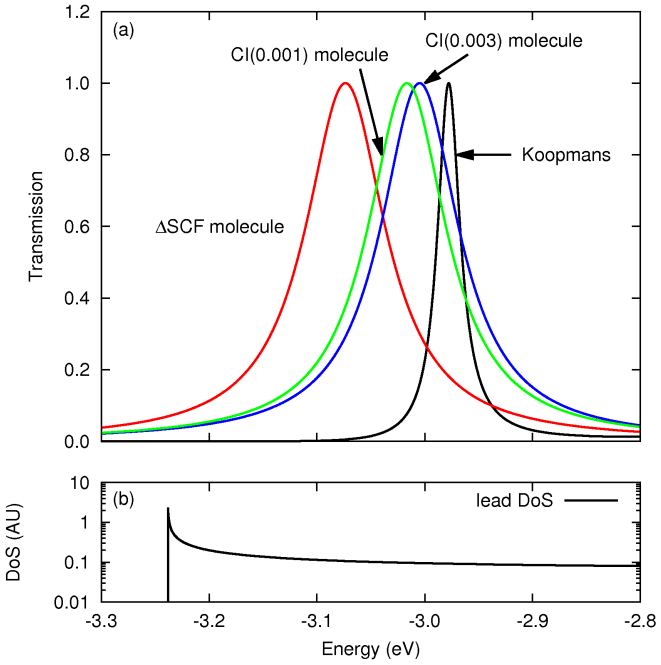

(b) LUMO quasiparticle peaks.

Fig. 4.7: Quasiparticle HOMO and LUMO levels for the 0.40 nm separated system, calculated using molecular orbitals localised on the molecular region only. Koopmans approximation is in black, ΔSCF is red, and CI resonances with c_{min} 0.003 in blue and 0.001 in green. Panel (b) shows the density of states on the lead.

4.3.2 Extended device excitations

In this section, the effect of including lead excitations is studied. Previous work using an interacting two-level model by Galperin *et al* predicted that the coupling of electrode excitations to the molecular excitations can significantly alter the electron transport through a junction [112]. This section considers whether the same is true for atomic chains. The results of ΔSCF and CI calculations are illustrated in Figure 4.8 for both cases considered in this work. As before, the ΔSCF approximation narrows the energy gap with respect to the Koopmans values. However, the energy shift is much larger than with MOs localised on the molecular region as discussed in the previous section. There is also a significant increase in resonant broadening for the ΔSCF calculation, especially for the stronger coupling case.

For the weakly coupled case, the HOMO state lifetime decreases from the Koopmans estimate of 223 fs to 18 fs from the ΔSCF approximation. While the width of the LUMO does not change much from the Koopmans lifetime of 121 fs to the ΔSCF lifetime of 85 fs. The introduction of electron correlations renormalises the band gap as was the case for molecular only excitations.

Notably, the correlated resonances are no longer bracketed by ΔSCF and Koopmans peaks. Introduction of correlations broadens the LUMO peak significantly more than the HOMO level. While the HOMO resonance remains approximately the same when correlations are included as with ΔSCF, the LUMO lifetime decreases from 121 fs to 21 fs.

The resonance behaviour in the stronger coupled case is qualitatively different compared to the previous cases as illustrated in Figure 4.8b. The band gap is reduced more significantly than in the weaker coupled system. The broadening and position of HOMO is approximately the same for both weakly and strongly coupled systems. However, the LUMO level is much broader than that for the junction with 0.45 nm lead-molecule gap. The LUMO lifetime is approximately 2 fs. One can recall that studying LUMO is equivalent to studying EA within Koopmans approximation, that is an $(N+1)$-electron state within the ΔSCF framework is considered. A closer look at the CSFs included in the CI-singles vector reveals that the the $(N+1)$ state is multi-referenced, that is more than one CSF is strongly contributing to the overall wavefunction. One of the CSFs has an additional electron in the molecule's LUMO state, whereas the other contains an extra electron in a lead orbital. This explains why the state broadening is larger: the electrode and molecule regions are strongly coupled through the multi-reference character of the state.

Introducing electron correlations has a different effect on the strongly coupled system than the weakly coupled one. The position and broadening of the HOMO level remains approximately unchanged for ΔSCF and MCCI calculations, compared to the noticeable shift seen in the weakly coupled case. The inclusion of electron correlations decouples the LUMO level and results in a single dominant CSF in the CI vector. This is also reflected in the resonance being less broad reducing to a lifetime of approximately 7 fs. The resonance shifts upwards by approximately 1 eV, a much larger shift than found in the earlier approximations.

These results illustrate that including electrode excitations significantly changes the behaviour of HOMO and LUMO levels. It is expected that this will have a strong effect on electron transport, which is considered next.

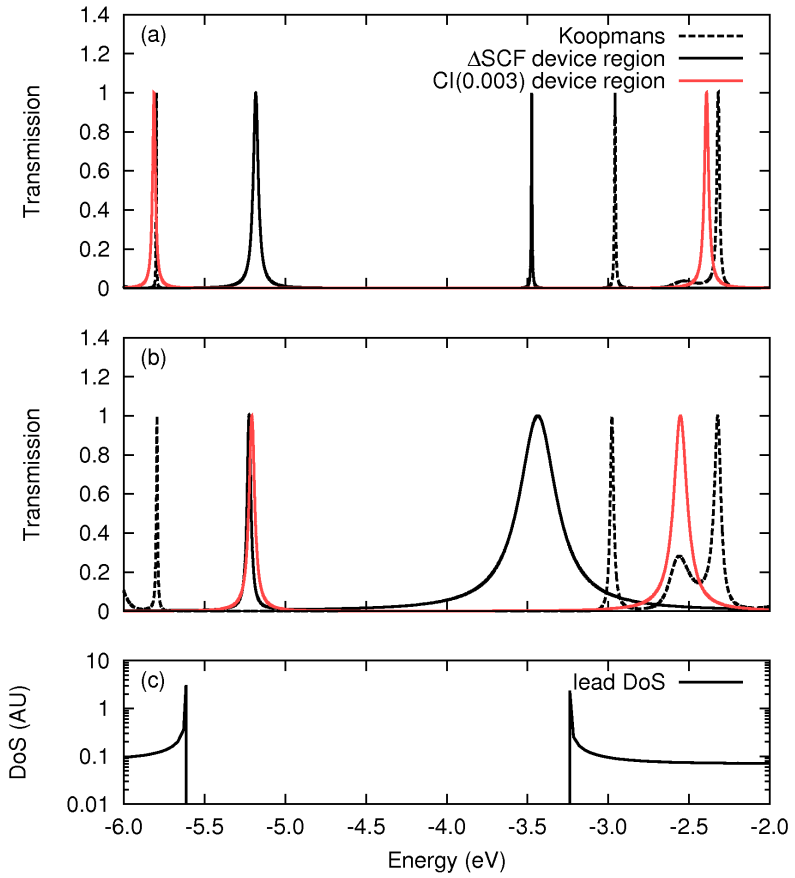

Fig. 4.8: The position of quasiparticle HOMO and LUMO peaks for the (a) 0.45 nm and (b) 0.40 lead-device separation junctions with the inclusion of lead excitations. The density of states of the leads is plotted in (c).

4.3.3 Electron Transport

The effect of the above treatments on conductance for a strongly coupled junction with 0.40 nm molecule-lead separation is illustrated in this section. The Landauer formalism is used. The left lead states are filled up to the chemical potential μ_L, and the right lead states are filled up to μ_R. In equilibrium, the two chemical potentials are equal and there is no current flow. Applying the bias voltage, V, shifts the chemical potentials and the current flows. The Landauer expression for the steady-state current through the device region for applied bias V is

$$I(V) = \frac{2e}{h} \int_{-\infty}^{+\infty} T(E,V)[f(E+\mu_L) - f(E-\mu_R)]dE, \qquad (4.10)$$

where f is the Fermi distribution function and $T(E,V)$ is the transmission probability for electrons from the left to the right lead with energy E and at a voltage difference $V = (\mu_L - \mu_R)/e$, where e is electron charge. The Landauer approach is known for its lack of self-consistency. However, in their recent work Ke *et al* [121] have shown that non-self-consistent approaches can qualitatively reproduce $I-V$ characteristics obtained with self-consistent schemes for a chain of carbon and aluminium atoms as molecular regions sandwiched between aluminium electrodes. Their device was described within DFT, while the electrodes were included using an NEGF approach. In the treatment presented in this chapter, the orbital relaxation of both neutral and charged states is included, except for the case of the Koopmans' values.

Figure 4.9 presents the $I-V$ curves for the strongly coupled system.

It is noted, that the broad extended device LUMO state observed in the ΔSCF approximation results in strong early onset of conductances as illustrated in Figure 4.9a. This is in contrast to the Koopmans' current which is very low as HF overestimates the size of the band gap and conduction states do not enter the bias window at low voltages. A similar trend is observed when correlated resonances are used, shown in Figure 4.9b. The extended device current is larger than when only molecular type excitations are included, which is in agreement with the model calculations by Galperin *et al.*

It is noted that the correlated HOMO and LUMO widths are similar for the molecule localised orbitals and complete device excitations. This leads to less of a difference between transmission CI(0.003)-molecule and CI(0.003)-device as shown in Figure 4.9. Introducing electron correlations narrows the LUMO state compared to the ΔSCF case shown in Figure 4.8b and shifts it higher in energy, resulting in a smaller conductance onset.

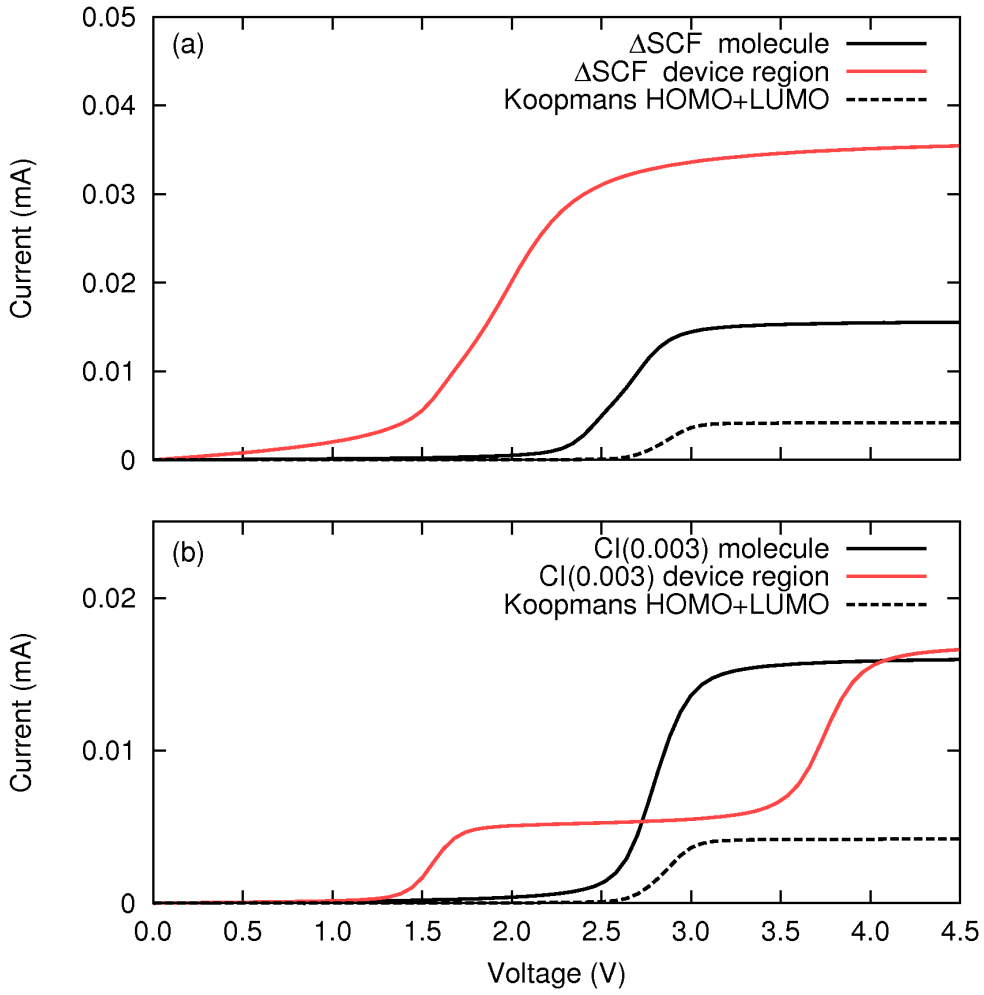

Fig. 4.9: $I-V$ characteristics for the 0.40 nm separated junction. In panel (a) the current from both molecule (black solid line) and device (red solid line) localised orbitals with the ΔSCF approximation is plotted in conjunction with the molecule only Koopmans current (black dashed line). Panel (b) illustrates the CI spectra compared to Koopmans transmission. The equilibrium Fermi energy was chosen to lie in the middle of the band gap of the leads at -4.42 eV, and the electrochemical potentials in the electrodes are taken to move apart symmetrically as voltage is applied.

4.4 Effect of Metal Electrodes on Junction Electronegativity

In this section, the BDA, Au-BDA-Au and chain-BDA-chain systems are studied using DFT and KS orbitals, as outlined in Section 4.2.1, to investigate the effect of electron correlations and environment on tunnel junction electronegativity.

4.4.1 Electronic Spectra

The influence of introducing metal electrodes on electronic spectra of BDA by considering molecular DFT/PBE HOMO and LUMO levels is summarised in Figure 4.10 and Table 4.1. The molecular HOMO and LUMO were identified by considering Mulliken analysis[2]: the highest occupied state with a dominant molecular character was chosen as HOMO, and similarly for the molecular LUMO.

	BDA	Au-BDA-Au	chain-BDA-chain
LUMO	-0.78	-1.88	-2.49
HOMO	-4.07	-7.13	-7.50
Band gap	3.29	5.25	5.01

Tab. 4.1: A summary of molecular HOMO, LUMO and band gap values in eV for the three BDA based systems described within DFT/PBE formalism.

[2] The Mulliken population for a given atom A is defined as $D_{pop} = \sum_{\mu \in A}^{K} \sum_{\nu}^{K} \rho_{\mu\nu} S_{\mu\nu}$, where $\rho_{\mu\nu} S_{\mu\nu}$ is an off-diagonal element representing the number of electrons shared by AOs μ and ν with ρ being the density matrix and S is the overlap matrix. The contributions from all AOs on atom A are summed up to give the total number of electrons on A. In Mulliken population analysis, the contribution of basis functions from two atoms is divided equally [77, 122].

It is noted that a significant decrease of 3 eV in the position of the molecular HOMO energy as single gold atom contacts are bonded to the amine linkers. Bonding of atomic chain electrodes decreases the HOMO energy further from the Au-BDA-Au value of -7.12 eV to -7.50 eV for the chain-BDA-chain. This change of 0.37 eV in the position of HOMO level is due to attaching semi-infinite leads, and is substantially less than the effect of forming a chemical bond. A decrease of approximately 1 eV in the position of the LUMO is seen when gold contacts are added to the free BDA molecule, with a further decrease of 0.61 eV upon addition of atomic chain electrodes.

It has been found in Section 4.3 that the position of transmission resonances and their broadening, *i.e.* molecular HOMO and LUMO states plays an important role in the description of electron current, where a too large Koopmans band gap resulted in too weak a current onset, and on the contrary ΔSCF values overestimate electron transport. Figure 4.10 demonstrates that the shift in the position of the molecular band gap is largely due to the chemical bonding to metal atoms. Next, the effect of electronegativity is studied using junction IP and EA levels, different to the molecular entities used in the above.

Electronegativity is studied as the difference between many-body N- and $(N+1)$-electron states for EA and N and $(N-1)$-electron states for IP as in equations (4.8) and (4.9), respectively. For the DFT treatment, IP and EA are calculated as differences between total energies for the charged states, *i.e.* DFT-ΔSCF. In the MCCI calculations, excitations originating from both the molecule localised orbitals and lead orbitals

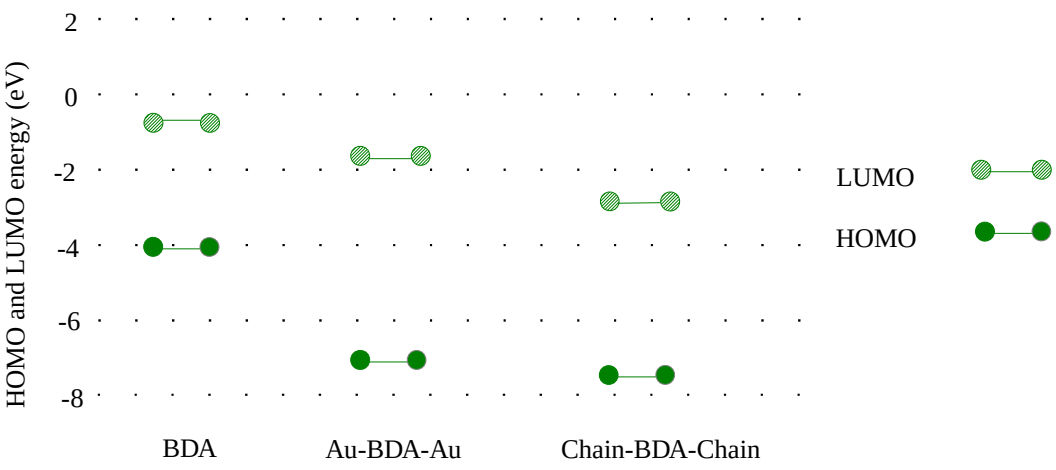

Fig. 4.10: The DFT energy of molecular HOMO and LUMO states is followed as metal electrodes are introduced. A significant shift in the energy of the HOMO is noted going from BDA to Au-BDA-Au, indicating strong coupling between the molecular and metal states, while further addition of contacts decreases the energy levels further.

were allowed, since the importance of lead excitations has been demonstrated in this work and in ref. [112]. The IP and EA values in Figure 4.11 and Table 4.2 are for the entire junction, which is what would be obtained experimentally. The molecular tunnel junction's electronegativity is studied as these determine the polarisability of the system. As will be discussed in Chapter 5, an improved treatment of the junction's polarisability leads to an improved RDM and improved transport description.

It is known that DFT/PBE underestimates the band gap due to the presence of self-interaction errors [55]. This is corrected by explicitly introducing electron correlations within MCCI treatment for all three systems as illustrated in Figure 4.11. The IP energy obtained for BDA with MCCI of -6.95 eV agrees well with the experimental result from

	BDA	Au-BDA-Au	chain-BDA-chain
DFT/PBE			
EA	1.78	-2.12	-4.24
IP	-6.71	-6.11	-5.41
MCCI			
EA	4.15	0.53	-2.79
IP	-6.95	-6.37	-5.31

Tab. 4.2: A summary of junction electronegativity values in eV for DFT and MCCI treatments of the three systems.

ultraviolet photoelectron spectroscopy (UPS) of -7.34 eV [123], while *GW* treatment by Strange *et al* [62] resulted in the energy of -6.2 eV with the use of a double-ζ basis set.

The EA of BDA is large and positive at 1.78 eV in DFT and with an even higher value of 4.15 eV from MCCI, which indicates that BDA does not easily form an anion state. Adding metallic character, lowers EA to -2.12 eV for Au-BDA-Au and -4.24 eV for chain-BDA-chain within DFT, meaning the affinity for an added electron is increased. The drop in MCCI calculated energy for EA is pronounced, with a decrease of 3.62 eV going from BDA to Au-BDA-Au, and a further decrease of 3.32 eV for chain-BDA-chain. A steady increase in the position of the IP level is seen, as the system becomes more metallic. In this work, it is found that DFT and CI treatments give a good agreement for the junction IP levels: for a free BDA molecule the difference between DFT and MCCI IP peaks is 0.24 eV, similarly for Au-BDA-Au the difference is 0.26 eV and for chain-BDA-chain the difference is 0.10 eV. As can be seen from Figures 4.10 and 4.11, although the molecular LUMO couples strongly with the

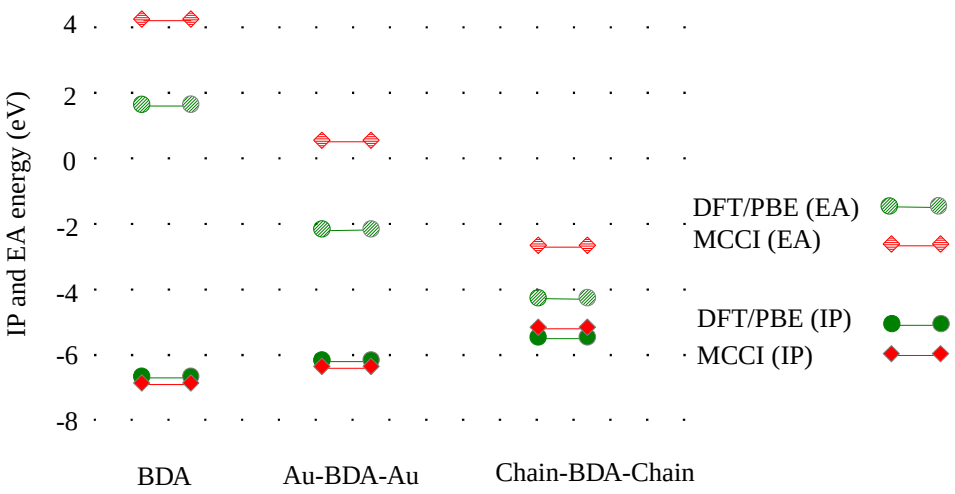

Fig. 4.11: IP (solid filled symbols) and EA (hatched symbols) energies for the three systems considered. As expected, DFT/PBE (shown in green circles) underestimates the band gap, while CI treatment (red diamonds) re-normalises it.

electrodes and lowers in energy, it is the much more lower lying hybridised molecule-electrode states that govern the junction electronegativity and hence polarisability.

The effect of opening the BDA junction by including chain electrodes using CAPs is considered next. As illustrated in Figure 4.11, no noticeable shift in the position of IP and EA values is seen compared to a closed junction, thus indicating that opening a system does not introduce a significant energy shift, the primary effect of opening the system is to introduce a finite state lifetime as illustrated in Figure 4.12.

As can be seen in Figure 4.11, a significant disagreement in the EA values of DFT and MCCI are observed. To understand this further, the CSF expansion of the CI vector for chain-BDA-chain open to the

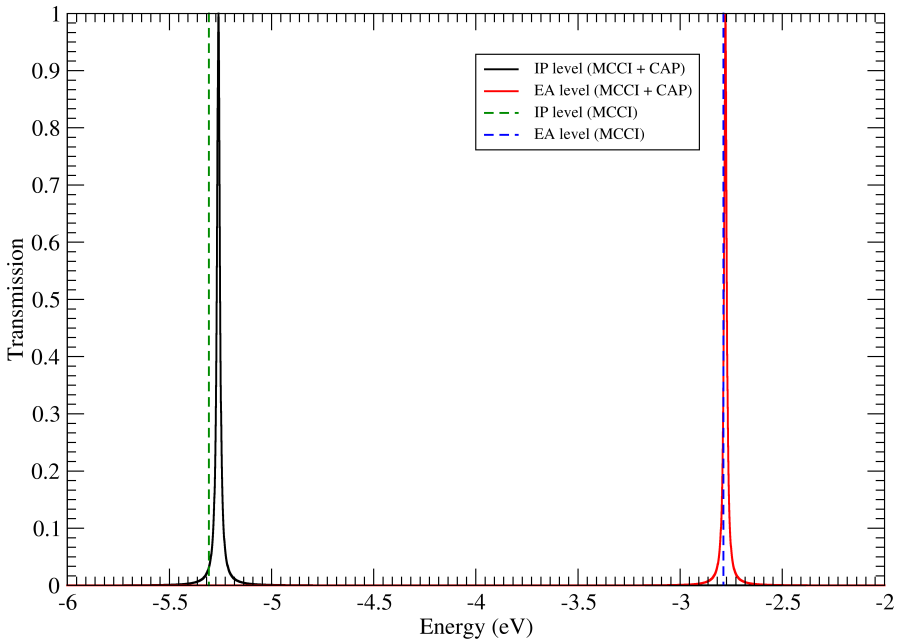

Fig. 4.12: The relative position of IP and EA levels for chain-BDA-chain junction. The dashed line peaks are the result of MCCI calculations where electron correlations are considered but the system remains closed. In solid lines the MCCI-CAP results are shown where the system is open and the influence of the electrodes is seen in the shift and broadening of the peaks.

environment by including CAPs is considered.

4.4.2 Multi-Reference Character of Tunnel Junctions

A single particle approximation assumes that a system can be described by a single determinant. This is true in the limit of weak coupling and negligible electron correlations, as will be discussed in Chapter 5. In Table 4.3, a summary of top contributing CSF coefficients from the MCCI calculations for the three BDA-based systems is given. The single-reference nature of the BDA molecule is noted, while bonding to metal

	N	$(N+1)$	$(N-1)$
BDA	0.97	0.97	0.97
Au-BDA-Au	0.67, 0.67, 0.34	0.95, 0.14, 0.12	0.93, 0.40, 0.14
Chain-BDA-Chain			
Closed:	0.56, 0.55, 0.35	0.82, 0.15, 0.13	0.79, 0.19, 0.14
Open:	0.57, 0.55, 0.34	0.82, 0.15, 0.12	0.80, 0.18, 0.14

Tab. 4.3: Summary of the top three contributing CSF coefficients for single BDA molecule, Au-BDA-Au and chain-BDA-chain for the N-, $(N+1)$- and $(N-1)$-electron states. Note, that BDA remains single-reference, whereas upon addition of the metal a multi-reference character is observed.

atoms is seen to introduce a multi-reference character, especially in the ground state for both Au-BDA-Au and chain-BDA-chain. This can be attributed to a strong metal-molecule hybridisation that is seen for metal containing junctions.

The ground state for chain-BDA-chain is multi-referenced for both closed (MCCI calculation) and open (MCCI+CAP treatment) systems. While the multi-referenced character for the $(N+1)$- and $(N-1)$-electron states is somewhat less pronounced.

As can be seen from Table 4.3 several CSFs of the CI vector expansion contribute to the description of the N-electron state of the open chain-BDA-chain system. One of the configurations (0.57) is that of a vacant junction HOMO level and a filled in LUMO level which could be due to the narrow junction band gap, as adding metallic character enhances screening and narrows the gap. While the second most contributing CSF (0.55) is that of a filled in junction HOMO. For the open chain-BDA-chain $(N+1)$-electron state, the leading CSF (0.82)

is that of the $(N+1)$-electron state itself, that is a single electron in the junction LUMO orbital. The junction HOMO and LUMO levels for the chain-BDA-chain system are metallic in character as was calculated from Mulliken population analysis. The multi-reference nature of the resulting states suggests they cannot be treated using a single-determinant approach and require an explicit CI description.

To confirm that the system's multi-reference character is not an artefact of the single particle basis set employed, the idempotency of the density matrix is calculated. The relationship between density matrix and electron correlations is studied further in Chapter 5. A density matrix is expressed in terms of orbitals as discussed in Section 2.5

$$\rho(\mathbf{x}', \mathbf{x}) = \sum_{p,q} \rho_{pq} \psi_p(\mathbf{x}) \psi_q^*(\mathbf{x}'), \tag{4.11}$$

with p and q labelling general states. When diagonalised, the eigenvalues ρ_{ii} refer to the orbital occupation numbers. If a wavefunction can be described by a single determinant, the density matrix is said to be idempotent $\rho = \rho^2$. Hence, calculation of idempotency of a density matrix can serve as a measure of the degree of correlation of a system. The larger the difference between ρ and ρ^2, the more non-idempotent is the matrix and the more correlated is the system. For the open chain-BDA-chain system the non-idempotency is 0.039 for the N-electron state, while the BDA non-idempotency value for the same state is 0.017. The higher non-idempotency of the chain-BDA-chain N-electron state can be related to the top three CSFs being significant contributors to the wave-

function description, thus making the system highly multi-determinant. The calculated non-idempotency values can be thought of as the amount of correlation per one active electron (*i.e.* frozen orbitals are neglected). Hence, it is correct to characterise the junction as a multi-reference system.

4.5 Conclusion

In this chapter, the impact of electronic structure treatment on quasiparticle energies and lifetimes for two different models described in HF and DFT bases was studied. A correct description of molecule-lead coupling will lead towards a better description of electron transport. The quasiparticle states were related to electron EA and IP values, which in turn can be related to the junction electronegativity. In Chapter 5, a further discussion of how accurate prediction of electronegativity contributes towards a better description of electron transport.

The work in this chapter validates the CAPs formalism extended beyond a tight-binding chain model as discussed in Chapter 3. The use of CAPs enabled a systematic inclusion of metal electrodes into CI calculations to study both the effect of a lead and correlation energy on the electronic spectrum of the device region. An excellent agreement between the CAPs and self-energy based transmissions was obtained showing that electrodes can be accounted for with the use of this energy-independent potential. The use of the CAP in the current study enabled the investigation of quasiparticle lifetimes within an explicit correlated wavefunction

method.

The two coupling regimes studied for the chain model showed a similar behaviour when only molecular excitations are included, however including the leads resulted in significantly different behaviour. Including only molecular excitations yields quasiparticle values qualitatively similar to that of an isolated molecule, similar to findings for linear chains [124]. However, including the leads caused the wavefunction to be multi-referenced resulting in a much broader LUMO state, which then decouples when correlations are introduced. It is noted that the quasiparticle states are heavily influenced by electron correlations and the coupling strength, implying that detailed treatments of the electronic structure are necessary to accurately model charge transport.

The effect of electron correlations and environment were investigated using BDA based junctions described with DFT orbitals. The molecular HOMO and LUMO levels have been seen to significantly shift as BDA was bonded to metal. A large shift in the position of the HOMO when gold contacts are introduced highlights that the change in the level position is largely due to the chemical bonding. A further decrease in energy of the HOMO is noticed as the system is made open by bonding to semi-infinite leads shows the influence of the environment on the molecular energy states.

The junction electronegativity has also been studied within DFT and CI formalisms. The junction IP was shown to be well described by both DFT with the PBE exchange correlation potential and MCCI. Less of an agreement is seen in the description of the EA state, with correlated

resonances being significantly higher in energy compared to their DFT counterparts. Opening the chain-BDA-chain junction by introducing the CAP did not result in a significant shift in the position of the IP and EA values compared to the correlated treatment of the closed junction. This indicates that the majority of electron correlation energy is due to the chemical bonding of the junction and not to the extended environment.

A further investigation of the nature of the CI vectors involved in metal bonded BDA systems revealed multi-reference behaviour is observed. Similar to the strongly coupled case in the chain model, multi-reference behaviour was seen for the Au-BDA-Au and chain-BDA-chain junctions, while single BDA molecule can be described as a single-reference state. This is because strong interaction between molecular and metal states exists and lead excitations heavily influence the system as was shown in the calculations of the gold atomic chain model presented in this work. This is particularly evident when considering the N-electron state of the open chain-BDA-chain model, where the filled in HOMO has approximately as equal a contribution as a vacant HOMO and filled in LUMO levels. It is of note, that these are the junction HOMO and LUMO levels and are metallic in character. We find that the multi-reference behaviour is not due to the choice of basis sets as was shown by considering the idempotency of the density matrix. The need for multi-determinant treatment of junctions has been raised by Geskin and co-workers [69]. In their study, the authors used a collection of organic donor-acceptor molecules within CI descriptions to study electron transfer in weakly coupled system. The findings pointed towards the need

to explicitly describe many-body effects and the deficiencies of standard DFT techniques. The work in this chapter points that multi-reference states are clearly present when treating electron tunnel junctions and an accurate description of such states can be achieved with many-body formalisms. In particular, this chapter has shown that the DFT treatment significantly underestimates the position of the junction EA states which are found to have a multi-reference character when described within CI.

5. ELECTRONEGATIVITY AND TRANSPORT IN MOLECULAR TUNNEL JUNCTIONS

5.1 Introduction

Electronegativity can be thought of as increasing or decreasing the system's affinity for electrons. When designing a molecular tunnel junction, the electronegativity of the molecule can be modified by using EDGs or EWGs, as discussed in Section 1.3. In what follows, electronegativity is shown to control charge transfer, energy level alignment, and electron currents in a single molecule tunnel junction, all of which are described through the density matrix (introduced in Section 2.5) [119]. The Mulliken electronegativity is given as $\frac{IP+EA}{2}$ and is a useful measure of charge transfer, which determines molecular level alignments relative to electron reservoir energies [46, 47]. The accurate prediction of the energy level alignment between the molecule and the electrode is essential for accurate predictions of current-voltage characteristics [2].

In Section 1.4, the importance of inclusion of electron correlations into the description of electronic structure of junctions has been mentioned. In this chapter, correlation corrections to independent particle models are considered and conditions on the one-electron Green's function and re-

duced density matrix for calculations of currents within non-equilibrium theories are related. Correlation corrections are shown to correspond to improving IPs and EAs on a molecular junction. One can think of IP and EA as description of HOMO and LUMO levels and consequently the band gap. By considering the effect of correlations on IP and EA, electron transport can be discussed in terms of electronegativity, *i.e.* the impact of electronegativity on charge transfer, level alignment and current magnitudes.

In what follows, a model of hexa-1,3,5-triene-1,6-dithiol (referred to as hexatriene in this chapter) bonded between two electrodes is studied. In an analytical model a parameter is used to increase electron-electron correlation while examining its effect on electronegativity and electron transport. The obtained results for current-voltage ($I-V$) curves are then compared to explicit electronic structure treatments for the same junction.

5.2 One-electron RDM and Green's Function

In Section 2.5 an introduction to reduced density matrices (RDMs) was given, where it was noted that any one-body quantity can be obtained from the one-electron RDM. The electron current density can be calculated from the RDM [66, 94] as

$$J(\mathbf{r}) = \frac{1}{2i}\left[\bigtriangledown_{\mathbf{r}} - \bigtriangledown_{\mathbf{r}'}\right]\rho(\mathbf{r},\mathbf{r}')\mid_{\mathbf{r}'=\mathbf{r}} \tag{5.1}$$

with J being the current density, $\mathbf{r}$ and $\mathbf{r}'$ are position vectors, and ρ the one-electron RDM. Current density is a one-electron operator, so to obtain an accurate prediction for current, an accurate prediction of the one-electron RDM is needed. Alternatively, advanced (superscript a) and retarded (superscript r) Green's functions $G^{a,r}$ can be used and an application of Landauer-type formula [3, 125, 126] determines electron current:

$$I = \frac{2e}{h} \int dE \left[f_L(E;\mu_L) - f_R(E;\mu_R) \right] Tr \left[\Lambda_L(\epsilon) G^a(E) \Lambda_R(E) \Upsilon G^r(E) \right], \tag{5.2}$$

with electron energy E, spectral densities[1] $\Lambda_{L,R}$, energy distribution $f_{L,R}$ with $\mu_{L,R}$ as chemical potentials in the left and right electron reservoirs, and Υ is the correction due to the correlations weighted by the spectral density of the electrodes and electron-electron spectral density on the molecule [125, 126]. In Section 2.7 it was shown that Green's function can be related to the RDM via integration over a Coulson contour as

$$\rho(\mathbf{r},\mathbf{r}') = \frac{1}{2\pi} \oint dE\, G(\mathbf{r},\mathbf{r}';E). \tag{5.3}$$

It is known that the RDM obtained from a many-electron wavefunction corrected to second-order in electron correlation is equivalent to the reduced density matrix arising from correcting IPs and EAs in the Green's function to second-order in the electron self-energy [127].

The perturbation expansion to correct the HF density matrix leads

[1] Spectral density can be thought of as a generalisation of the density distribution of states.

to the first-order correction from HF orbitals vanishing [128] giving the density matrix correct to second-order as,

$$\rho \approx \rho^{(0)} + \lambda^2 \rho^{(2)}. \tag{5.4}$$

The RDM may be represented as an infinite expansion over single electron states ψ

$$\rho(\mathbf{r}, \mathbf{r}') = \sum_{pq} \rho_{pq} \psi_q^*(\mathbf{r}') \psi_p(\mathbf{r}), \tag{5.5}$$

where p and q denote general states. The density matrix coefficients may be calculated using a perturbation expansion of a many-body wavefunction [127].

The poles of the Green's function correspond to IPs and EAs and can also be thought of as transmission resonances. It has also been mentioned, that introducing electron-electron correlation to the Hartree-Fock Green's function will improve the prediction of IPs and EAs. Hence, it can be assumed that if an independent particle picture is chosen to optimise IPs and EAs, then the prediction of currents from the Green's function approach, equation (5.2), will also be improved. In this context, a model for transport is measured in terms of reproducing the correct molecular electronegativity.

The Green's function corrected in second-order self-energy as studied

in ref. [127] leads to the following approximation,

$$\begin{aligned}\left[G^{(2)}(E)\right]^{-1}_{pq} &= \left[G^{(0)}(E)\right]^{-1}_{pq} + \Sigma^{(2)}(E)_{pq} \\ &= (E-\epsilon_p)\delta_{pq} \\ &- \frac{1}{2}\sum_{iab}\frac{\langle ab||pi\rangle\langle qi||ab\rangle}{E+\epsilon_i-\epsilon_a-\epsilon_b} \\ &- \frac{1}{2}\sum_{ija}\frac{\langle ij||pa\rangle\langle qa||ij\rangle}{E+\epsilon_a-\epsilon_i-\epsilon_j},\end{aligned} \tag{5.6}$$

where i and j label occupied states, a and b label virtual states, p and q label general states, and the lowest order Koopmans' IPs and EAs obtained from the diagonal elements of $G(E)$. The improvement of Koopmans' IPs and EAs is achieved *via* the second-order correction in electron self-energy as shown in Section 2.7 and ref. [127]. Within this approximation, it is also possible to determine the density matrix directly from equation (5.3) which will coincide exactly with the density matrix corrected to second-order in electron correlation [127, 128]. This means that both approaches will lead to the same prediction of electron currents, as identical one-electron RDMs will predict identical currents.

A way to select an independent particle model for electron transport is to select a set of single particle states yielding an approximate density matrix with maximal overlap to the exact reduced density matrix [129]. The single electron states that diagonalise the RDM are natural orbitals (NOs) [130], and their eigenvalues ρ_{ii} are known as natural occupations. To approximate the exact RDM in equation (5.5), the best

finite expansion $\tilde{\rho}$ is found to minimise the least squares error,

$$\int \mid \rho - \tilde{\rho} \mid^2 \; d\mathbf{r}d\mathbf{r}' = \min, \tag{5.7}$$

which is satisfied by including n NOs with the largest occupancies into the expansion of equation (5.5) [128].

One can consider the coupling between density matrix coefficients by partitioning the density matrix ,

$$\rho = \begin{bmatrix} \rho_{ij} & \rho_{ia} \\ \rho_{ai} & \rho_{ab} \end{bmatrix}, \tag{5.8}$$

using the same index as before for labelling states: (ij) denotes occupied-occupied coupling, (ab) unoccupied-unoccupied and (ia) occupied-unoccupied state interactions, with occupations referring to the zeroth-order wavefunction. The NOs to second-order in electron correlation are given by the eigenfunctions of equation (5.8). Then to build the best single particle approximation, an occupied single Slater determinant of the first N NOs is constructed. Numerically it was shown that a single Slater determinant composed of the largest occupation number of NOs can lead to essentially the same results as many-body treatment for tunnelling through a weakly correlated system such as alkanes [129]. In this case, the density matrix is idempotent, *i.e.* $\rho^2 = \rho$, since only the first N occupations are equal to one and the rest are zero (single determinant approximation). If the coupling between the occupied and unoccupied states becomes stronger (correlation increased), *i.e.* ρ_{ia} and ρ_{ai} in equa-

tion (5.8) increases, then the idempotency condition no longer holds and the single particle approximation is no longer useful as a zeroth-order many-body wavefunction. This has been demonstrated in Chapter 4, where for a strongly coupled system of gold atomic chains and metal coupled BDA, multi-reference behaviour was seen.

So for weak to moderate correlations, the Green's function corrected to second-order in self-energy can achieve improved IPs and EAs. But as natural occupancies in the zeroth-order wavefunction become much less than unity, a perturbation expansion about an independent particle model loses its applicability even when including higher order corrections. This means that the IPs and EAs will be no longer correctly treated. This is especially true for multi-determinant ground states [114] or in strongly correlated electron transport [61, 131, 132].

The above concepts are illustrated using an analytical model where electron-electron correlation is increased by using a numerical parameter. The obtained results are then compared to treating the same junction but using electronic structure theories such as HF and DFT.

5.3 Correlated Analytical Model

In this section, a correlated model is introduced to demonstrate the effect of over- and underestimation of electronegativity on electron transport. A hexatriene molecule bonded between two metal electrodes is considered.

A model Hamiltonian used is

$$\begin{aligned}
\hat{H} &= -\gamma_L \sum_{n<-3} (\hat{c}_n^\dagger \hat{c}_{n-1} + h.c.) \\
&+ \sum_{n<-3} (\epsilon_L + V_L)\hat{c}_n^\dagger \hat{c}_n - \gamma_{LM}(\hat{c}_{-4}^\dagger \hat{b}_{-3} + h.c.) \\
&+ \sum_{n=-3}^{+3} (\epsilon_M + V_n)\hat{b}_n^\dagger \hat{b}_n \\
&- \gamma_M(\hat{b}_{-3}^\dagger \hat{b}_{-2} + \hat{b}_{-1}^\dagger \hat{b}_1 + \hat{b}_2^\dagger \hat{b}_3 + h.c.) - \Gamma_M(\hat{b}_{-2}^\dagger \hat{b}_{-1} + \hat{b}_{-2}^\dagger \hat{b}_{-1} + h.c.) \\
&- \gamma_{MR}(\hat{b}_{+3}^\dagger \hat{c}_{+4} + h.c.) + \sum_{n>+3} (\epsilon_R + V_R)\hat{c}_n^\dagger \hat{c}_n \\
&- \gamma_R \sum_{n>+3} (\hat{c}_n^\dagger \hat{c}_{n+1} + h.c.), \qquad (5.9)
\end{aligned}$$

where *h.c.* stands for "Hermitian conjugate". The hexatriene molecule is modelled as six central sites labelled $-3, -2, -1, 1, 2, 3$ (there is no 0 site) with electron creation operator $\hat{b}^\dagger$ and electron annihilation operator $\hat{b}$. The alternating single and double bonds are represented by Γ_M and γ_M, respectively, and the on-site energy is ϵ_M. While the hexatriene-electrode coupling is determined by $\gamma_L = \gamma_R$. The electron reservoirs (leads) extend to the left and to the right of the molecule and are described $\hat{c}^\dagger$ and $\hat{c}$ electron creation, annihilation operators, respectively. The on-site energy for the lead region is $\epsilon_{R/L}$ for the right (R) and left (L) reservoirs. The voltage applied across the junction is $V_L \neq V_R$ in the reservoirs and the voltage drop V_n across the molecular region is scaled linearly between the values of V_L and V_R.

The eigenstates of the molecular Hamiltonian are found with the electron-electron self-energy, while the exact electrode self-energies are

introduced to describe the molecule coupling to the electrodes.[2]

The resulting single electron states are taken as the expansion functions for the correlated version which is obtained from $\hat{H}_0 \rightarrow \hat{H}_0 + \hat{\nu}$, where $\hat{\nu}$ is the pairwise interactions. Current-voltage characteristics are calculated using equation (5.2). A simplified form of self-energy is used such that the interaction matrix elements in equation (5.6) are approximated as $\langle pq||rs\rangle \approx U$.

In Figure 5.1 the current-voltage $(I-V)$ characteristics are presented. The independent particle model or uncorrelated model occurs for $U = 0$ (labelled as "no $\Sigma^{(2)}$ correction"). Increasing U is equivalent to increasing the electron correlations on the molecular region. At $U = 0$, currents at low voltages are much lower than when the $\Sigma^{(2)}$ correction is allowed to improve the IPs and EAs. So the highest lying occupied states are too low, corresponding to high IPs and the lowest lying unoccupied single electron states are too high, giving too low EAs with respect to the Fermi level. Under these conditions neither occupied nor unoccupied states enter the voltage bias window at low voltages.

Increasing the U parameter, the highest occupied states near the Fermi level enter the bias window at low voltages, while the lower unoccupied states enter at higher voltages. This sequence of introducing the states is due to the relative position of the Fermi level in this system, that is, the Fermi level is closer in energy to the occupied states. That is, introducing correlations on the molecular region shifts up the occupied

[2] It is important to distinguish between electron-electron self-energy which is a correction term to the HF Hamiltonian described in Section 2.7 and the electrode self-energy which describes the effect of a semi-infinite lead, Section 3.2

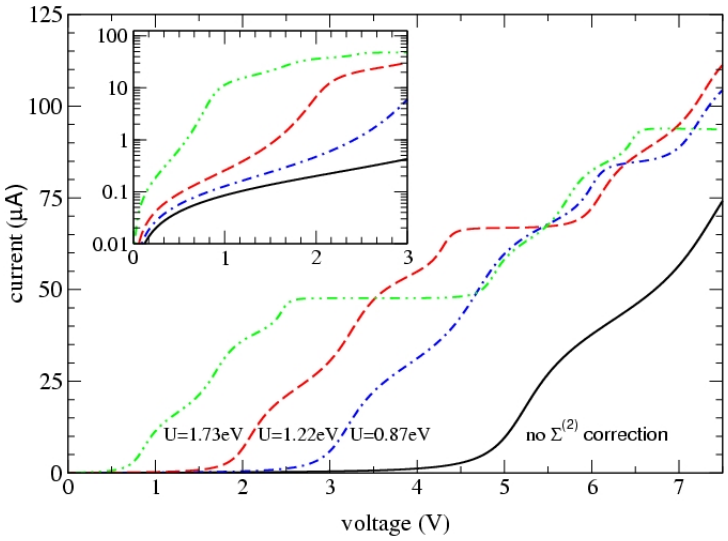

Fig. 5.1: Current-voltage characteristics for the model Hamiltonian. Electronegativity is modified by varying U, with values labelled within the figure. Inset: $I-V$ characteristics with current displayed on a logarithmic scale.

levels relative the Fermi level leading to reduced IP values. Similarly, with increased correlation the lowest lying unoccupied states are lowered in energy leading to the lower EA values. Increasing correlations *via* U keeps reducing IPs and increasing EAs values eventually leading to an underestimated band gap and large current magnitudes. In Figure 5.2 the observed trend for HOMO-LUMO gap as a function of increasing U is shown. It is clear that as correlations are increased, the band gap narrows.

The discussion is taken a step further and electronic structure treatment is applied to this chain-hexatriene-chain junction as an intermediate step before studying a more realistic system. The results for the HOMO-LUMO gap for the molecular region are given in Figure 5.3, illustrating

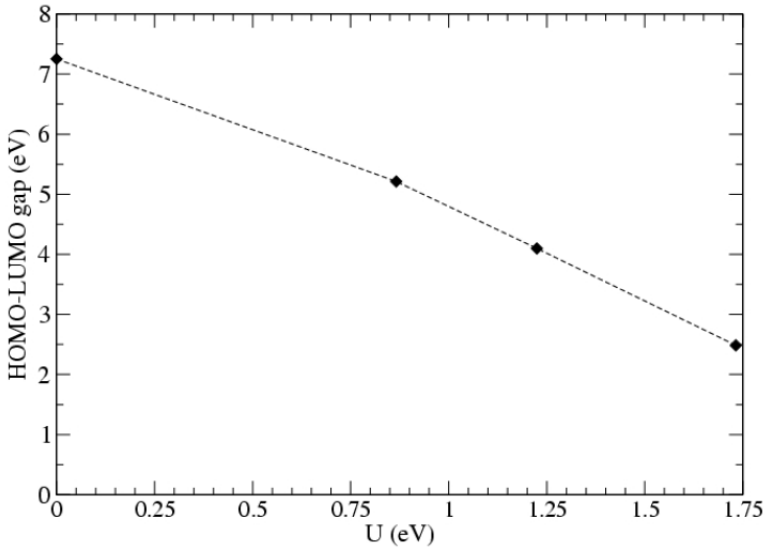

Fig. 5.2: HOMO-LUMO gap for the correlated model defined by equation (5.9) as a function of electron-electron self-energy as varied through interaction parameter U. The reduction in the gap demonstrates the effect of electron correlation on molecular electronegativity.

that the electronegativity on the molecular region changes as different treatments are applied. From this, it is noted that for a large HOMO-LUMO gap or weak electronegativity, charge transfer is small. For small HOMO-LUMO gap, typical of GGA and LDA, the charge transfer is overestimated as illustrated in Figure 5.3. While hybrid functionals correct charge transfer to some extent, this correction is not systematic [133].

5.4 Electronic Structure Theory Results

In this section, the electron transport calculations are carried out for a gold-hexatriene-gold tunnel junction shown in Figure 5.4, using DFT and HF treatments for electronic structure. The relationship between differ-

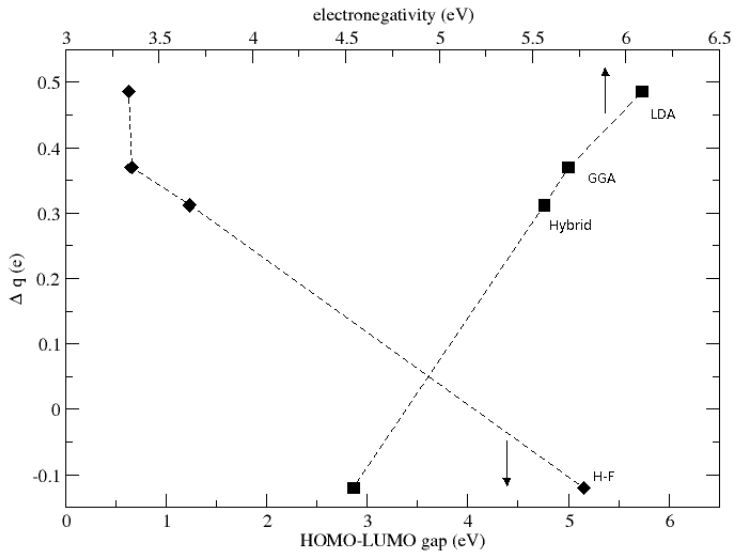

Fig. 5.3: Charge transfer versus HOMO-LUMO energy gap and electronegativity for hexatriene-dithiol bonded to two linear gold chains. Calculations have been performed with the Turbomole [116] program package. The auc-cc-pVDZ basis set was used for all carbon atoms [134] and all the other atoms were treated with split valence polarised basis, including a 60 electron effective core potential for the gold atoms [116].

ent electronic structure treatments and the analytical model system with increasing correlation outlined in the previous section can be compared. The electronic structure calculations are performed with Fock matrices built from the Turbomole [116] package using HF and DFT.

The Turbomole split valence polarised Gaussian basis were used for all atoms on the hexatriene-dithiol molecule. In the gold leads, the three gold atoms in each electrode which bond to the sulphur atoms are also treated with a split valence/polarised basis set in conjunction with a sixty electron effective core potential [116]. All other gold atoms are treated

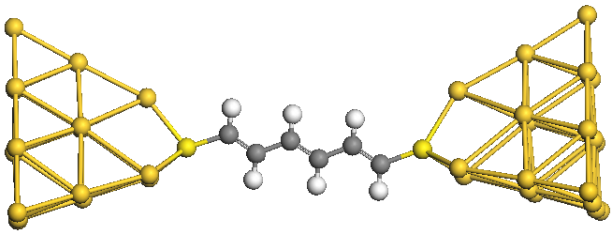

Fig. 5.4: Hexatriene bonded to two gold contacts. The last two planes of the contacts were used to model periodic infinite leads.

with a modified 6s orbital basis set used with a 68 electron effective core potential [115].

Calculations have been performed using HF, DFT with a hybrid exchange-correlation functional (DFT/hybrid), GGA (DFT/GGA), and Local Density Approach (DFT/LDA). In DFT the exact correlation and exchange functionals are not known, however approximations exist, such as hybrid functionals, GGA and local density approach, which are used in these calculations. The B3LYP hybrid functional, so called after Becke for the exchange approximation part, and Lee, Yang and Parr for correlation, is combined with the exact energy from HF theory. Three parameters define the hybrid function, hence B3LYP [135], specifying how much mixing of the exact exchange is chosen. The Perdew, Burke, Ernzerhof GGA functional [117] which improves the description of the local spin density by using the gradient approach is used. For DFT/LDA, the Perdew-Wang (PW) functional [136] is used, where an analytical representation of correlation energy was proposed for a uniform electron gas. A full geometry relaxation is performed on the junction for each

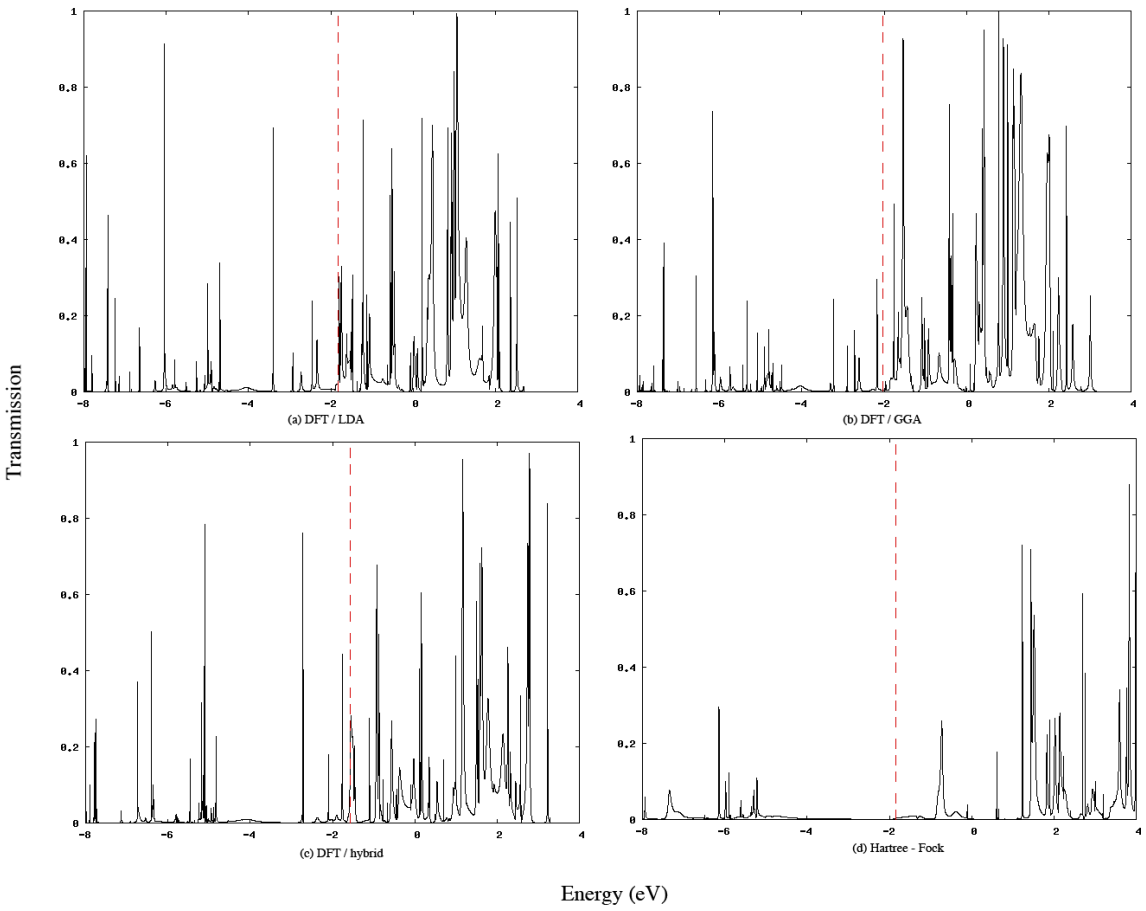

Fig. 5.5: Comparison of electron transmission calculated from different electron structure treatments for the hexatriene-dithiol molecular junction: (a) DFT/LDA, (b) DFT/GGA, (c) DFT/hybrid and (d) HF. The Fermi energy (dashed red line) is taken to be the HOMO energy in the leads.

electronic treatment.

Electron transport is calculated using the Green's function approach implemented within the TiMeS scattering program [101], using the junction Hamiltonians in an atomic orbital basis as extracted from a modified version of Turbomole [116]. The resulting electron transmission as a func-

tion of energy is given in Figure 5.5. As can be seen, the overestimation of electronegativity within the LDA results in a narrow band gap around the Fermi level yielding a higher density of states with the energy range in the transport window. This is similar to having a high correlation regime, that is a large U parameter in terms of the analytical model calculation. On the other hand, the underestimation of electronegativity within the HF approximation results in a low density of states around the Fermi level and within the voltage bias window of a few volts. A comparison can be drawn between the HF band gap and that obtained at $U = 0$.

The current-voltage characteristics are plotted in Figure 5.6 for the hexatriene tunnel junction. Comparing to Figure 5.1, it can be noticed that at the highest value of U and DFT/LDA are comparable, both methods underestimate the band gap and overestimate the transport properties. Similarly, in the single-determinant picture, $U = 0$, the current-voltage curve is comparable to the HF treatment with too small of an electronegativity, too little charge transfer between the molecule and electrodes. The GGA and hybrid approximations tend to lie between the extremes of the LDA and HF approximations, as can be seen in Figure 5.6. Similar findings in the context of the effect of differing exchange-correlation treatments on electron currents have been reported by Thygesen [56] within the context of GW studies. This work focused on the role of improving the electronegativity to improve the overlap to the exact RDM as shown in Section 5.1.

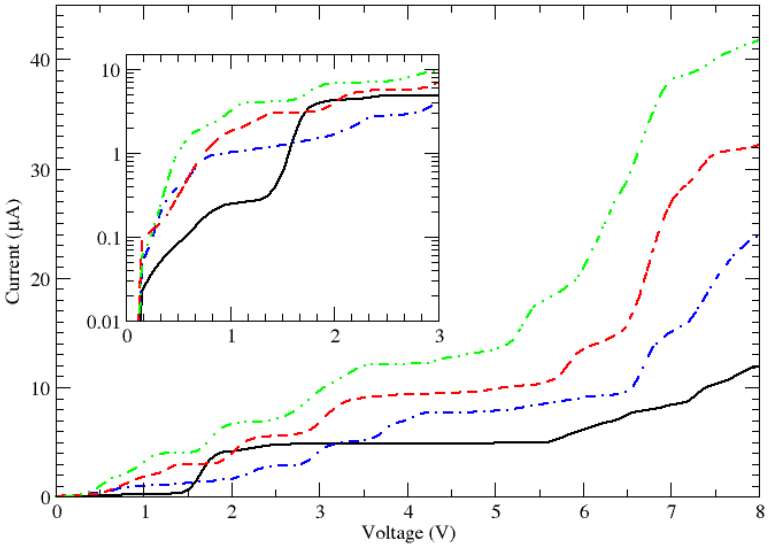

Fig. 5.6: Current-voltage characteristics for the electronic structure calculations of hexatriene bonded between two gold contacts; the colors correspond green-DFT/LDA, red-DFT/GGA, blue-DFT/hybrid, black-HF. Inset: $I-V$ characteristics with current displayed on a logarithmic scale.

5.5 Conclusion

In this chapter, the effect of a correct description of electronegativity on electron current has been studied. Correcting electronegativity is equivalent to maximising overlap to the exact density matrix. The true value of electronegativity is found at the exact density matrix and many-body solution. Improving the description for the IP and EA levels with the methods outlined in Section 5.2 will lead to improved prediction of electron current for medium and weak correlations. This is characteristic

of the electron currents obtained with DFT/GGA and DFT/hybrid. Poor correction for electron correlations results in an overestimated band gap and too low an electron current as was shown to be the case for HF. While overestimating this interaction leads to too narrow a band gap and a large electron current as seen with DFT/LDA treatment. The ability to improve electron transport, within this context, is hence understood as the ability to improve the description of IP and EA levels.

In the case of strong electron-electron correlations, off-diagonal terms of the density matrix in equation (5.8) become important. It then becomes inadequate to use single particle approximations to predict electronegativity and perturbation corrections about a single reference state fail, thus complicating treatment of molecular junctions with Green's function methods. This is also a key limitation of the *GW* approach, as it can not describe multi-reference states explicitly.

Overall, the correct description of electronegativity is improved by explicit treatment of electron correlations which can be achieved within many-body treatments such as CI. The improvement in treating electronegativity will lead to an improved description of the one-electron RDM, and thus to a better description of currents in molecular tunnel junctions.

6. CONCLUSION AND REMARKS

In this thesis, the molecule-metal interface that is formed in single molecule junctions was studied. Electronic structure of a molecule in a junction is different to free species: molecular levels broaden with a lifetime τ and shift from their original positions. The aim of this thesis was to describe and understand the behaviour of such resonances.

The method of CAPs was further developed and enabled the study of electron lifetimes in a junction (Section 3.3.2). The essence of the CAP method is to transmit the information within energy-dependent self-energies to an energy-independent potential, hence the better the CAP mimics the self-energy, the better the approximation. This was validated using an atomic chain model, yielding an excellent agreement between the two methods with varying molecule-electrode coupling, especially in the HOMO-LUMO region of the junctions (demonstrated in Section 4.2.3). Further, the method was used on junctions described within a HF and DFT basis to demonstrate its applicability.

Incorporating CAPs into MCCI as a one-electron operator enabled the study of electron state lifetimes in Chapter 4. Considering atomic gold chain junctions, it was found that lead excitations play a significant role in the description of electronegativity and electron transport.

Including excitations originating from orbitals localised on the molecule only resulted in the electronic spectra qualitatively similar to an isolated molecule. A much broader LUMO state was seen when lead excitations were added within single particle approximation. This state then decoupled upon inclusion of electron correlations, but the resulting energy levels are a complicated consequence of electrode coupling and electron correlation. Similarly, it was seen that a free BDA molecule can be approximately described by a single determinant, while bonding metal electrodes resulted in a strong metal-molecule interaction and multi-reference behaviour within the CI approach.

The electron transport resulting from different electronic structure treatments was studied in Chapter 5, pointing out that an underestimated band gap such as for DFT leads to the conducting states entering the bias window at too low voltages and overestimation of electron current. On the contrary, not including electron correlation corrections as is the case for HF results in an overestimated band gap and too low an electron current. To improve the description of electronegativity means to maximise the overlap of an approximate RDM to the exact density matrix. This conclusion can be achieved *via* a second-order correction in self-energy to the Green's function methods, or second-order density matrix corrections. However, these approximations are only valid in a weak to moderate correlations regime. For strongly correlated systems the off-diagonal interaction elements of the density matrix become important and can only be described by multi-determinant many-body theories. In this work, it has been shown that the use of single-particle methods is not

suitable in the limit of a strong coupling regime (*i.e.* a strong electron-electron interaction). Hence, an explicit treatment of electronegativity achieved through many-body formalisms will lead to a better description of electron correlations and electron transport.

APPENDIX

A. COMPLEX ABSORBING POTENTIALS FOR 3D ELECTRODES

In this appendix[1], the future generalisation needed to apply the CAPs method to 3D electrodes is discussed. In particular, non-Hermitian quantum dynamics are discussed in a greater detail, followed by what causes failure in adiabatic method when evaluating complex eigenvalues in certain systems. In these cases, the adiabatic method for generating a CAP used in this thesis fails, although the general formalism for building the CAP from the open system eigenvalues and eigenvectors remains valid. A proposed solution is provided in the last section of this appendix for constructing CAPs in more general systems.

A.1 Non-Hermitian Quantum Mechanics

In Chapter 3 open systems were discussed in relation to molecular electronics. The CAPs method deals with open systems leading to a non-Hermitian quantum mechanical description. This means that many methods used to describe Hermitian Hamiltonians may not apply or be special cases of a more general non-Hermitian approach. Properties of Hermitian Hamiltonians are considered first, then the difference in the behaviour of

[1] Here, atomic units (a.u.) are used, that is energy is measured in Hartrees.

the eigenvectors and eigenvalues as the system is exposed to the environment is examined.

Before going on to discuss non-Hermitian Hamiltonians, it is useful to consider a symmetric Hermitian time-independent matrix Schrödinger equation [104],

$$\hat{H}|U_j\rangle = \epsilon_j|U_j\rangle, \tag{A.1}$$

where $|U_j\rangle$ is a right-hand vector. For a symmetric Hermitian Hamiltonian, one can write $\hat{H} = \hat{H}^\dagger$, then taking the conjugate transpose of the above gives,

$$\langle U_i|\hat{H} = \langle U_i|\epsilon_i, \tag{A.2}$$

from which the scalar product can be written as

$$\langle U_i|U_j\rangle = \delta_{ij}. \tag{A.3}$$

Since the Hamiltonian is symmetric, the eigenvalues of $\hat{H}$ and $\hat{H}^T$ are equal.

Now a symmetric non-Hermitian Hamiltonian as used in CAP generation is considered. Since the Hamiltonian is non-Hermitian, then $\hat{H} \neq \hat{H}^\dagger$, but it is symmetric yielding $\hat{H} = \hat{H}^T$. Starting with equation (A.1) and taking Hermitian adjoint will not yield the same result as above due non-Hermiticity of the Hamiltonian, instead one has,

$$(\hat{H}|U_j\rangle)^T = (\epsilon_j|U_j\rangle)^T \tag{A.4}$$

with eigenvalues of $\hat{H}$ and $\hat{H}^T$ being equal, one can write the left-hand vectors as,

$$\langle U_i^*|\hat{H} = \langle U_i^*|\epsilon_i, \tag{A.5}$$

which yields the generalised scalar product, the so-called c-product [137, 138], defined as

$$\langle U_i^*|U_j\rangle = \delta_{ij}. \tag{A.6}$$

For ease of notation, $\langle V|$ is used for the left-hand vectors and $|U\rangle$ is used for the right-hand vectors.

The next section will deal with the particular behaviour of non-Hermitian operator's eigenvalues and eigenvectors.

A.2 Complex Resonances and Exceptional Points

It has been seen in Section 3.1 that a resonance encompasses a shift from the starting position in the real part and broadening in the imaginary part of an eigenvalue. If a system with a dense energy spectrum couples to the continuum *via* some coupling constant, then at some values of that coupling parameter the vectors become ill-defined. These points are exceptional points (EPs) and are generally defined as singularities within the eigenvalue space. The EPs are also called crossing point (CP) because the eigenvalues can cross: in imaginary space, when the widths overlap or real space where the trajectories shift. Changes in level repulsion and small changes in width pass into width bifurcation and level clustering [139]. Since in this work only the crossing of eigenvalues is considered,

the terms EP and CP are used interchangeably.

EPs determine the spectroscopic properties of realistic quantum systems in the regime of overlapping resonances [140], that is, almost all systems under realistic conditions where level broadening is similar to level spacing, $\gamma \approx \Delta\epsilon$.

The concept of crossing points is not unique to the field of open quantum systems, but is also prominent in other fields and often under different names, for *e.g.* in scattering theory EPs are observed as double poles of the S-matrix [141]. To best understand the occurrence of EPs, a model used by Rotter and Sadreev consisting of two quantum dots (QDs) attached to two reservoirs and a device region between them as illustrated in Figure A.1 [142] is studied.

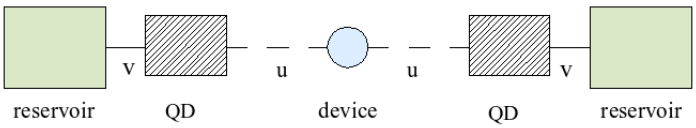

Fig. A.1: A model system used to study the behaviour of crossing points: two single energy level QDs connected to the device region which could be a wire or a molecule and to two semi-infinite reservoirs. Figure from ref. [142].

The model that is used in this thesis for comparison consists of three lead unit cells, the center unit cell will be considered a device region with Hamiltonian $\mathbf{H}_D$; and the QD is comparable to a lead unit cell ($\mathbf{H}_0$) that denotes a lead; the reservoirs having the same role in both models. For simplicity, it is assumed the interaction between the device and QD is symmetric. A major difference between the model from ref. [142] and

the one used in this thesis, is that the interaction between the device region and the leads in this work is described by matrices as oppose to scalar parameters. The bare Hamiltonian is then [142],

$$\mathbf{H}_B = \begin{pmatrix} \epsilon_1 & u & 0 \\ u & \epsilon_D & u \\ 0 & u & \epsilon_1 \end{pmatrix}, \tag{A.7}$$

where u is the coupling between the QD and the device.

Opening a system is achieved by incorporating a self-energy in both models. A varying parameter ν is introduced to control the strength of this coupling in Rotter and Sadreev's model, which can be compared to λ used in the adiabatic coupling method. The solution of the resulting Schrödinger equation is outlined in ref. [142], which leads towards identification of the crossing and diabolic points. Below the relevant findings are outlined:

1. The points of eigenvalue coalescence for a real (closed) system occur when $u = 0$. This leads to diabolic points (DPs) which are not meaningful for a realistic system that interacts with its surrounding and will not be discussed here.

2. For an open system, coalescence of two or more eigenvalues occurs when the states become degenerate. Both coupling parameters u and ν are not zero, thus the system has a realistic character, that is, it interacts with the surrounding. This occurs at different values of u and ν for various systems.

The EPs are accompanied by a shift in the phase of the wavefunctions which become linearly dependant as the norm of the eigenvector diverges. For example, if ψ_k is an eigenvector of $\mathbf{H}$, it can be written as:

$$\psi_k = \sum a_{kl}\psi_l^B, \tag{A.8}$$

where ψ_l^B is the wavefunction of the bare Hamiltonian $\mathbf{H}_B$. If the wavefunction is normalised, then $\sum_l (a_{kl})^2 = 1$ and the c-product normalisation condition is met. However, at the points of coalescence $\mid a_{kl} \mid = \infty$, that is the coefficients of the wavefunction normalised using the c-product diverge [140].

Bearing the QD-device-QD system in mind, with eigenvalues $z_{1,3}$ and eigenvector components a, b, Rotter and Sadreev [142] obtain the diagrams in Figure A.2

The phase shift that is seen at the CP does not appear suddenly but is a gradual effect [139]. The phase change by an angle β is connected to the wavefunction rotation through this angle and the loss of phase rigidity [140], defined as in [143]

$$r_\lambda = \frac{\langle \psi_\lambda^* | \psi_\lambda \rangle}{\langle \psi_\lambda | \psi_\lambda \rangle} = \frac{1}{(Re(\psi_\lambda))^2 + (Im(\psi_\lambda))^2} = \frac{1}{A_\lambda}. \tag{A.9}$$

In approaching an EP, the wavefunction's norm diverges $\langle \psi_\lambda | \psi_\lambda \rangle \equiv A_\lambda \rightarrow \infty$. In a physical sense [140], phase rigidity measures the overlap between a resonance state with one of the scattering states. Some states decouple, that is become sharp single particle states, to a certain extent from the environment, as other states couple to the environment.

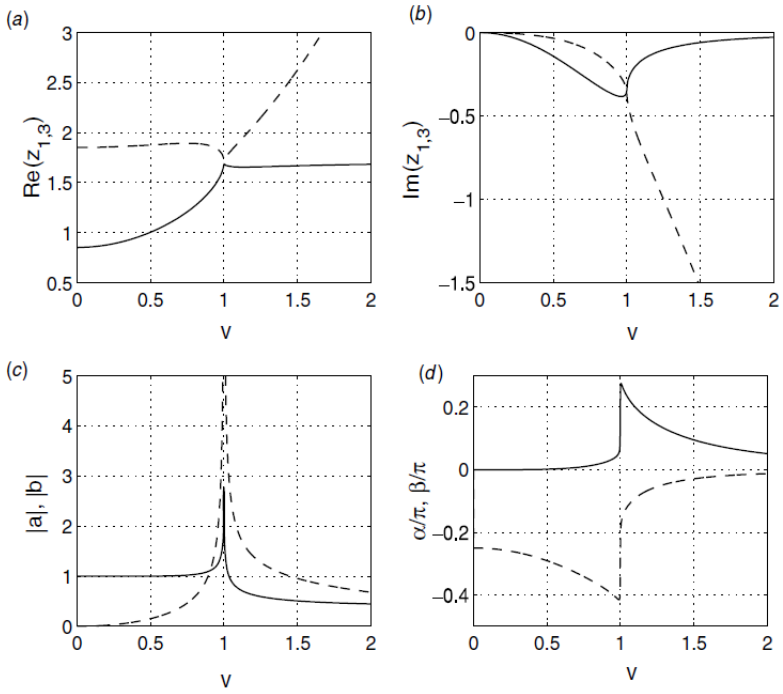

Fig. A.2: An evolution of eigenvalues $z_{1,3}$ and eigenvector components a, b for QD-device-QD system as described in ref. [142]. The behaviour of z_1 (solid lines) and z_3 (dashed lines) showing a crossing point in the real plane in (a) while the eigenvalues avoid cross in the corresponding imaginary plane (b). The components of the eigenvector a (dashed lines) and b (solid lines) are seen to diverge at the critical point in (c), this is accompanied by a phase shift of the maximum of $\pi/4$ at the critical point itself (d). Figure from ref. [142]

To measure the phase change, one needs to define the phase of a starting vector and the open system vector, the difference between these two phases will lead to a jump at the EP [140]. The phase difference is calculated between the phase of ψ_B, *i.e.* the wavefunction of the bare Hamiltonian $\mathbf{H}_B$ and the current state ψ. If the phases of the original vectors are fixed, then $\mid \beta - \beta_B \mid = \pm\pi/4$ at the CP. The phases of the wavefunctions vary on approach of the EP, with only the $\pi/4$ jump

occurring exactly at the CP [139].

In their review of complex absorbing potentials, Santra and Cederbaum also observe the existence of critical points [95]. They illustrate the coalescence using a 2×2 model Hamiltonian in a similar fashion as discussed above based on Rotter and Sadreev's QD-Device-QD system.

Next, the method of generating the CAPs is explained. This involves non-Hermitian mechanics and demonstrates that exceptional points are encountered in general when considering CAPs for electrodes with a dense set of states.

A.3 CAPs for 3D Electrodes

In this section, the development of CAPs concept is taken further and the possibilities to generalise the method to be applicable to general 3D systems is discussed. This is done by considering the algorithm first and then studying the eigenvalue behaviour of a test metal cluster.

A.3.1 Definition of Variables

Since self-energy is a property of a lead, the CAP is also calculated on the lead region. Before the CAP generation algorithm is explained, a summary of the variables used is given in Table A.1.

As in Section 3.3, vectors $\mathbf{U}$ and $\mathbf{V}$ with eigenvalues ω_i result from solving equations 3.23 and 3.24, while $\mathbf{X}$ and ϵ_i are those of the bare Hamiltonian at $\lambda = 0$.

Variable	Description
λ	adiabatic coupling constant that varies from $\lambda = 0$ to $\lambda = 1$
m	number of intervals between $\lambda = 0$ and $\lambda = 1$
$\delta\lambda$	one interval λ/m
λ_m	value of λ at the m'th step
λ_{m-1}	value of λ at the $(m-1)$'th step
J_{Opt}	index at which best overlap of U_{λ_m} and $U_{\lambda_{m-1}}$ is achieved

Tab. A.1: A summary of variables used in describing the CAPs algorithm.

A.3.2 Algorithm

The adiabatic coupling of a closed region (device) to that of the continuum states (electrodes) relies on the idea that, provided the adiabatic steps are small enough, the trajectory of eigenvalues will be smooth. This is the basis for the current CAP method. Let us assume the calculation is defined to have m steps between $\lambda = 0$ and $\lambda = 1$, then let $\lambda_m = m\delta\lambda$ and $\lambda_{m-1} = (m-1)\delta\lambda$. For each λ_m, the new Hamiltonian $\mathbf{H}_0 + \lambda_m\mathbf{\Sigma}_L + \lambda_m\mathbf{\Sigma}_R$ is evaluated leading to a new matrix of complex eigenvalues, $\boldsymbol{\omega}_{\lambda_m}$ and corresponding left and right eigenvectors $\mathbf{U}_{\lambda_m}$ and $\mathbf{V}_{\lambda_m}$. Figure A.3 outlines the steps in the algorithm.

The process of calculating the eigenvalue ω_{λ_m} and the eigenvectors $|U_{\lambda_m}\rangle$, $\langle V_{\lambda_m}|$ is initiated by obtaining two sets of ω_{λ_m} shown in Figure A.3a. First, the expectation value of the new operator, $\langle\omega_{exp_m}\rangle$ is evaluated using the vectors from previous iteration

$$\langle\omega_{exp_m}\rangle = \frac{\mathbf{V}_{\lambda_{m-1}}[\mathbf{H_0} + \mathbf{\Sigma}_L(\omega_{\lambda_{m-1}}) + \mathbf{\Sigma}_R(\omega_{\lambda_{m-1}})]\mathbf{U}_{\lambda_{m-1}}}{\mathbf{V}_{\lambda_{m-1}}\mathbf{S}_0\mathbf{U}_{\lambda_{m-1}}}, \qquad \text{(A.10)}$$

assuming that U_{λ_m} approaches $U_{\lambda_{m-1}}$ adiabatically, the above expectation value will be a good initial guess for the eigenvalues of the current step.

Secondly, the matrix of eigenvalues $\boldsymbol{\omega}_{\lambda_m}$ is obtained from solving $\mathbf{H}_0 + \lambda_m \boldsymbol{\Sigma}_L(\omega_{exp_m}) + \lambda_m \boldsymbol{\Sigma}_R(\omega_{exp_m})$. The difference between $\langle \omega_{exp_m} \rangle$ and each value ω_{λ_m} is calculated, if there is an eigenvalue that matches $\langle \omega_{exp_m} \rangle$ within a specified tolerance (stated as "Tol" in Figure A.3b), it is chosen. Otherwise, one solves for a suitable ω_i self-consistently as shown in Figure A.3b.

Within the self-consistent loop for finding the best matching eigenvalue to $\langle \omega_{exp_m} \rangle$, the algorithm searches for the vector that most closely resembles the $U_{\lambda_{m-1}}$ (or $V_{\lambda_{m-1}}$) state. Let a measure of the overlap $\mathfrak{S}_{\lambda_m \lambda_{m-1}}$ between vectors the m'th and $(m-1)$'th iterations be calculated as,

$$\begin{aligned} \mathfrak{S}_{\lambda_m \lambda_{m-1}} = & \left[\left[\frac{[\mathbf{V}_{\lambda_m} \mathbf{S}_0 \mathbf{V}_{\lambda_{\mathbf{m-1}}}][\mathbf{U}_{\lambda_m} \mathbf{S}_0 \mathbf{U}_{\lambda_{\mathbf{m-1}}}]}{[\mathbf{V}_{\lambda_m} \mathbf{S}_0 \mathbf{V}_{\lambda_{\mathbf{m}}}][\mathbf{U}_{\lambda_m} \mathbf{S}_0 \mathbf{U}_{\lambda_{\mathbf{m}}}]} \right] \right. \\ & \left. \times \left[\frac{[\mathbf{V}_{\lambda_m} \mathbf{S}_0 \mathbf{V}_{\lambda_{\mathbf{m-1}}}][\mathbf{U}_{\lambda_m} \mathbf{S}_0 \mathbf{U}_{\lambda_{\mathbf{m-1}}}]}{[\mathbf{V}_{\lambda_m} \mathbf{S}_0 \mathbf{V}_{\lambda_{\mathbf{m}}}][\mathbf{U}_{\lambda_m} \mathbf{S}_0 \mathbf{U}_{\lambda_{\mathbf{m}}}]} \right]^* \right]^{3/2} \end{aligned} \tag{A.11}$$

with the maximum value of $\mathfrak{S}_{\lambda_m \lambda_{m-1}} \approx 1$ corresponding to the best matching index (J_{Opt} in the flow chart Figure A.3) and consequently the correct eigenvalue and set of right and left eigenvectors for the m'th step. If $\mathbf{U}_{\lambda_m}$ and $\mathbf{U}_{\lambda_{m-1}}$ are similar, then the value of $\frac{\mathbf{U}_{\lambda_m} \mathbf{S}_0 \mathbf{U}_{\lambda_{m-1}}}{\mathbf{U}_{\lambda_m} \mathbf{S}_0 \mathbf{U}_{\lambda_m}}$ will be close to 1. Similarly for $\mathbf{V}_{\lambda_m}$ and $\mathbf{V}_{\lambda_{m-1}}$. The factor of 3/2 is a heuristic factor that amplifies the deviation from unity for numerical purposes. The self-consistent procedure, Figure A.3b is repeated until convergence is reached and the closest eigenvalue obtained. The algorithm then continues on to the next index and value of λ. Upon reaching $\lambda = 1$, a complete array of new complex energies and vectors is obtained, Figure A.3c. The

construction of the CAP is in practice done using the final eigenvalues ω_i obtained at $\lambda = 1$ but using the initial real eigenvectors from $\lambda = 0$, that is,

$$\mathbf{W} = \mathbf{S}_0 \mathbf{X} \boldsymbol{\omega} \mathbf{X}^\dagger - \mathbf{H}_0, \tag{A.12}$$

with $\mathbf{S}_0$ a diagonal metric. The reason why this approximation is used is to express the CAP in the real MO basis, facilitating its use in the subsequent CI calculations. The dimensions of $\mathbf{W}$ are the same as of the lead region Hamiltonian $\mathbf{H}_0$ on which it was calculated.

As has been shown in Section A.1, at an EP two or more eigenvectors may become linearly dependant. That is, it is no longer possible to choose just one $\mathbf{U}_{\lambda_m}$ or $\mathbf{V}_{\lambda_m}$ that corresponds well to $\mathbf{U}_{\lambda_{m-1}}$ or $\mathbf{V}_{\lambda_{m-1}}$. This condition is investigated further next.

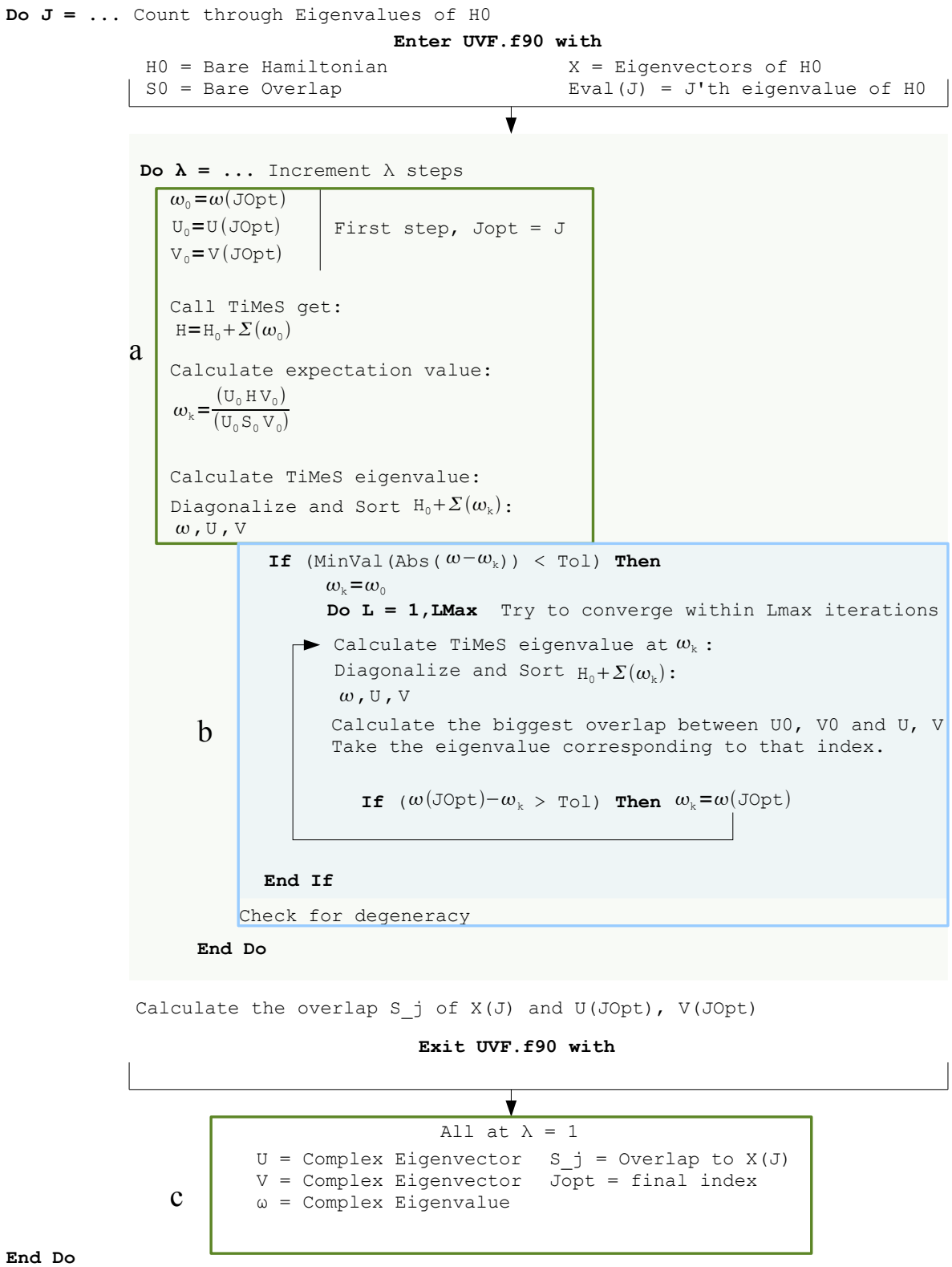

Fig. A.3: Flow chart of building a CAP as is implemented in the current version of algorithm. (a) initiation of algorithm and evaluation of two sets of complex eigenvalues, (b) self-consistent calculation of eigenvalues, (c) final eigenvalues and eigenvectors are obtained.

Behaviour at Exceptional Points

The origin and behaviour of EPs have been discussed in Section A.2. Here the numerical consequences of encountering an EP within the CAPs approach are highlighted. A lead unit cell of sixteen gold atoms arranged into alternating 10 and 6 atom planes is considered and is shown schematically in Figure A.3.2. Three such unit cells are taken so that to obtain inter-cell interaction matrices $\mathbf{H}_{1L}$ and $\mathbf{H}_{1R}$. The atoms are treated with a modified $6s$ orbital basis set used with a 68 electron effective core potential [115], and HF orbitals are used.

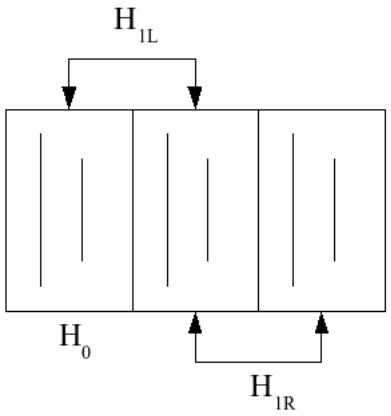

Fig. A.4: A schematic representation of a region on which the CAP is calculated. The left $\mathbf{W}_L$ and right $\mathbf{W}_R$ matrices are calculated separately and summed together to give the overall CAP.

The size of the $\mathbf{H}_0$ matrix is determined by the number of atoms and basis orbitals present,

$$N = \sum_{i}^{N_{total}} N^i_{atoms} \times N^i_{orbitals}$$

thus leading to a 16×16 matrix and 16 eigenvalues. The complex eigenvalue problem, equations (3.23) and (3.24) are solved until the corresponding ω_i value is obtained at $\lambda = 1$, as outlined in Section A.3. The Hamiltonian $\mathbf{H}_0$ is not sparse due to the fact that each atom interacts with a large number of other atoms in a cell.

At certain values of λ_m, the ill-defined behaviour of eigenvectors is seen which inhibit convergence of the self-consistent loop. This behaviour is shown to indicate approaching an EP [95, 140]. Three occupied energy states in close proximity of each other as in Table A.2 are considered.

Eigenvalue #	Value (H)
5	-0.2400
6	-0.2393
7	-0.2261

Tab. A.2: Three occupied energy states of a 16 atom lead unit cell that are used to demonstrate crossing points. Eigenvalues 5 and 6 can be thought of as nearly degenerate.

The calculation is initiated at the 7'th eigenvalue, ϵ_7, and its evolution, as a function of m steps from $\lambda = 0$ to $\lambda = 1$ as the system is opened is followed. In Figure A.5, it is clearly seen that a sudden change in both real and imaginary components of ω_7 occur. To investigate this further, the calculation was repeated, changing m to see if the sudden jump occurred regardless of the interval size, as illustrated in Figure A.5. It is clear that a shift in eigenvalues is seen in approximately the same region, independent of m. It is believed this is a signature of an EP being approached and consequently, characteristic irregular behaviour of the eigenvectors should be observed [95, 140].

This is investigated further by keeping λ_m stationary at a fixed value just before the energy jump and studying the behaviour of the self-consistent loop.

The self-consistent loop is allowed to have 1000 cycles to reach a convergence tolerance of 10^{-2} as the evolution of ϵ_7 towards ω_7 is followed. In this context, a cycle is defined as one evaluation of the self-consistent routine in Figure A.3b, where "Lmax" corresponds to the maximum number of cycles, *i.e.* 1000. In Figures A.6a and A.7 oscillations in resonance components are seen. This is due to different indices controlled by $\mathfrak{S}_{\lambda_m\lambda_{m-1}}$ in equation (A.11) being chosen, which indicates a mixing of vectors at this point in the adiabatic evolution of the eigenvalue. Since the vectors are becoming linearly dependent as the EP is approached, it means that more than one vector can be picked to match $U_{\lambda_{m-1}}$ (or $V_{\lambda_{m-1}}$) which means that vectors are no longer even approximately orthogonal and, hence, are mixing. This is illustrated in Figure A.8a. It is clear that the points of eigenvalue oscillations coincide with the change of index of a newly picked eigenvector. This is because at a certain given self-consistent cycle, several linearly dependent vectors produce a good match to $U_{\lambda_{m-1}}$ (or $V_{\lambda_{m-1}}$). In Figure A.8b the irregular behaviour of $\mathfrak{S}_{\lambda_m\lambda_{m-1}}$ is plotted. In an ideal adiabatic scenario the value of $\mathfrak{S}_{\lambda_m\lambda_{m-1}}$ will remain close to one to allow for a smooth evolution from ϵ_i to ω_i. Instead, it is observed that two other indices U_5 and U_6 interact with U_7, thus indicating that $\mathfrak{S}_{\lambda_m\lambda_{m-1}} \neq 1$ for any single eigenvector. This mixing of eigenvectors and eigenvalues is difficult to resolve and highlights the ill-defined behaviour of an EP.

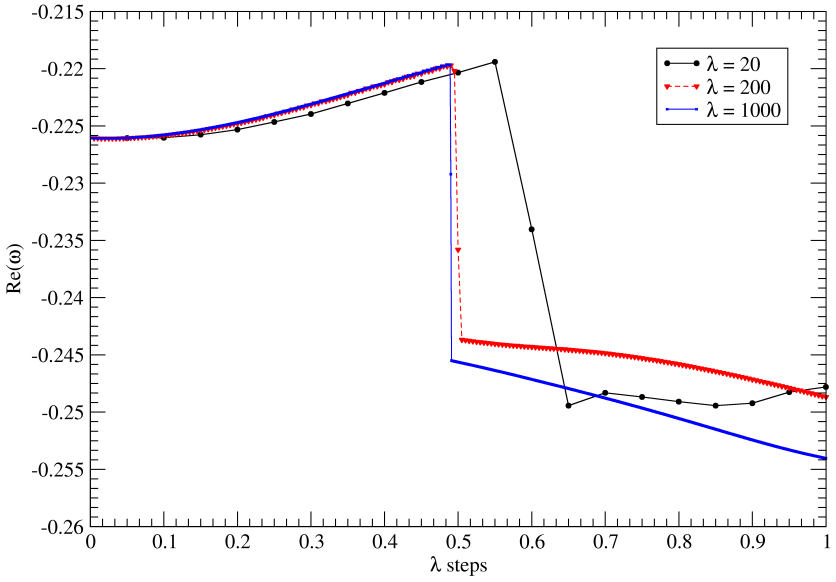

(a)

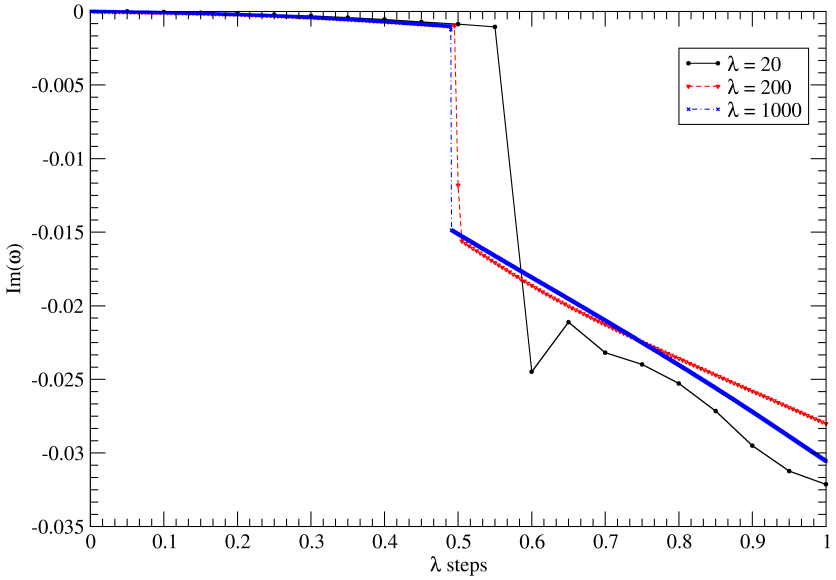

(b)

Fig. A.5: The energy shifts in the real (a) and imaginary (b) components of ω_7 with varying λ. The jump occurs approximately at the same point for the smaller intervals of $m = 200$ and $m = 1000$.

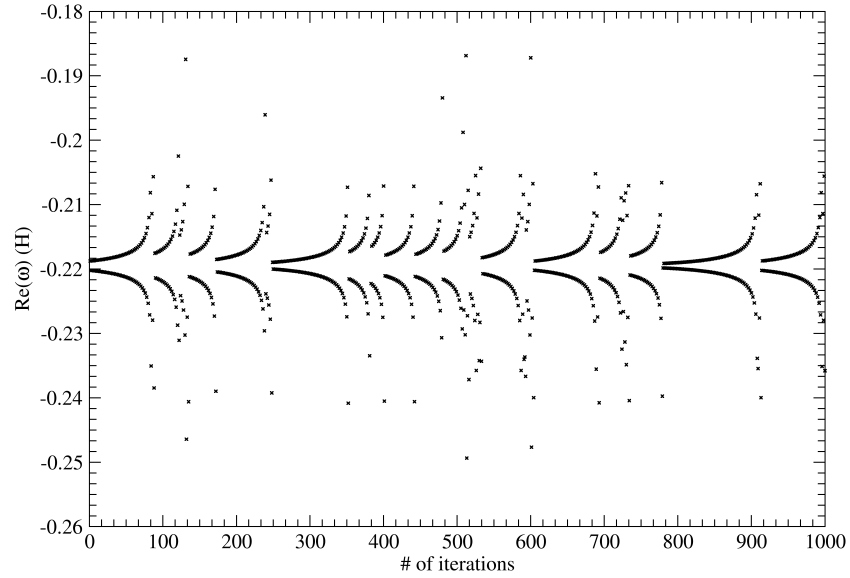

(a) Behaviour of the real component of the complex resonance ω_7 at one single stationary λ_m point. The x axis gives the number of self-consistent iterations allowed to obtain convergence.

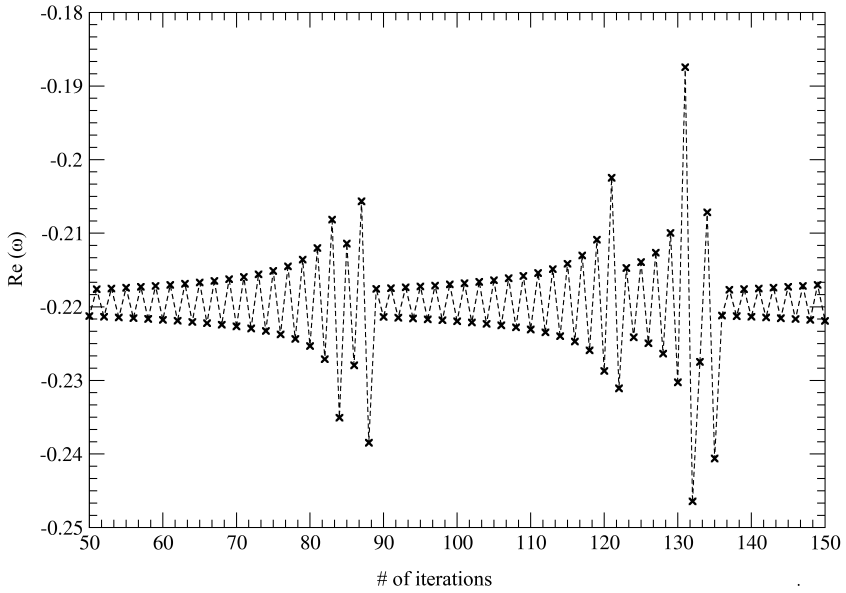

(b) Close-up of the oscillations region with a dashed lined used to indicate the behaviour.

Fig. A.6: Behaviour of the real component of ω_7 at a single λ_m point.

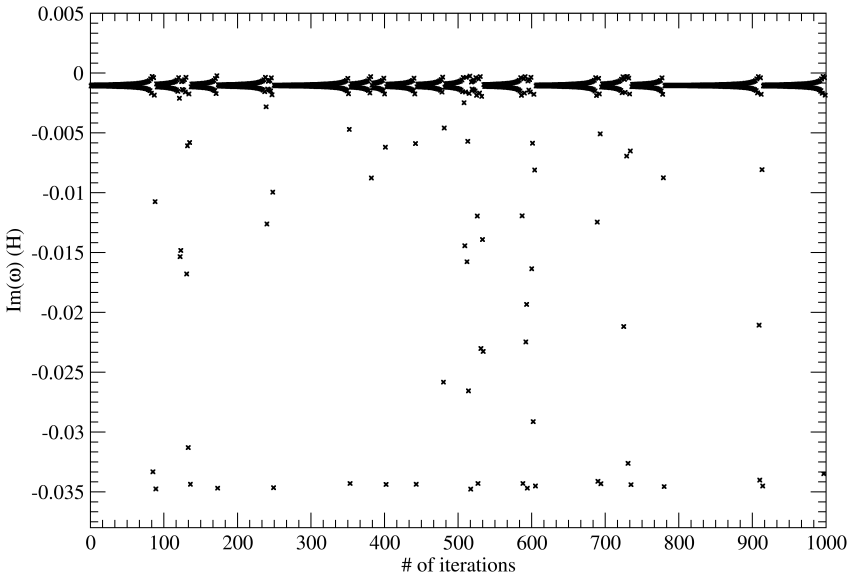

Fig. A.7: Behaviour of the imaginary component of the complex resonance ω_7 at one single λ_m point. Similar oscillations for the real component are observed at the same self-consistent iteration values.

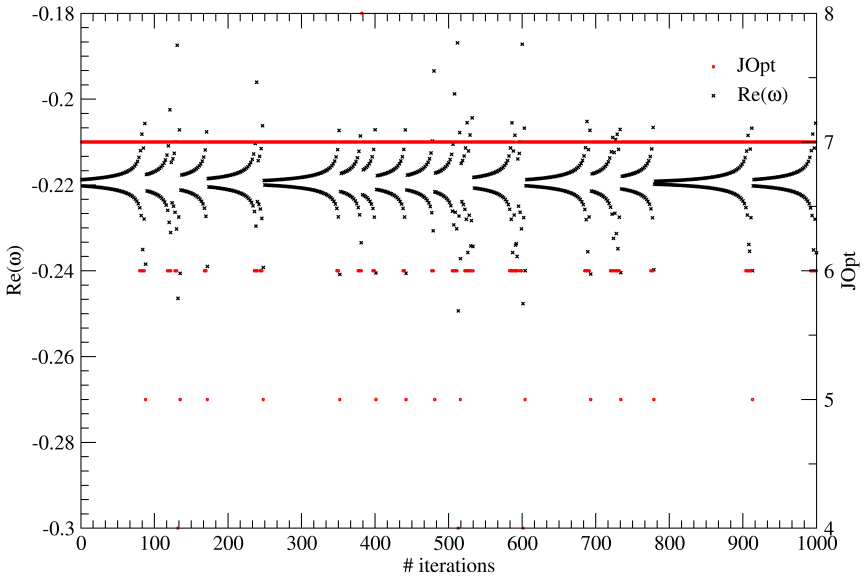

(a) Change of original eigenvalue index, JOpt, is observed at the same points where both real and imaginary components of ω_7 resonance oscillate.

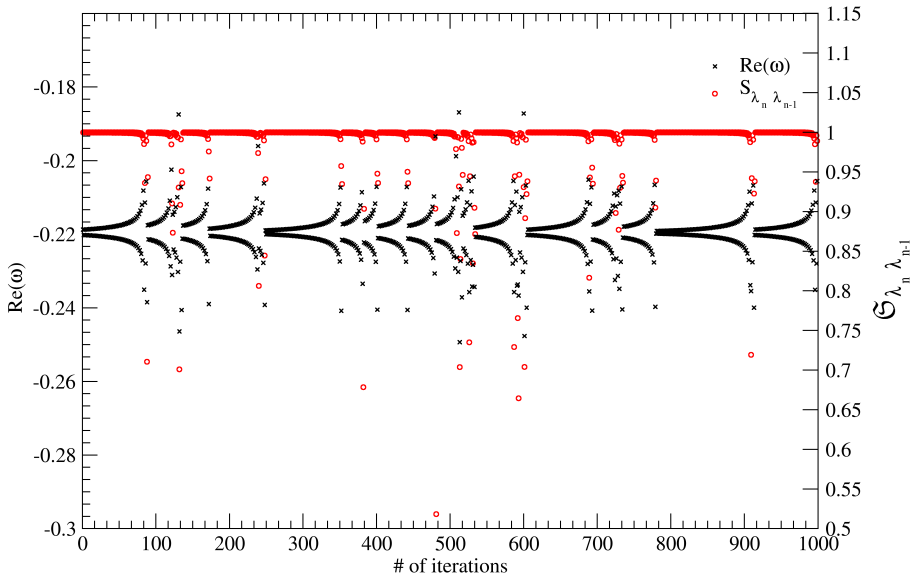

(b) Behaviour of the real component of energy superimposed with the varying values of $\mathfrak{S}_{\lambda_m \lambda_{m-1}}$ indicating that oscillating behaviour of energy corresponds to the points of linear dependence of eigenvectors.

Fig. A.8: Oscillating behaviour of ω_7 complex resonance for a fixed λ_m value.

A.4 Conclusion

In this appendix the challenges in constructing a CAP for 3D electrodes with densely packed energy levels was highlighted. The adiabatic coupling method fails to describe the behaviour of the eigenvalues and eigenvectors of such systems and a new methodology is needed to identify the correct energy and corresponding states of the open system needed to define the CAP.

Another approach that it is thought should overcome some of the discussed challenges is a grid method. Instead of assuming adiabatic behaviour, this method will divide the eigenvalue space into an equally spaced grid. The essence of the grid method is to avoid evaluating the $\mathbf{H}_0+\mathbf{\Sigma}_L+\mathbf{\Sigma}_R$ Hamiltonian at each eigenvalue of $\mathbf{H}_0$ but instead at the grid points. This means that the eigenvalues which could potentially become EPs will be avoided. The grid range must extend beyond the minimum and maximum values of ϵ_i to allow for the shift and broadening of the final complex resonance ω_i. The knowledge of how the system might potentially behave is required *a priori* to determine the size of the grid. At each grid point, the eigenvalue will be calculated self-consistently and stored. If convergence cannot be reached within the self-consistent routine, then this eigenvalue can be discarded, thus taking out points from the grid. It should be noted that the resulting CAP matrix $\mathbf{W}$ should be of the same dimensions as the bare Hamiltonian $\mathbf{H}_0$ of a lead unit cell, therefore a method should be developed to have the same number of final complex energies ω_i as there was starting eigenvalues ϵ_i to avoid

rectangular matrices. Another point to consider is the construction of the CAP: currently due to the adiabatic coupling the final resonances ω_i could be related to the initial energy states ϵ_i and their corresponding vectors $\mathbf{X}$, however in the grid method this will not be the case. As the adiabatic approximation breaks down, the correlation between the states of the closed and open systems is lost. Hence the CAP needs to be constructed using the complex basis $\mathbf{U}$ and $\mathbf{V}$ of ω_i of the open system.

B. LIST OF ACRONYMS

a.u. atomic units

AO atomic orbital

BDA benzene-di-amine

BDT benzene-di-thiol

CAP complex absorbing potential

CI configuration interaction

CP crossing point

CSF configuration state function

DFT Density Functional Theory

DP diabolic point

EA electron affinity

EDG electron donating group

EM extended molecule

EP exceptional point

EWG electron withdrawing group

FCI full configuration interaction

GGA Generalized Gradient Approach

HF Hartree-Fock

HOMO highest occupied molecular orbital

IETS inelastic electron tunnelling spectroscopy

IP ionisation potential

IR infra-red

KS Kohn-Sham

LCAO linear combination of atomic orbitals

LDA Local Density Approach

LUMO lowest unoccupied molecular orbital

MCBJ mechanically controllable break junctions

MCCI Monte-Carlo configuration interaction

MO molecular orbital

MP Møller-Plesset

NEGF non-equilibrium Green's function

NO natural orbital

PL principal layer

QD quantum dot

RDM reduced density matrix

SCF self-consistent field

SES smooth exterior scaling

STM scanning tunnelling microscope

TERS tip-enhanced Raman spectroscopy

TiMeS Transport in mesoscopic systems

UPS ultraviolet photoelectron spectroscopy

BIBLIOGRAPHY

[1] G. E. Moore. Cramming more components onto integrated circuits. *Electronics*, 65(8), 1965.

[2] Y. Xue, S. Datta, and M. A. Ratner. Charge transfer and "band lineup" in molecular electronic devices: A chemical and numerical interpretation. *J. Chem. Phys.*, 115(9):4292–4299, 2001.

[3] S. Datta. *Quantum Transport: Atom to Transistor*. Cambridge University Press, 2005.

[4] T. Henderson, G. Fagas, E. Hyde, and J. C. Greer. Determination of complex absorbing potentials from the electron self-energy. *J Chem Phys*, 125:244104, 2006.

[5] A. Aviram and M. A Ratner. Molecular rectifiers. *Chem. Phys. Lett.*, 29(2):277–283, 974.

[6] C. Joachim and M. A. Ratner. Molecular electronics: some views on transport junctions and beyond. *Proceedings of the National Academy of Sciences of the United States of America*, 102(25):8801–8, 2005.

[7] A. Nitzan and M. A. Ratner. Electron transport in molecular wire junctions. *Science*, 300(5624):1384–9, 2003.

[8] G. Cuniberti, G. Fagas, and K. Richter. *Introducing Molecular Electronics*. Springer, 2005.

[9] R. L. McCreery, H. Yan, and A. J. Bergren. A critical perspective

on molecular electronic junctions: There is plenty of room in the middle. *Phys. Chem. Chem. Phys.*, 15(4):1065–1081, 2013.

[10] M. Tsutsui and M. Taniguchi. Single molecule electronics and devices. *Sensors*, 12:7259–7298, 2012.

[11] K. Moth-Poulsen and T. Bjornholm. Molecular electronics with single molecules in solid-state devices. *Nature Nanotech.*, 4:551–556, 2009.

[12] N. J. Tao. Electron transport in molecular junctions. *Nature Nanotechnology*, 1(3):173–81, 2006.

[13] L. Venkataraman, J. E. Klare, I. W. Tam, C. Nuckolls, M. S. Hybertsen, and M. L. Steigerwald. Single-molecule circuits with well-defined molecular conductance. *Nano Lett.*, 6(3):458–62, 2006.

[14] M. S. Hybertsen, L. Venkataraman, J. E. Klare, A. C. Whalley, M. L. Steigerwald, and C. Nuckolls. Amine-linked single-molecule circuits: systematic trends across molecular families. *J. Phys.: Condens. Matt.*, 20(37):374115, 2008.

[15] M. Dell'Angela, G. Kladnik, A. Cossaro, A. Verdini, M. Kamenetska, I. Tamblyn, S. Y. Quek, J. B. Neaton, D. Cvetko, A. Morgante, and L. Venkataraman. Relating energy level alignment and amine-linked single molecule junction conductance. *Nano Lett.*, 10(7):2470–2474, 2010.

[16] C. Bruot, J. Hihath, and N. Tao. Mechanically controlled molecular orbital alignment in single molecule junctions. *Nature Nanotech.*, 7:35–40, 2012.

[17] Y. Kim, T. Pietsch, A. Erbe, W. Belzig, and E. Scheer. Benzedithiol: A broad-range single-channel molecular conductor. *Nano Lett.*, 11:3734–3738, 2011.

[18] C. D. Lindstorm, M. Muntwiler, and X.-Y. Zhu. Electron transport across the alkanethiol self-assembled monolayer/au(111) interface: Role of chemical anchor. *J. Phys. Chem.*, 109(46):21492–21495, 2005.

[19] G. Fagas and J. C. Greer. Tunnelling in alkanes anchored to gold electrodes via amine end groups. *Nanotech.*, 18(42), 2007.

[20] M. A. Reed, C. Zhou, C. J. Muller, T. P. Burgin, and J. M. Tour. Conductance of a molecular junction. *Science*, 278(5336):252–254, 1997.

[21] F. Chen, X. Li, J. Hihath, Z. Huang, and N. Tao. Effect of anchoring groups on single-molecule conductance: Comparative study of thiol-, amine-, and carboxylic-acid-terminated molecules. *J. Am. Chem. Soc.*, 128(49):15874–15881, 2006.

[22] W. Chen, J. R. Widawsky, H. Váquez, S. T. Schneebeli, M. S. Hybertsen, R. Breslow, and L. Venkataraman. Highly conducting conjugated molecular junctions covalently bonded to gold electrodes. *J. Am. Chem. Soc.*, 133(43):17160–17163, 2011.

[23] B. Xu, H. He, and N. J. Tao. Controlling the conductance of atomically thin metal wires with electrochemical potential. *J. Am. Chem. Soc.*, 124(45):13568–13575, 2002.

[24] R. Landauer. Spatial variation of currents and fields due to localized scatterers in metallic conduction. *IBM Journal of Research and Development*, 1(3):223, 1957.

[25] J. I. Pascual, J. Mendez, J. Gomez-Herrero, A. M. Baro, N. Garcia, and V. T. Binh. Quantum contact in gold nanostructures by scanning tunneling microscopy. *Phys. Rev. Lett.*, 71(12):1852–1855, 1993.

[26] H. Ohnishi, Y. Kondo, and K. Takayanagi. *Nature*, 395(22), 1998.

[27] C. Joachim, J. K. Gimzewski, and A. Aviram. Electronics using hybrid-molecular and mono-molecular devices. *Nature*, page 541, 2000.

[28] B. Xu and N. J. Tao. Measurement of single-molecule resistance by repeated formation of molecular junctions. *Science*, 301(5637):1221–1223, 2003.

[29] H. Park, J. Park, A. K. L. Lim, E. H. Anderson, A. P. Alivisatos, and P. L. McEuen. Nanomechanical oscillations in a single c60 transistor. *Nature*, 407:57–60, 2000.

[30] M. Tsutsui, M. Taniguchi, K. Shoji, K. Yokota, and T. Kawai. Inelastic electron tunneling spectroscopy of single-molecule junctions using a mechanically controllable break junction. *Nanotech.*, 20:434008, 2009.

[31] H. Song, Y. Kim, H. Jeong, M. A. Reed, and T. Lee. Intrinsic charge transport of conjugated organic molecules in electromigrated nanogap junctions. *J. App. Phys.*, 109:102419, 2011.

[32] C. J. Muller, J. M. Krans, T. N. Todorov, and M. A. Reed. Quantization effects in the conductance of metallic contacts at room temperature. *Phys. Rev. B*, 53(3):1022–1025, 1996.

[33] S. Kubatkin, A. Danilov, M. Hjort, J. Cornil, J. L. Bredas, N. Stuhr-Hansen, P. Hedegard, and T. Bjornholm. Single-electron transistor of a single organic molecule with access to several redox states. *Nature*, 425(6959):698–701, 2003.

[34] X. Xiao, B. Xu, and N. J. Tao. Measurement of single molecule conductance: Benzenedithiol and benzenedimethanethiol. *Nano Lett.*, 4(2):267–271, 2004.

[35] A. Kumar, R. Hembuch, B. Poelsema, and H. J. Zandvliet. Controlled transport through a single molecule. *J. Phys. Condens. Matter*, 24:082201, 2012.

[36] L. Venkataraman, J. E. Klare, C. Nuckolls, M. S. Hybertsen, and M. L. Steigerwald. Dependence of single-molecule junction conductance on molecular conformation. *Nature*, 442(7105):904–7, 2006.

[37] M. Frei, S. V. Aradhya, M. Koentopp, M. S. Hybertsen, and L. Venkataraman. Mechanics and chemistry: Single molecule bond rupture forces correlate with molecular backbone structure. *Nano Lett.*, 11:1518–1523, 2011.

[38] L. Venkataraman, Y. S. Park, A. C. Whalley, C. Nuckolls, M. S. Hybertsen, and M. L. Steigerwald. Electronics and chemistry: varying single-molecule junction conductance using chemical substituents. *Nano Lett.*, 7(2):502–6, 2007.

[39] J. Klein, A. Leger, M. Belin, and D. Defourneau. Inelastic electron-tunneling spectroscopy of metal-insulator-metal junctions. *Phys. Rev. B*, 7(6):2336–2348, 1973.

[40] H. Song, Y. Kim, Y. H. Jang, H. Jeong, M. A. Reed, and T. Lee. Observation of molecular orbital gating. *Nature*, 402:1039–1043, 2009.

[41] M. Galperin, M. A. Ratner, and A. Nitzan. Inelastic electron tunneling spectroscopy in molecular junctions: Peaks and dips. *J. Chem. Phys.*, 121(23):11965–11979, 2004.

[42] K. W. Hipps and U. Mazur. Inelastic electron tunneling spectroscopy: An alternative molecular spectroscopy. *J. Phys. Chem.*, 97(30):7803–7814, 1993.

[43] Z. Liu, S-Y. Ding, Z-B. Chen, X. Wang, J-H. Tian, J.R. Anema, X-S. Zhou, D-Y. Wu, B-W. Mao, X. Xu, B. Ren, and Z-Q Tian. Revealing the molecular structure of single-molecule junctions in different conductance states by fishing-mode tip-enhanced raman spectroscopy. *Nat. Commun.*, 2(305), 2011.

[44] E. Bailo and V. Deckert. Tip-enhanced raman scattering. *Chem. Soc. Rev.*, 37:921–930, 2008.

[45] F. Mirjani, J. M. Thijssen, and M. A. Ratner. Probing charge states in molecular junctions using Raman spectroscopy. *J. Phys. Chem. C*, 116(43):23120–23129, 2012.

[46] R. Stadler. Conformation dependence of charge transfer and level alignment in nitrobenzene junctions with pyridyl anchor groups. *Phys. Rev. B*, 81(16):165429, 2010.

[47] R. Stadler and K. W. Jacobsen. Fermi level alignment in molecular nanojunctions and its relation to charge transfer. *Phys. Rev. B*, 74(16):161405, 2006.

[48] J. B. Neaton, M. S. Hybertsen, and S. G. Louie. Renormalization of molecular electronic levels at metal-molecule interfaces. *Phys. Rev. Lett.*, 97(21):216405, 2006.

[49] R. Stadler. Fermi level alignment in single molecule junctions and its dependence on interface structure. *J. Phys.: Conference Series*, 61(1):1097, 2007.

[50] K. Stokbro, J. Taylor, M. Brandbyge, J.-L. Mozos, and P. Ordejón. Theoretical study of the nonlinear conductance of di-thiol benzene coupled to au(111) surfaces via thiol and thiolate bonds. *Comput. Mat. Sci.*, 27(12):151 – 160, 2003.

[51] H. Basch, R. Cohen, and M. A. Ratner. Interface geometry and molecular junction conductance: geometric fluctuation and stochastic switching. *Nano letters*, 5(9):1668–75, 2005.

[52] D. J. Mowbray, G. Jones, and K. S. Thygesen. Influence of functional groups on charge transport in molecular junctions. *J. Chem. Phys.*, 128:111103, 2008.

[53] Y. Xue and M. A. Ratner. Theoretical principles of single-molecule electronics: A chemical and mesoscopic view. *J. Quantum. Chem.*, 102:911, 2005.

[54] R. O. Jones and O. Gunnarsson. The density functional formalism, its applications and prospects. 61(3):689–746, 1989.

[55] C. Toher, A. Filippetti, S. Sanvito, and K. Burke. Self-interaction errors in density-functional calculations of electronic transport. *Phys. Rev. Lett.*, 95(14):146402, 2005.

[56] K. S. Thygesen. Impact of exchange-correlation effects on the *iv* characteristics of a molecular junction. *Phys. Rev. Lett.*, 100(16):166804, 2008.

[57] S.-H. Ke, H. U. Baranger, and W. Yang. Role of the exchange-correlation potential in ab initio electron transport calculations. *J. Chem. Phys.*, 126(20):201102, 2007.

[58] F. Evers, F. Weigend, and M. Koentopp. Conductance of molecular wires and transport calculations based on density-functional theory. *Phys. Rev. B.*

[59] S. Y. Quek, L. Venkataraman, H. J. Choi, S. G. Louie, M. S. Hybertsen, and J. B. Neaton. Amine-gold linked single-molecule circuits: Experiment and theory. *Nano Lett.*, 7(11):3477–3482, 2007.

[60] C. Toher and S. Sanvito. Efficient atomic self-interaction correction scheme for nonequilibrium quantum transport. *Phys. Rev. Lett.*, 99(5):056801, 2007.

[61] P. Darancet, A. Ferretti, D. Mayou, and V. Olevano. Ab initio GW electron-electron interaction effects in quantum transport. *Phys. Rev. B*, 75(7):075102, 2007.

[62] M. Strange, C. Rostgaard, H. Häkkinen, and K. S. Thygesen. Self-consistent GW calculations of electronic transport in thiol- and

amine-linked molecular junctions. *Phys. Rev. B*, 83(11):115108, 2011.

[63] P. Darancet, J. R. Widawsky, H. J. Choi, L. Venkataraman, and J. B. Neaton. Quantitative current-voltage characteristics in molecular junctions from first principles. *Nano Lett.*, 12(12):6250–6254, 2012.

[64] L. Hedin. New method for calculating the one-particle Green's function with application to the electron-gas problem. *Phys. Rev.*, 139(3A):A796–A823, 1965.

[65] M. S. Hybertsen and S. G. Louie. Electron correlation in semiconductors and insulators: Band gaps and quasiparticle energies. *Phys. Rev. B*, 34(8):5390, 1986.

[66] P. Delaney and J. C. Greer. Correlated electron transport in molecualr electronics. *Phys. Rev. Lett.*, 93(3):036805–1–036805–4, 2004.

[67] S. McDermott, C. B. George, G. Fagas, J. C. Greer, and M. A. Ratner. Tunnel currents across silane diamines/dithiols and alkane diamines/dithiols; a comparative computational study. *J. Phys. Chem.C*, 113:744–750, 2009.

[68] C. A. Martin, D. Ding, H. S. J. van der Zant, and J. M. van Ruitenbeek. Lithographic mechanical break junctions for single-molecule measurements in vacuum: possibilities and limitations. *New. J. Phys.*, 10:065008, 2008.

[69] V. Geskin, R. Stadler, and J. Cornil. Multideterminant assessment of mean-field methods for the description of electron transfer in weak-coupling regime. *Phys. Rev. B*, 80:085411, 2009.

[70] A. Szabo and N. S. Ostlund. *Modern Quantum Chemistry: Introduction to Advanced Electronic Structure Theory.* Dover Publications, Inc., 1996.

[71] W. Kohn and L. J. Sham. Self-consistent equations including exchange and correlation effects. *Phys. Rev.*, 140(4A):A1133–A1138, 1965.

[72] J. C. Greer. Estimating full configuration interaction limits from a Monte-Carlo selection of the expansion space. *J. Chem. Phys.*, 103:1821–1828, 1995.

[73] J. C. Greer. Monte-Carlo Configuration Interaction. *J. Comput. Phys.*, 146(1):181–202, 1998.

[74] Győrffy Werner. *Monte Carlo Configuration Interaction Method for Calculation of Electronic Spectra of Molecules.* PhD thesis, University College Cork, 2007.

[75] J. C. Slater. The theory of complex spectra. *Phys. Rev.*, 34:1293–1322, 1929.

[76] J. C. Slater. Atomic shielding constants. *Phys. Rev.*, 36:57–64, 1930.

[77] F. Jensen. *Introduction to Computational Chemistry.* Wiley, 2007.

[78] L. H. Thomas. The calculation of atomic fields. *Mathematical Preceedings of the Cambridge Philosophical Society*, 23(5):542, 1927.

[79] R. M. Martin. *Electronic Structure: Basic Theory and Practical Methods.* Cambridge University Press, 2010.

[80] P. Hohenberg and W. Kohn. Inhomogeneous electron gas. *Phys. Rev.*, 136(3B):B864–B871, 1964.

[81] J. K. L. MacDonald. Successive approximations by the Rayleigh-Ritz variation method. *Phys. Rev.*, 43(10):830–833, 1933.

[82] L. Tong, M. Nolan, T. Cheng, and J. C. Greer. A Monte Carlo configuration generation computer program for the calculation of electronic states of atoms, molecules, and quantum dots. *Comput. Phys. Commun.*, 131:142 – 163, 2000.

[83] W. Győrffy, T. M. Henderson, and J. C. Greer. Statistical estimates of electron correlations. *J. Chem. Phys.*, 125(5):054104, 2006.

[84] J. A. Larsson, L. Tong, T. Cheng, M. Nolan, and J. C. Greer. A basis set study for the calculation of electronic excitations using Monte-Carlo configuration interaction. *J. Chem. Phys.*, 114(15), 2001.

[85] W. Győrffy, R. J. Bartlett, and J. C. Greer. Monte Carlo configuration interaction predictions for the electronic spectra of Ne, CH2, C2, N2, and H2O compared to full configuration interaction calculations. *J. Chem. Phys.*, 129(6):064103, 2008.

[86] J. P. Coe, D. J. Taylor, and M. J. Paterson. Calculations of potential energy surfaces using Monte Carlo configuration interaction. *J. Chem. Phys.*, 137(19):194111, 2012.

[87] J. P. Coe, D. J. Taylor, and M. J. Paterson. Monte Carlo configuration interaction applied to multipole moments, ionisation energies and electron affinities. *J. Comput. Chem.*, 34:1083–1093, 2013.

[88] J. C. Greer. Consistent treatment of correlation effects in molecular dissociation studies using randomly chosen configurations. *J. Chem. Phys.*, 103:7996, 1995.

[89] P. Delaney, J. C. Greer, and A. Larsson. Spin-polarization mechanisms of the nitrogen-vacancy center in diamond. *Nano Lett*, 10(2):610–614, 2010.

[90] M. Szepieniec, I. Yeriskin, and J. C. Greer. Quasiparticle energies and lifetimes in a metallic chain model of a tunnel junction. *J. Chem. Phys.*, 138:144105, 2013.

[91] T. Sommerfeld and F. Tarantelli. Subspace iteration techniques for the calculation of resonances using complex symmetric hamiltonians. *J. Chem. Phys.*, 112(5):2106–2110, 2000.

[92] J. P. Coe and M. J. Paterson. Development of Monte Carlo configuration interaction: Natural orbitals and second-order perturbation theory. *J. Chem. Phys.*, 137(20):204108, 2012.

[93] R. McWeeny. *Methods of Molecular Quantum Mechanics*. Academic Press, 1992.

[94] W. R. Frensley. Boundary conditions for open quantum systems driven far from equlibrium. *Rev. Mod. Phys.*, 62(3):745–79, 1990.

[95] R. Santra and Cederbaum L. S. Non-Hermitian electronic theory and application to clusters. *Phys. Rep.*, 368:1–117, 2002.

[96] S. Datta. ECE 659 Lecture Notes. `www.nanohub.org/resources/6172`, 2003.

[97] A. F. J. Siegert. On the derivation of the dispersion formula for nuclear reactions. *Phys. Rev.*, (56):750–752, 1939.

[98] T. Helgaker and P. R. Taylor. World Scientific, Singapore, 1995.

[99] J. G. Muga, J. P. Palao, B. Navarro, and I. L. Egusquiza. Complex absorbing potentials. *Phys. Rep. - Review Section Of Physics Letters*, 395(6):357–426, 2004.

[100] R. Santra and L. S. Cederbaum. Complex absorbing potentials in the framework of electron propagator theory. I. General formalism. *J. Chem. Phys.*, 117(12):5511–5521, 2002.

[101] R. Gutierrez, G. Fagas, K. Richter, F. Grossmann, and R. Schmidt. Conductance of a molecular junction mediated by unconventional metal-induced gap states. *Europhys. Lett.*, 62(1):90–96, 2003.

[102] G. Fagas. *Vibrational properties of complex solids*. PhD thesis, Lancaster University, 2000.

[103] D. Sharma. *Investigation of numerical atomic orbitals for first-principles calculations of the electronic and transport properties of*

silicon nanowire structures. PhD thesis, University College Cork, March 2012.

[104] N. Moiseyev. Quantum theory of resonances: Calculating energies, widths and cross-sections by complex scaling. *Phys. Rep.*, 302, 1998.

[105] R. Kosloff and D. Kosloff. Absorbing boundaries for wave-propagation problems. *J. Comput. Phys.*, 63(2):363–376, 1986.

[106] J. A. Driscoll and K. Varga. Calculation of self-energy matrices using complex absorbing potentials in electron transport calculations. *Phys. Rev. B*, 78(24):245118, 2008.

[107] U. V. Riss and H. D. Meyer. Calculation of resoannce energies and widths using the complex absorbing potential method. *J. Phys. B*, 26(23):4503–4536, 1993.

[108] R. Santra. Why complex absorbing potentials work: A discrete-variable-representation perspective. *Phys. Rev. A*, 74(3):034701, 2006.

[109] N. Nilius, T. M. Wallis, and W. Ho. Development of one-dimensional band structure in artificial gold chains. *Science*, 297(5588):1853–1856, 2002.

[110] A. I. Yanson, G. Rubio Bollinger, E. van den Brom, N. Agraït, and J. M. van Ruitenbeek. Formation and manipulation of a metallic wire of single gold atoms. *Nature*, 395:783–780, 1998.

[111] N. D. Lang. Resistance of atomic wires. *Phys. Rev. B*, 52(7):5335–5342, 1995.

[112] M. Galperin, A. Nitzan, and M. A. Ratner. Molecular transport junctions: Current from electronic excitations in the leads. *Phys. Rev. Lett.*, 96:166803, 2006.

[113] I. Tamblyn, P. Darancet, S. Y. Quek, S. A. Bonev, and J. B. Neaton. Electronic energy level alignment at metal-molecule interfaces with a GW approach. *Phys. Rev. B*, 84(20):201402, 2011.

[114] Y. Pavlyukh and W. Hübner. Configuration interaction approach for the computation of the electronic self-energy. *Phys. Rev. B*, 75(20):205129, 2007.

[115] P. Fuentealba, H. Stoll, L. von Szentpaly, P. Schwerdtfeger, and H. Preuss. On the reliability of semi-empirical pseudopotentials: simulation of Hartree-Fock and Dirac-Fock results. *J. Phys. B*, 16(11):L323, 1983.

[116] R. Ahlrichs, M. Bar, M. Haser, H. Horn, and C. Kolmel. Electronic-structure calculations on workstation computers - The program system Turbomole. *Chem. Phys. Lett.*, 162(3):165–169, 1989.

[117] J. P. Perdew, K. Burke, and M. Ernzerhof. Generalized gradient approximation made simple. *Phys. Rev. Lett.*, 77(18):3865–3868, 1996.

[118] D. J. Thouless. Stability conditions and nuclear rotations in the Hartree-Fock theory. *Nuc. Phys.*, 21:225–232, 1960.

[119] I. Yeriskin, S. McDermott, R. J. Bartlett, G. Fagas, and J. C. Greer. Electronegativity and electron currents in molecular tunnel junctions. *J. Phys. Chem. C*, 114(48):20564–20568, 2010.

[120] J. P. Lowe and K. A. Peterson. *Quantum Chemistry*. Elsevier, 3rd edition, 2006.

[121] S. H. Ke, H. U. Baranger, and W. Yang. Electron transport through molecules: Self-consistent and non-self-consistent approaches. *Phys. Rev. B*, 70(8):085410, 2004.

[122] R. S. Mulliken. Electronic population analysis on LCAOMO molecular wave functions. I. *J. Chem. Phys.*, 23:1833, 195.

[123] D. E. Cabelli, A. H. Cowley, and M. J. S. Dewar. UPE studies of conjugation involving Group 5A elements. 1. Phenylphosphines. *J. Am. Chem. Soc.*, 103(12):3286–3289, 1981.

[124] F. Goyer and M. Ernzerhof. Correlation effects in molecular conductors. *J. Chem. Phys.*, 134(17):174101, 2011.

[125] Y. Meir and N. S. Wingreen. Landauer formula for the current through an interacting electron region. *Phys. Rev. Lett.*, 68(16):2512–2515, 1992.

[126] A. Ferretti, A. Calzolari, R. Di Felice, and F. Manghi. First-principles theoretical description of electronic transport including electron-electron correlation. *Phys. Rev. B*, 72(12):125114, 2005.

[127] B. T. Pickup and O. Goscinski. Direct calculation of ionization energies: I. Closed shells. *Mol. Phys.*, 26(4):1013–1035, 1973.

[128] E. R. Davidson. Properties and uses of natural orbitals. *Rev. Mod. Phys.*, 44(3):451–464, 1972.

[129] G. Fagas, P. Delaney, and J. C. Greer. Independent particle descriptions of tunneling using the many-body quantum transport approach. *Phys. Rev. B*, 73(24):241314, 2006.

[130] P.-O. Löwdin. Quantum theory of many-particle systems: I. Physical interpretations by means of density matrices, natural spin-orbitals, and convergence problems in the method of configurational interaction. *Phys. Rev.*, 97(6):1474–1489, 1955.

[131] K. S. Thygesen and A. Rubio. Nonequilibrium gw approach to quantum transport in nano-scale contacts. *J. Chem. Phys.*, 126(9):091101, 2007.

[132] X. Wang, C. D. Spataru, M. S. Hybertsen, and A. J. Millis. Electronic correlation in nanoscale junctions: Comparison of the GW approximation to a numerically exact solution of the single-impurity Anderson model. *Phys. Rev. B*, 77(4):045119, Jan 2008.

[133] E. Ruiz, D. R. Salahub, and A. Vela. Charge-transfer complexes: Stringent tests for widely used density functionals. *J. Phys. Chem.*, 100(30):12265–12276, 1996.

[134] R. A. Kendall, T. H. Dunning Jr, and R. J. Harrison. Electron affinities of the first-row atoms revisited. Systematic basis sets and wave functions. *J. Chem. Phys.*, 96(9):6796–6806, 1992.

[135] A. D. Becke. Density Functional thermochemistry IV: A new dynamical correlation functional and implications for exact exchance-correlation mixing. *J. Chem. Phys.*, 104:1040–46, 1996.

[136] J. P. Perdew and Y. Wang. Accurate and simple analytic representation of the electron-gas correlation energy. *Phys. Rev. B*, 45(23):13244–13249, 1992.

[137] N. Moiseyev. Quantum theory of resonances: calculating energies, widths and cross-sections by complex scaling. *Phys. Rep.*, 302(5-6), 1998.

[138] N. Moiseyev, P. R. Certain, and F. Weinhold. Resonance properties of complex-rotated hamiltonians. 78(6):1613–1630, 1978.

[139] M. Müller and I. Rotter. Exceptional points in open quantum systems. *J. Phys. A*, 41(24):244018, 2008.

[140] I. Rotter. A non-hermitian hamilton operator and the physics of open quantum systems. *J. Phys. A*, 42(15):153001, 2009.

[141] S. Cavalli and D. De Fazio. Coalescence of metastable states in chemical rections: Double poles of the scattering matrix and exceptional points. *Theor. Chem. Acc.*, 129:141–150, 2011.

[142] I. Rotter and A. F. Sadreev. Singularities caused by coalesced complex eigenvalues of an effective Hamilton operator. *Int. J. Theor. Phys.*, 46(8), 2007.

[143] E. N. Bulgakov, I. Rotter, and A. F. Sadreev. Phase rigidity and avoided level crossings in the complex energy plane. *Phys. Rev. E*, 74:1–6, 2006.